Aus der Klinik für Medizinische und Poliklinik III
Direktor: Herr Prof. Dr. Stefan R. Bornstein

In vivo characterization of Ca^{2+} dynamics in pancreatic β-cells of Zebrafish

Dissertationsschrift

zur Erlangung des akademischen Grades

Doktor der Biomedizin
Doctor rerum medicinalium (Dr. rer. medic.)

vorgelegt
der Medizinischen Fakultät Carl Gustav Carus
der Technischen Universität Dresden

von
MSc. Luis Fernando Delgadillo Silva

Geboren 9st June, 1988 aus Guadalajara, Mexiko

Dresden, 2020

1. Gutachter:
Prof. Stephan Speier
Paul Langerhans Institute Dresden of the Helmholtz Center Munich at the University Clinics and Medical Faculty Carl Gustav Carus at TU Dresden
Molekulare Diabetologie Fetscherstraße 74
01307 Dresden Germany

2. Gutachter:
Dr. Anthony Gavalas
Paul Langerhans Institute Dresden of the Helmholtz Center Munich at the University Clinics and Medical Faculty Carl Gustav Carus at TU Dresden
Molekulare Diabetologie Fetscherstraße 74

3. Gutachter:
Prof. Guy Rutter
Faculty of Medicine, Department of Metabolism, Digestion and Reproduction
Department of Medicine, Imperial College London, London, UK

Tag der mündlichen Prüfung: , 2020.

gez.: Prof. Dr. Michele Solimena
Vorsitzender der Promotionskommission

Paul Langerhans Institute Dresden of the Helmholtz Center Munich at the University Clinics and Medical Faculty Carl Gustav Carus at TU Dresden
Molekulare Diabetologie Fetscherstraße 74 01307 Dresden Germany

Anmerkung:
Die Eintragung der Gutachter und Tag der mündlichen Prüfung (Verteidigung) erfolgt nach Festlegung von Seiten der Medizinischen Fakultät Carl Gustav Carus der Technischen Universität Dresden. Die oben genannten Eintragungen werden durch die Doktoranden nach der Verteidigung zwecks Übergabe der fünf Pflichtexemplare an die Zweigbibliothek Medizin in gedruckter Form oder handschriftlich vorgenommen.

Abstract

Glucose homeostasis is fundamental for all living organisms. In vertebrates, the hormone insulin regulates the metabolism of carbohydrates, fats and proteins. In order to sustain the glucose homeostasis, the pancreatic β-cells, which produce and secrete insulin, must coordinate their efforts to secrete the right amounts of insulin required by the organism. *In vitro* studies, have suggested that a subpopulation of β-cells, referred to as "hub-cells", coordinate islet Ca^{2+} dynamics during insulin secretion. However, it is unclear whether the hub-cell model pertains to an *in vivo* scenario, where the islet is densely vascularized and innervated. In this thesis, we employed the genetically-encoded calcium indicator GCaMP6, confocal imaging and optogenetics, to characterize the Ca^{2+} dynamics of the zebrafish β-cells *in vivo*. We found that pancreatic β-cells present endogenous Ca^{2+} spikes *in vivo* under basal conditions. These Ca^{2+} spikes are rapidly suppressed after lowering glucose levels via insulin administration. In addition, the temporal inhibition of blood flow decreases the Ca^{2+} spikes, suggesting that β-cells are systemically connected. Furthermore, β-cells show a synchronized response to a pericardial glucose injection. Specifically, we found that Ca^{2+} spikes originate and emanate from a subset of β-cells that are the first to respond to a glucose stimulus. We define these cells as "leader-cells". We tested if these cells could coordinate the islet *in vivo* by employing 2-photon laser ablation. Whereas ablation of control cells had no significant effect on the amplitude and duration of the subsequent Ca^{2+} spikes responses, ablation of leader cells led to a reduction in the Ca^{2+} response. Furthermore, we developed systems for optogenetic interrogation of β-cells *in vivo*. We show that the light-gated Cl^- ion pump halorhodopsin (NpHR) can be applied to inhibit β-cell depolarization in the zebrafish. We also present the optically orthogonal system of the red Ca^{2+} indicator K-GECO1 in combination with the blue-shifted channelrhodopsin CheRiff to activate individual β-cell *in vivo*. Using these new tools, we provide examples where the activation of individual β-cells showed heterogeneous potential to trigger influx of Ca^{2+} in the rest of the β-cells. Overall, our results led us to propose a hierarchical model of islet coordination. In contrast to the majority of β-cells, which occupy the bottom of the hierarchy since they present low capability to recruit other cells, the leader cells occupy the top levels, being capable to coordinate a majority of the islet's β-cells.

Keywords: Diabetes, β-cells, zebrafish, live imaging, optogenetics.

Abstract

Abstract

Die Glukosehomöostase ist für alle lebenden Organismen von grundlegender Bedeutung. Bei Wirbeltieren reguliert das Hormon Insulin den Stoffwechsel von Kohlenhydraten, Fetten und Proteinen. Um die Glukosehomöostase aufrechtzuerhalten, müssen die β-Zellen der Bauchspeicheldrüse, welche Insulin produzieren und absondern, ihre Bemühungen koordinieren, um die richtigen Mengen an Insulin zu sekretieren, die der Organismus benötigt. In-vitro-Studien haben gezeigt, dass eine Subpopulation von β-Zellen, die als „Hub-Zellen“ bezeichnet werden, die Insulinsekretion der Inseln koordiniert. Es ist jedoch unklar, ob sich die Hub-Cell-Theorie auf ein in-vivo-Szenario bezieht, bei dem die Insel dicht vaskularisiert und von Neuronen innerviert ist. In dieser Arbeit verwendeten wir den genetisch kodierten Calcium-Indikator GCaMP6, konfokale Bildgebung und Optogenetik, um die Ca^{2+}-Dynamik der Zebrafisch-β-Zellen *in vivo* zu charakterisieren. Wir fanden heraus, dass Pankreas-β-Zellen *in vivo* unter basalen Bedingungen endogene Ca^{2+}-Spitzen aufweisen. Diese Ca^{2+}-Spitzen werden nach Senkung des Glukosespiegels durch Insulinverabreichung schnell unterdrückt. Darüber hinaus verringert die zeitliche Hemmung des Blutflusses die Ca^{2+}-Spitzen, was darauf hindeutet, dass β-Zellen systemisch verbunden sind. Darüber hinaus zeigen β-Zellen eine synchronisierte Reaktion auf die perdikale Glukoseinjektion. Insbesondere fanden wir heraus, dass Ca^{2+}-Spitzen von den β-Zellen hervorgerufen werden, die zuerst auf den Glukosestimulus reagieren. Wir definieren diese Zellen als "Leader-Zellen". Wir haben *in vivo* durch den Einsatz einer 2-Photonen-Laserablation getestet, ob diese Zellen die Insel koordinieren können. Während die Ablation von Kontrollzellen keinen signifikanten Einfluss auf die Amplitude und Dauer der nachfolgenden Ca^{2+}-Spitzenreaktionen hatte, führte die Ablation von Leader-Zellen zu einer signifikanten Verringerung der GCaMP-Reaktion. Darüber hinaus haben wir Systeme für die optogenetische Abfrage von β-Zellen *in vivo* entwickelt: Wir zeigen, dass die lichtgesteuerte Cl^-Ionenpumpe Halorhodopsin (NpHR) angewendet werden kann, um die Depolarisation von β-Zellen *in vivo* zu hemmen. Wir präsentieren auch das optisch orthogonale System des roten Ca^{2+}-Indikators K-GECO1 in Kombination mit dem blauverschobenen Channelrhodopsin CheRiff, um einzelne β-Zellen *in vivo* abzufragen. Unter Verwendung dieser neuen Werkzeuge liefern wir Beispiele, bei denen die Aktivierung einzelner β-Zellen ein heterogenes Potenzial für die Auslösung des Ca^{2+}-Einstroms in die übrigen β-Zellen *in vivo* zeigte. Insgesamt bietet diese Studie Hinweise darauf, dass eine Untergruppe von β-Zellen ein hohes Potenzial zur Koordination der Ca^{2+}-Dynamik

Abstract

der Insel *in vivo* aufweist.

Schlüsselwörter: Diabetes, β-Zellen, Zebrafisch, Live-Bildgebung, Optogenetik.

Contents

Contents

Contents

List of figures

List of Tables

1. Introduction

1.1. Diabetes and insulin

Physicians have fought diabetes for over 3,500 years; the first documentation of diabetes dates back to an Egyptian ancient papyrus found in the grave of Thebes. The papyrus is a medical compendium where the Egyptian physician Hesy-Ra (1552 BC) noted: “to regulate - excessive urine”, referring to a diabetic patient. The Indian physicians Chackrat and Syshrut at around 500 BC made the observation of the urine sweetness in diabetes after noticing ants congregating around the urine of diabetic patients. Yet, at around 230 BC, the prefix “diabetes” was used for the first time to refer to an illness of excessive urine passage by the Egyptian physician Apollonius Memphites. Diabetes derives from the Greek verb word *διαβαινω* which means “pass”, and the word *διαβήτης* (which means wine-pourer or siphon) is believed to have been coined by Demetrios of Apamaia in 200-250 BC, and it was the Greek physician Aretaeus of Cappadocia (81-138 AD). They used this word to describe a dreadful disease characterized by excessive urination, a melting down of flesh and limbs into urine. Typical treatments against diabetes involved limiting food and water, usually leading to death by sever starvation and dehydration. Hence, diabetes was an obscure and mortal disease with no possible treatment until the discovery of insulin in the 19th century (Ahmed, 2002; Poretsky, 2010)

The relationship between the pancreas and diabetes was not clear until 1840, when the physiologist Claude Bernard ligated the pancreatic duct of a dog, which led to pancreas degeneration and diabetes (Vecchio et al., 2018). The same results were produced by Oscar Minkowski Joseph von Mering and Gustave-Edouard Laguesse; Minkowski and

Mering reported in 1889 that dog pancreas removal leads to a permanent diabetes. In 1869, the German pathologist Paul Langerhans, identified in his thesis a new kind of cells, which he described as “heaps of cells” dispersed across the acini of the pancreas and called them “islet cells”. Finally, in 1921, in acidic ethanol extracts from dog pancreas, the insulin protein was finally isolated and purified by Frederick Banting, Charles Best and John Macleod. In 1922, Banting and Macleod administered insulin to the 14 years old Leonard Thompson, who suffered from T1D; Miraculously, Leonard survived to the age of 27. This accomplishment earned the Nobel Prize for the insulin discovery to Frederick Banting and John Macleod in 1923 (Poretsky, 2010). Nowadays, diabetes is recognized as a multifactorial disease and even though insulin does not cure diabetes, it is considered as one of the major medical discoveries.

1.2. The endocrine pancreas

The pancreas is a glandular organ composed of two types of tissues, the exocrine tissue that produces and secretes digestive enzymes into the duodenum, and the endocrine tissue, consisting of the islets of Langerhans. The islets of Langerhans constitute ~2% of the pancreas and are composed of 5 different types of cells: α-cells, β-cells, δ-cells ε-cells and PP-cell, producing the hormones glucagon, insulin, somatostatin, ghrelin and pancreatic polypeptide, respectively (Figure 1) (Barrett et al., 2010).

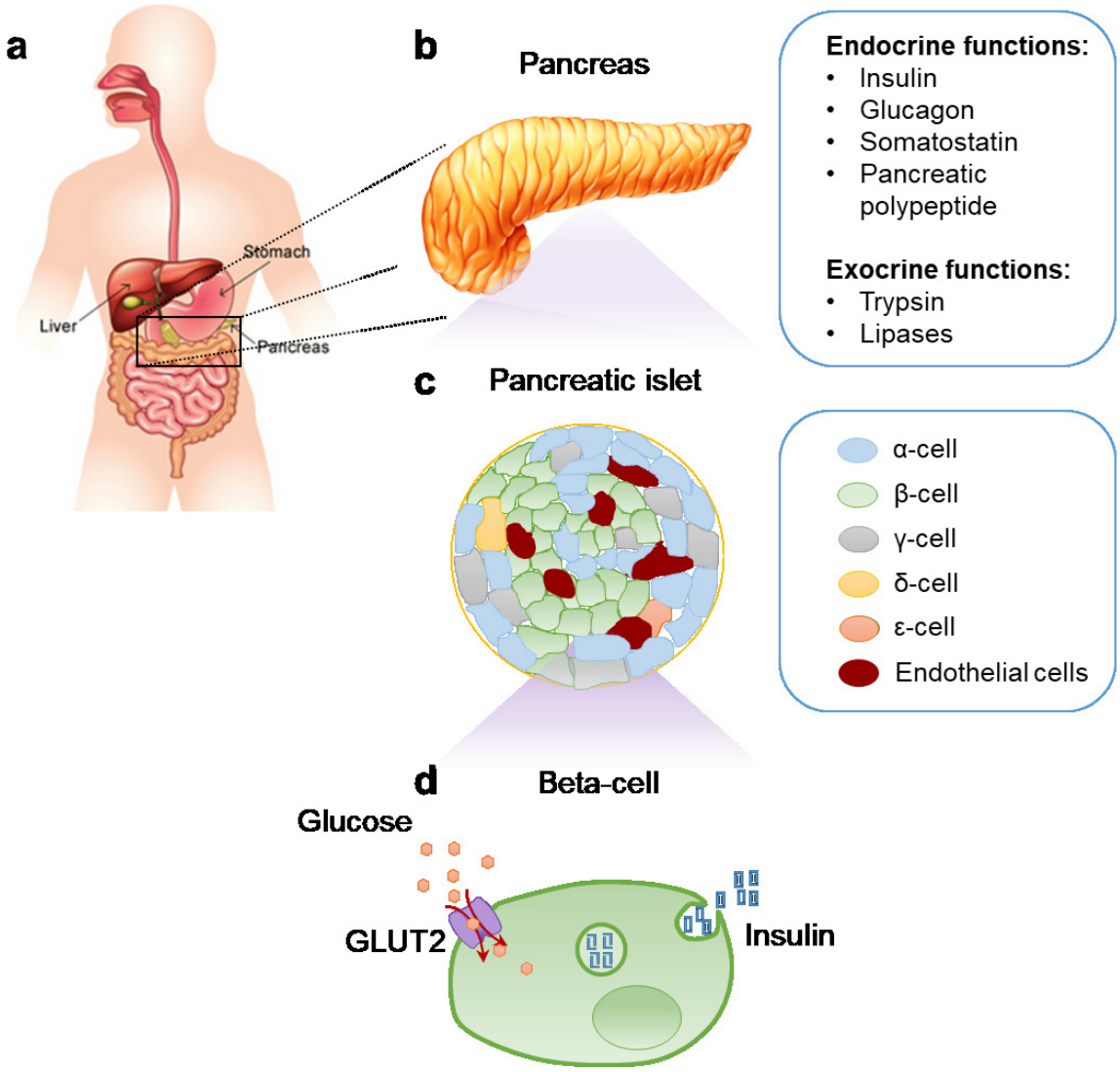

Figure 1. Human pancreas anatomy. a. The pancreas is located behind the stomach and surrounded by the liver, intestine and spleen. **b.** The pancreas is composed of exocrine and endocrine tissue. **c.** The islets of Langerhans are composed of insulin producing β-cells, glucagon producing α-cells, ghrelin producing epsilon-cells, somatostatin producing δ-cells and pancreatic polypeptide producing PP-cells. **d.** When the glucose levels in blood increases, it is transported inside the β-cells by glucose transporter such as GLUT2, and then secrete insulin into the blood stream promoting glucose uptake by peripheral tissues such as the liver and muscle.

1.3. The diabetes pandemic

Diabetes mellitus affects almost 1/8 of the world's population, and consumes >10% of the healthcare budged in western societies (https://www.idf.org/). Diabetes mellitus can be broadly classified in two distinct types: Type 1 and Type 2. Type 1 diabetes mellitus (T1DM) is known as an autoimmune disease, characterized by the destruction of the pancreatic β-cells by the immune system and the requirement of lifelong insulin therapy (Katsarou et al., 2017). Type 2 diabetes mellitus (T2DM) is the predominant type of diabetes, which is characterized by insulin resistance and hyperglycemia. T2DM affects more than 415 million people worldwide and is predicted to afflict over 640 million people by 2040. Genetic predisposition, age, obesity, pregnancy and sedentary life style are risk factors for diabetes development (Kahn et al., 2014). Other types of diabetes include rare monogenic forms derived from single-gene mutations in genes involved in β-cell function or development such as INS, GCK and PDX1 (Ashcroft and Rorsman, 2012; Bell and Polonsky, 2001; Murphy et al., 2008; Poretsky, 2010).

1.4. β-cell development in zebrafish and mammals

The zebrafish pancreas contains primary and secondary islets. The primary islet is located at the anterior head of the pancreas and is established during embryonic development. During embryogenesis, the first wave of β-cells appears at 15 somites stage (15s) or 17 hours post fertilization (hpf) along the bilateral mid-line in the endoderm adjacent to the notochord. At 24 hpf the dorsal bud is fully formed. The transcription factor pancreatic and duodenal homeobox 1 (*Pdx1*), is one of the earliest markers of β-cells, and plays an important role in pancreatic development. Zebrafish *Pdx1* mutants show islet formation but impaired islet expansion and a lower number of β-cells, resembling *Pdx1*$^{-/-}$ mice (Kimmel et al.,

2015). At 32hpf, the second wave of differentiation comes from the ventral domain of the gut, which forms the ventral pancreatic bud. The dorsal and ventral buds coalesce at around 48hpf to form the pancreas containing the primary islet. The ventral bud generates exocrine cells as well as some endocrine cells. The secondary islets start to appear at around 5-7 days post fertilization (dpf) and spread over the tail of the zebrafish pancreas (Kinkel and Prince, 2009).

Similarly to the fish, the mouse pancreas originates from the dorsal and ventral buds formed from the foregut endoderm. Two temporal waves of endocrine differentiation have been identified. The first transition occurs from embryonic day (E) 9, with the formation of the dorsal bud from the dorsal foregut endoderm and the ventral bud from of the hepatic/biliary evagination. During this stage, in the dorsal bud the first expressing glucagon and insulin cells and some bi-hormonal cells are detected, it is still controversial if these first endocrine cells contributes to the mature islets. At E11.5, as dorsal and ventral buds fuse, the pancreatic epithelium segregates progressively into the tip and truck domains, containing the progenitors for acinar cells and the bipotent progenitors for endocrine/duct cells, respectively. During the secondary transition, between E12.5 and E15.5, the epithelial plexus forms. This transition is characterized by a fast expansion and differentiation of endocrine and exocrine tissues and the maturation and specification of the endocrine cells. The endocrine progenitors in the epithelial plexus are labelled by the expression of *Pdx1* and the transient expression of *Neurogenin-3 (Ngn3)*. *Pdx1* is necessary for pancreas expansion but is not essential for endocrine formation (Spooner et al., 1970). *Pdx1*$^{-/-}$ mice form pancreatic buds with endocrine progenitors but fail to complete the pancreas development. Meanwhile, *Ngn3*$^{-/-}$ mice, do not develop any endocrine cells (Gradwohl et al., 2000). As Ngn3 expression peaks, the progenitors commit to an endocrine fate. Endocrine differentiation is controlled by the Notch signaling pathway via lateral inhibition in the ductal epithelium. Notch signaling sustains the progenitor state, as upon Notch signaling inhibition, cells start to express higher levels of *Ngn3* and commit to the endocrine lineage. This leads them to exit the cell cycle, delaminate from the ductal epithelium and coalesce in proto-islets (Ackermann and Gannon, 2007). As the islet matures, they acquire a typical spherical

shape, blood vessel supply and innervation (Bastidas-Ponce et al., 2017). Finally, during the tertiary transition from E16.5–postnatal, differentiated PP-expressing cells appears. This stage is characterized by further maturation of endocrine cells, the migration of individual differentiated endocrine cells to organize in clusters to form the mature islets, where the β-cells form the core, and α-, δ- and PP-cells localize at the periphery with some ϵ-cells distributed throughout the islet (Rukstalis and Habener, 2009).

As early as E9.5, the Ngn3+ endocrine progenitors start to differentiate, resulting in the emergence of early glucagon-producing cells. At day E10.5, the first insulin-producing cells are detected and at E14.5, the somatostatin-expressing cells are formed. All the endocrine cells derive from *Ngn3* progenitors. Collombat *et al*. showed that the specification towards alpha and β-cell occurs via mutual inhibition between *Pax4* and *Arx* expression. Both transcription factors are induced by *Ngn3*. While $Arx^{-/-}$ mice do not present α-cells, an increased number of β and δ-cells is observed. Similarly, $Pax4^{-/-}$ mice do not present β-cells and δ-cells, but show an increased number of α-cells. Congruently, $Arx^{-/-}$ and $Pax4^{-/-}$ mice show an increase in δ-cells at the expenses of α-and β-cell mass. It is not clear which cues help to make the final commitment towards each endocrine lineage, or if the lack of *Arx* and *Pax4* leads to a default δ-cell fate (Bastidas-Ponce et al., 2017; Collombat et al., 2005; Collombat et al., 2003). A similar genetic program is found in zebrafish β-cell specification, however *Ngn3* is not expressed in the endocrine progenitors, yet, they express *NeuroD*, which is expressed in early precursors that give rise to all endocrine cells and labels the endocrine cells similarly to the mammalian systems (Kinkel and Prince, 2009).

1.5. β-cells function and heterogeneity

The main function of β-cells is to secrete insulin accordingly to the blood glucose levels. After a carbohydrate-rich meal, the blood glucose increases and enters the β-cells by glucose transporters such as GLUT2 (Figure 2a-b). Then, the glucose is quickly metabolized to produce ATP.

As the intercellular ratio of ATP/ADP increases, it leads to the closure of the ATP-dependent K^+ channels (Figure 2c-e). The closure of the K^+ channels depolarizes the cell membrane, triggering the activation of the voltage dependent Ca^{2+} channels (Figure 2f-h). The rapid increase of intracellular Ca^{2+} stimulates insulin secretion by exocytosis, releasing insulin into the blood flow (Figure 2i). The insulin then promotes the glucose uptake by the peripheral tissues such as the liver, brain and muscles. Insulin secretion presents two phases: during the first phase, a rapid transient peak of insulin release is detected lasting for about 10 min. The second phase has a more sustained insulin release. Patients with T2DM show defects in the first-phase and reduced second-phase insulin secretion, hence, the importance to clarify the cellular and molecular mechanism on how β-cells coordinate insulin secretion (Ivanova et al., 2013; Poretsky, 2010; Rorsman and Renstrom, 2003).

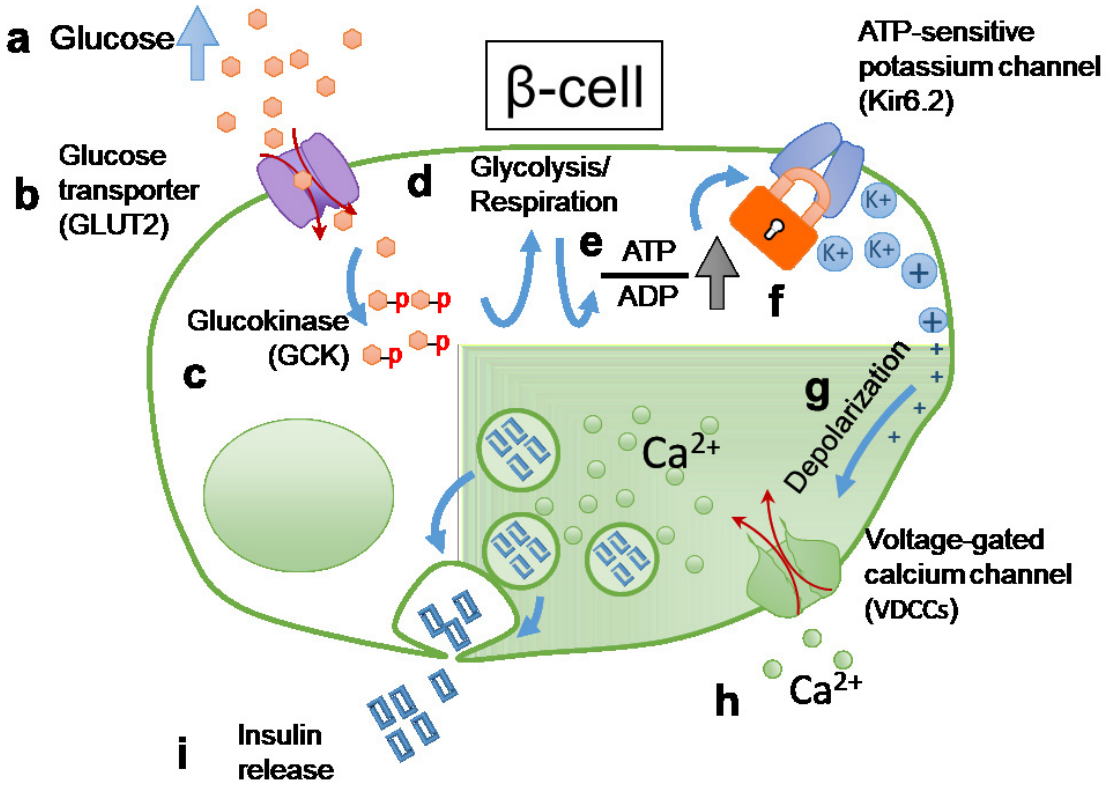

Figure 2. Process of insulin secretion by the β-cells. a. After a glucose-rich meal, the glucose levels rise. **b.** Then, the glucose is internalized by the glucose transporters (GLUT2) inside the β-cells. **c.** The glucokinase (GCK) phosphorylates the glucose generating glucose-6-phospate. **d**. The glucose-6-phospate is metabolize to generate ATP. **e.** The ratio

of ATP/ADP increases, and this event closes the ATP-sensitive potassium channel (Kir6.2). **f.** Once the potassium cannot leave the cell, the membrane starts to acquire a positive charge inside, triggering depolarization of the cell membrane. **g.** The membrane depolarization activates the Voltage-gated calcium channels (VDCCs) **h.** Then, the intracellular Ca^{2+} rises. **i.** High intracellular Ca^{2+} stimulates insulin secretion by exocytosis into the blood stream.

The β-cells have been considered as a rather uniform cell population, as the islet behave as a syncytium, in which glucose triggers synchronized insulin secretion (Nadal et al., 1999). However, new studies have pointed out the existence of heterogeneity among β-cells. Sub-population of β-cells have been identified based on differential cell-surface markers, gene expression profiles, topological location and even their embryonic origin (Ackermann et al., 2016; Bader et al., 2016; Ellenbroek et al., 2013; Katsuta et al., 2012; Li et al., 2016; Singh et al., 2017; Smukler et al., 2011; Xin et al., 2016). β-cell heterogeneity has been reported not only at a transcriptomic level, but also at the functional level. From *in vitro* studies Giordano *et al*. observed at least two discrete subpopulation of β-cells characterized by their responsive to glucose: Giordano *et al*., incubated dispersed β-cells with 16.7 mM glucose three consecutive times, and found that around 36% of the β-cells would respond to the incubation, while another 39% would not secrete insulin. Interestingly, around 75% of the β-cells would present a fixed pattern, either responsive or unresponsive to glucose incubations, meanwhile a proportion of around 25% would oscillate between responsive and unresponsive states (Giordano et al., 1991). Finally, Johnston *et al*., described a functional heterogeneity in which insulin secretion is coordinated by a subpopulation of β-cells, termed “hub-cells”. These hub-cells act as pacemakers dictating insulin secretion dynamics of the rest of the β-cells (Johnston et al., 2016). Of note, all these studies were performed *in vitro*. Therefore, if this heterogeneity has any functional significance *in vivo*, remains to be clarified.

1.6. β-cell coordination

Studies employing patch-clamp in β-cells from isolated mouse islets have shown that β-cells are electrically coupled to other β-cells, but not to non-β-cells in the islet. Zhang *et al.* suggested that β-cells are coupled to 6-7 other β-cells, and theoretically, it is possible to propagate Ca^{2+} waves at 80 microns per second, allowing whole islet synchronization (Zhang et al., 2008). From *in vitro* Ca^{2+} imaging of isolated islets, it was already noted that β-cells display synchronicity in Ca^{2+} oscillations upon glucose stimulation. Nadal *et al.* reported that β-cells are silent at low glucose levels (3mM) and as expected, upon glucose stimulation (11mM), β-cells show transient increases in intracellular Ca^{2+}, followed by the typical train of oscillations in synchronicity. This experiment led the authors to propose that the islet behaves as a functional syncytium (Nadal et al., 1999). It has also been observed that Ca^{2+} influx occurs in a synchronous and rhythmic fashion. This pattern derives from the underlying electrical bursting activity of the β-cells that leads to pulsatile insulin secretion (Ivanova et al., 2013; Poretsky, 2010; Rorsman and Renstrom, 2003).

One of the most important mechanism of cell coupling is mediated by gap-junctions. Gap-junctions are specialized intercellular channels formed by connexins. The connexins are transmembrane proteins that assemble and connect directly the cytoplasm of two cells, allowing electrical and metabolic coupling. These channels allow the passage from one cell to another of small molecules and ions, including inositol and Ca^{2+}. Particularly, in mouse β-cells, connexin 36 (Cx36) plays a major role in β-cell coupling (Serre-Beinier et al., 2000). Indeed, Magalie *et al.*, found that isolated islets of $Cx36^{-/-}$ mice, upon glucose stimulation, showed irregular Ca^{2+} oscillations, without the characteristic synchronicity. Furthermore, they found that pulsatile insulin secretion was not present in these islets, and that the islets presented higher basal insulin release (Ravier et al., 2005). Moreover, $Cx36^{-/-}$ mice were shown to lack of a proper first phase and second phase of insulin secretion. These mice showed glucose intolerance, despite showing normal insulin levels and insulin sensitivity (Head et al., 2012). This is important, since

T2DM patients usually presents defects in the first phase and second phase of insulin secretion. Recently, Cohrs *et al.* reported that β-cells from metabolically phenotyped T2DM and glucose intolerant (IGT) donors lack the typical first-phase peak insulin secretion. While the IGT individuals presented a normal second-phase insulin secretion, the T2DM individuals showed defects in both the first ant the second phases. Both groups presented an overall lower insulin secretion in comparison to non-diabetic individuals, however, they had unchanged β-cell mass. The authors suggested that β-cells dysfunction precedes loss of β-cell mass, reinforcing the concept that β-cell functional restoration might be major target for diabetes therapy (Cohrs et al., 2020). Altogether these studies clearly illustrates that β-cell synchronicity is key for proper insulin secretion and its impairment may contribute to disease progression.

Recently, using intact isolated mouse islets, fast Ca^{2+} confocal imaging (2-8Hz), photopharmacology and optogenetics, Johnston *et al*., mapped a subpopulation of β-cell, which serve as hubs cells and regulate the glucose response of the rest of the β-cells. They showed that optogenetic silencing of the hub cells via the chloride pump halorhodopsin (NpHR) was enough to impair Ca^{2+} coordination in the islet. The hub cells comprised around 1-10% of the total β-cell population and presented high glucokinase (GCK) expression, reduced insulin levels, reduced expression of sarcoplasmic reticulum Ca^{2+}/ATPase (SERCA2) and lower Pdx1 expression in comparison to other β-cells (Johnston et al., 2016). These observations showed that the β-cells synchronous behavior might be controlled by a subpopulation of β-cells. However, these experiments were conducted *in vitro*, and it is possible that the behavior of β-cells in the native microenvironment could differ significantly, since islets are continuously perfused with blood and receive complex neural inputs. Therefore, the next steps in the field of β-cells coordination would require a more physiological environment in order to better characterize the hub cell.

1.7. Genetically-encoded calcium indicators

Introduction

Calcium is ubiquitous in all cells. It plays critical roles in cell physiology and is involved in cell secretion, cell contraction and gene expression. Thus, the understanding of Ca^{2+} signaling is paramount in biology. The first observations between the requirements of extracellular Ca^{2+} and insulin release were made by Grodsky *et al.,* when they found that insulin secretion is inhibited in rat pancreas perfused without Ca^{2+} (Grodsky et al., 1967). Subsequently, Grapengiesser, *et al.,* using the fluorescent dye Fura-2 as a calcium indicator, showed for the first time that β-cells exhibit intracellular Ca^{2+} oscillations in response to glucose (Grapengiesser et al., 1988).

The first chemical calcium sensors were made by pioneer work in 1970s by Roger Tsien. These Ca^{2+} sensors were based on the Ca^{2+} chelating properties of EGTA (Tsien, 1980). The calcium sensors can be broadly classified in single wavelength indicators and ratiometric indicators. Single wavelength indicators increase their fluorescence upon Ca^{2+} binding without changing their excitation/emission wavelength. The ratiometric indicators exhibit changes in the peak wavelength of their excitation or emission wavelength upon Ca^{2+} binding (Paredes et al., 2008). The chemical calcium indicators have the following advantages: they present a broad range of calcium affinities, are commercially available (www.thermofisher.com), can be loaded onto the cells, and there is no need to transfect the cells. One of the major disadvantages of the chemical calcium indicators is the difficulty to target a particular type of cell. Furthermore, the chemical indicators tend to compartmentalize and diffuse outside the cell, making longitudinal experiments very difficult (Grienberger and Konnerth, 2012; Paredes et al., 2008).

The Genetically-Encoded Calcium Indicators (GECIs) are an alternative to chemical Ca^{2+} indicators and have the advantage to target defined cell populations. Different GECIs, such as the GCaMP family of sensors, consisting of a circularly permuted green fluorescent protein (cpGFP) linked to calmodulin (CAM) and the M13 peptide from myosin light-chain kinase (Chen et al., 2013; Nakai et al., 2001), have been developed. This system present low or high fluorescence depending on calcium concentration changes in the cell. At low calcium levels, the

GCaMP presents low fluorescence, and upon calcium binding into the CAM domain, the GCaMP undergoes a conformational change that increases its fluorescence. The GECIs systems have been successfully used to trace back neuronal activity and several variants have been created. In the GCaMP6 family, the sensor with the largest change of fluorescent upon calcium binding is GCaMP6s. GaMP6s has a dynamic range, defined as the maximum fluorescent intensity divided by the minimum fluorescence (F_{max}/F_{min}) of ~63, and can detect single action potential (AP) in neurons with a temporal resolution of ~150ms. It has an affinity for Ca^{2+} with a K_d of 144nM, which is similar to one of the most popular chemical dies Fura-2 which has an affinity for Ca^{2+} with a K_d of ~145nM (Paredes et al., 2008). The fastest calcium sensor is the GCaMP6f, which can resolve single AP in neurons if they are separated by 50ms. However the GCaMP6f has a much lower affinity for Ca^{2+} with a K_d of 375nM, making it less sensitive for Ca^{2+} transients (Table 1) (Chen et al., 2013; Nakai et al., 2001).

The GECIS has also been applied to study pancreatic β-cells. Specifically, since insulin secretion involves influx of calcium, GECIs can be used as a proxy to study β-cell function. Indeed, our laboratory has developed a zebrafish transgenic line expressing GCaMP6s under the *insulin* promoter, which allows real-time visualization of β-cell influx of calcium (Janjuha et al., 2018; Singh et al., 2017).

In addition to the GCaMP system, a new generation of Red fluorescent protein (RFP) derived GECIs have been created, including the JRCaMP, JRGECO and K-GECO families. The red GECIs have the inherent advantage of using longer wavelengths than the green GECIs, which translates into lower phototoxicity and deeper light penetration in tissues. They can also allow for multiple color imaging when combined with blue, cyan and green fluorophores. The red GECIs follow a similar design to the GCaMP family: in the C-terminus the circularly permuted red fluorescent protein is fused to calmodulin (CAM) and in the N-terminus they are fused to the M13 peptide from myosin light-chain kinase (Akerboom et al., 2013; Dana et al., 2016; Shen et al., 2018; Zhao et al., 2011).

Introduction

The jRGECO family uses as a template the circularly permuted mApple, which derives from Ds-Red isolated from the mushroom coral *Discosoma sp.* The JRGECO family of red GECIs has one of the most sensitive Red GECI reported to date: jRGECO1a, which presents a dynamic range of ~11 (F_{max}/F_{min}) and temporal resolution for a single AP in neurons of ~330ms (Table 1). However, the jRGECO family exhibits photoswitching under green-blue illumination (λ≤488). This particularity renders the jRGECO1a incompatible with multicolor imaging where blue-green (λ ≤ 488nm) illumination is necessary (Dana et al., 2016).

The JRCaMP and K-GECO families derives from circularly permuted mRuby and FusionRed fluorescent proteins. These two RFPs proteins were isolated from the bubble-tip anemone *Entacmaea quadricolor* (Akerboom et al., 2013; Dana et al., 2016; Shen et al., 2018). The jRCaMP1a presents a low dynamic range of ~3 (F_{max}/F_{min}) and temporal resolution for a single AP in neurons of ~500ms. Its advantage over jRGECO1a is that it does not suffer from photoswitching under blue illumination. The K-GECO1 presents a dynamic range of ~12 (F_{max}/F_{min}), however, under strong blue illumination (λ=488, 6.13 W/cm^2), it can present up to a ~20% increase in red fluorescence. Unfortunately, the temporal resolution for a single AP in neurons was not reported, but it was mentioned by the authors that it is similar to that of jRGECO1a (~330ms) (Table 1) (Akerboom et al., 2013; Dana et al., 2016; Shen et al., 2018; Zhao et al., 2011). So far, the equilibrium between multicolor imaging and dynamic range is probably the best with the K-GECO family (Table 1).

Table 1. General properties of commonly used GECIs.

	GCaMP6s[1]	GCaMP6f[1]	jRCaMP1a[2]	jRGECO1a[2]	K-GECO1[3]
Excitation peak (λ) 1p/2p	488/925	488/925	570/1140	561/1140	565/1140
Emission peak (λ)	515	515	600	600	590
Dynamic range ($\Delta F/F_0$) at 160 AP)	1680±48%	1314±56%	160 ± 25%	N.R.	N.R.
Temporal resolution for single AP	100–150 ms	50–75 ms	500 ± 45 ms	330 ± 16 ms	N.R.
$\Delta F/F_0$ per single action potential	23 ± 1.9%	19 ± 2.8%	15%	27%	26%

($\Delta F/F_0$) per 10 action potential	450%	340%	90%	156%	106%
dynamic range of purified sensor (F_{max}/F_{min})	63.2 ± 3.1	51.8±2.8	3.2± 0.1	11.6 ± 0.4	~12
Ca^{2+} k_d	144 nM	375 nM	214 nM	148 nM	165 nM

[1]Values obtain from Chen, *et al.* 2013

[2]Values obtain from Dana, *et al.* 2006

[3]Values obtain from Shen, *et al.* 2018

N.R. not reported.

1.8. Genetically-encoded optogenetic actuators

The optogenetic control of individual β-cells within the pancreas *in vivo* with high temporal precision would allow us to explore and interrogate how the β-cell coordination is achieved. Optogenetics, or "light-driven" actuators, integrates genetic engineering, microscopy and electrophysiology in order to allow functional interrogation with high temporal and spatial precision. This allows for precise cellular interrogation, where pharmacological or electrical methods cannot be applied.

Opsins are involved in light sensing, and one of the first reports in phototaxis dates back to more than 100 years ago (Mast, 1916). However, the relationship between rhodopsin and cation currents was not observed until 1991, when Harz *et al.* reported that flashes of light in *Chlamydomonas reinhardtii* cells produced cation currents. This led Harz to suggest that channelrhodopsins could depolarize membranes (Harz and Hegemann, 1991). Then, by expressing the channelrhodopsin-1 and 2 (ChR1 and ChR2) from *Chlamydomonas reinhardtii* in HEK cells and *Xenopus* oocytes, Nagel *et al*. showed that these rhodopsins are indeed light-gated channels capable of depolarizing the cells upon light illumination (Nagel et al., 2002; Nagel et al., 2003). This was soon exploited in neurobiology and Boyden *et al.* were the first to show that ChR2 can drive neurons spiking and synaptic transmission upon blue light illumination (Boyden et al., 2005).

One of the most sensitive and blue shifted channelrhodopsins

(ChR) was identified by *de novo* sequencing in plant genomes: Hochbaum, *et al.* characterized the blue shifted ChR from *Scherffelia dubia* and termed it CheRiff. The CheRiff is able to produce photocurrents of 1nA (enough to produce 1AP) with illuminations as dim as 22 mW/cm^2, which is 9-fold lower than required for ChR2 (Hochbaum et al., 2014; Lin, 2011; Mattis et al., 2011). The CheRiff system combines several desirable characteristics, such as high light sensitivity, large phothocurrents and optical orthogonality for red-light illumination (no activation upon illumination with λ>560nm) (Table 2).

The optogenetic activation of β-cells and their simultaneous recording of their calcium dynamics, would be an excellent system to study β-cells coordination *in vivo*. Unfortunately, most of the channelrhodopsins are activated under blue illumination, including the well characterized ChR2 and CheRiff, which have their maximum spectrum activation at ≈460-470 nm. Thus, due to the wavelength overlap for the activation of ChR2 or CheRiff and the excitation of GCaMP, their combination is not possible. Yet, the discovery of the red-light channelrhodopsin from *Chlamydomonas noctigama* (Chrimson) with a maximum spectrum activation at ≈590 nm light, i.e. 45 nm more red-shifted than any other channelrhodopsin, would theoretically allow reversible and temporal activation of β-cells while recording Ca^{2+} activity using the calcium sensor GCaMP (Table 2) (Oda et al., 2018).

In parallel, the light-sensitive archaeal inhibitory chloride pump halorhodopsin (NpHR) has been developed and successfully applied for optical manipulation of neuronal activity (Nagel et al., 2003; Zhang et al., 2007). The eNpHR3.0 has its maximum spectrum activation at ≈589 nm light and its activation can robustly inhibit neuronal membrane depolarization (Table 2). The NpHR has the advantage that it can be combined together with the GCaMP sensor, allowing to simultaneously record Ca^{2+} influx while inhibiting membrane depolarization. This means that it is possible to reversibly silence individual β-cells while recording the islet's Ca^{2+} activity.

Since the β-cells require depolarization of the membrane to elicit insulin secretion both optogenetic activators (ChR2) and inhibitors

(NpHR) have been expressed in rodent β-cells to successfully interrogate β-cells *in vitro* (Johnston et al., 2016; Reinbothe et al., 2014). If it were possible to use optogenetics *in vivo* for functional β-cell interrogation, new venues would be open to evaluate functional heterogeneity in normal and diabetic conditions.

Table 2. General properties of commonly used optogenetic actuators.

	ChR2[1]	**CheRiff[2]**	**ChRimsonR[3]**	**eNpHR3.0[4]**
Specie	*Chlamydomonas reinhardtii*	*Scherffelia dubia*	*Chlamydomonas noctigama*	*Natronomonas pharaonis*
Excitation peak (λ)	470nm	460nm	590nm	589nm
Reported conditions: λ and light intensity	470nm, 19.8 mW/mm^2	488nm, 500mW/cm^2	625 nm, 3.14 mW/mm^2	593 nm, 21.7 mW/mm^2
Light sensitivity/EC50	~11 mW/cm^2	~22 mW/cm^2	N.R.	N.R.
Peak current	~0.7nA	~2nA	~0.7nA	~0.74nA (outward)
Desensitization (steady-state current over peak current)	~0.22	~0.665	~0.58	N.R.
Opening rate $t_{(El'tseva\ et\ al.)}$	~1.21ms	~4.5ms	~9ms	~6.1ms
Closing rate $t_{(El'tseva\ et\ al.)}$	~13.5ms	~16ms	~15.8ms	~6.9ms
Ion specificity	Cations	Cations	Cations	Cl-

[1]Values obtain from Boyden, *et al*. 2005

[2]Values obtain from Hochbaum, *et al.* 2015

[3]Values obtain from Oda, *et al.* 2018

[4]Values obtain from F. Zhang *et al.* 2007

1.9. Models to study *In vivo* β-cell coordination

In order to study β-cell physiology, the microenvironment should be preserved. Pancreatic tissue slices is a methodology which preserves the β-cell microenvironment. This methodology avoids the isolation of the islets, which provokes a substantial chemical and mechanical stress in the

islet cells and is known to produce changes in cell physiology. Pancreatic tissue slices also preserve the morphology of the pancreas, thereby conserving the immediate microenvironment of the β-cells (Marciniak et al., 2014). This methodology has been successfully applied to study β-cell interaction with other cells, such as islet-resident macrophages (Weitz et al., 2018). Although the immediate islet environment is preserved, the blood flow and neuronal input are missing from these preparations, and the slices decay in about 4-7 days (Marciniak et al., 2013).

Imaging of the islet within the intact pancreas *in vivo* in mice is challenging and requires exteriorization of the whole organ. A powerful alternative for non-invasive *in vivo* imaging is to transplant islets into the anterior chamber of the eye (AC) of mice (Speier et al., 2008). Transplanted islets into the AC of mice mimics an *in vivo* environment, allowing longitudinal studies and Ca^{2+} imaging by fluorescent probes as a proxy for β-cell function and activity (Chen et al., 2016). Nevertheless, the process of islet revascularization can take several weeks after islet transplantation into the AC of mice. Also, the process of revascularization is postulated to be affected by the age of the donor: Cohrs *et al*. recently reported that aged islets from mouse (1-year-old), pig (3- to 5-year-old) and human (>19-year-old) had a significant decrease in the vessel fraction compared to the pancreatic endogenous vessel network found *in vivo,* after being transplanted into the AC of mice. Notably, they found that islets transplanted into the AC of mice of young pigs (<18-month-old) and mouse (12<weeks-old) have higher potential to rebuild their vascular network reaching similar values of vascular fraction compared to *in vivo* (Cohrs et al., 2017). Thus, preserving the original native environment, where the β-cells are properly vascularized and in constant communication with the metabolic state of the organism, and achieving *in vivo* singe-cell imaging resolution remain very challenging and time consuming.

To overcome these limitations, we used the zebrafish larvae as a window into β-cell activity *in vivo*. Zebrafish is an excellent model organism due to the relatively easy genetic manipulation, ability to regenerate almost every organ, high fecundity and the optical transparency at early stages of development. Also, during zebrafish

development, the yolk serves as a reservoir of nutrients and is metabolized to support grow. The zebrafish larvae present a peak in free glucose levels at around 5 days post fertilization (dpf), in comparison to earlier stages (<3dpf), due to increased gluconeogenesis as their yolk deposits deplete. This suggests that at 5dpf, the β-cells are exposed to circulating free glucose (Gut et al., 2013). Also, at 5 dpf, the β-cells of the zebrafish primary islet express mature markers such as *Ucn3l* and show *in vitro* response to glucose in the physiological range (Singh et al., 2017). Similar to the mouse islets, the zebrafish β-cells localize in the core of the islet, whereas most α-cells allocate to the periphery, although some α-cells can clearly be seen dispersed in the center of the islet, reminiscing the situation in human islets. The zebrafish islet is densely vascularized and innervated by neurons (Yang et al., 2018). Furthermore, genetic ablation of β-cells in this stage leads to glucose intolerance. In addition, the zebrafish shows conserved responses to glucose-lowering agents such as insulin or the antidiabetic drug metformin, showing that at 5dpf, the primary islet is glucose responsive and systemically connected organ controlling glucose levels. These special characteristics make the zebrafish a unique model to study islet β-cell activity *in vivo* (Eames et al., 2010; Nath et al., 2015)

2. *In vivo* β-cell Ca^{2+} dynamics

Sections of this chapter have been adapted from the following publication:

Victoria Salem, Luis Delgadillo Silva, Kinga Suba, Eleni Georgiadou, S. Neda Mousavy Gharavy, Nadeem Akhtar, Aldara Martin-Alonso, David C. A. Gaboriau, Stephen M. Rothery, Theodoros Stylianides, Gaelle Carrat, Timothy J. Pullen, Sumeet Pal Singh, David J. Hodson, Isabelle Leclerc, A. M. James Shapiro, Piero Marchetti, Linford J. B. Briant, Walter Distaso, Nikolay Ninov & Guy A. Rutter (2019). Leader β-cells coordinate Ca^{2+} dynamics across pancreatic islets *in vivo*. Nature Metabolism.

2.1. β-cells present endogenous Ca^{2+} spikes *in vivo*, which are not present *ex vivo*

Our group has recently characterized the functionality of zebrafish β-cell *in vitro* using the genetically-encoded calcium indicator GCaMP6s. Singh *et al*. showed that isolated islets from transgenic *Tg(ins:GCaMP6s)* zebrafish larvae exhibit Ca^{2+} influx upon glucose addition in a physiological relevant range (Singh et al., 2017). Due to the optical transparency of the zebrafish larvae at early stages of development, we hypothesized that they could serve as a unique window into β-cell activity *in vivo*. Thus, in order to investigate the islet β-cell activity *in vivo*, we developed a high-resolution, high-speed confocal protocol for β-cell Ca^{2+} imaging *in vivo*, using transgenic *Tg(ins:GCaMP6s)* zebrafish larvae expressing GCaMP6s under the insulin promoter.

To explore the Ca^{2+} dynamics of β-cells in their native environment with single-cell resolution, we employed the previously published transgenic lines *Tg(ins:GCaMP6s)* and the nuclear β-cell marker *Tg(ins:cdt1-mCherry*), which labels 86 ± 6.6% (mean ± SD) (*n=5* islets) of all β-cells at 4.5 days post fertilization (dpf) (Ninov et al., 2013; Singh et al., 2017). Anesthetized 4.5 dpf larvae were mounted in 1% low melting agarose. Live imaging was performed on an inverted laser scanning

confocal system. Previous reports in isolated islets had shown that β-cells do not present significant activity unless they are stimulated with glucose (Singh et al., 2017). Intriguingly, the cumulative fluorescent trace of the whole islet shows periods of high and low activity as measured using GCaMP fluorescence (Figure 3). In other words we found endogenous β-cell Ca^{2+} activity not previously observed *in vitro* (Figure 3c). Furthermore, the single-cell quantification of the GCaMP signal revealed that individual β-cells present different levels of activity over time, as shown by the changes in GCaMP signal for single-cells (Figure 3c´).

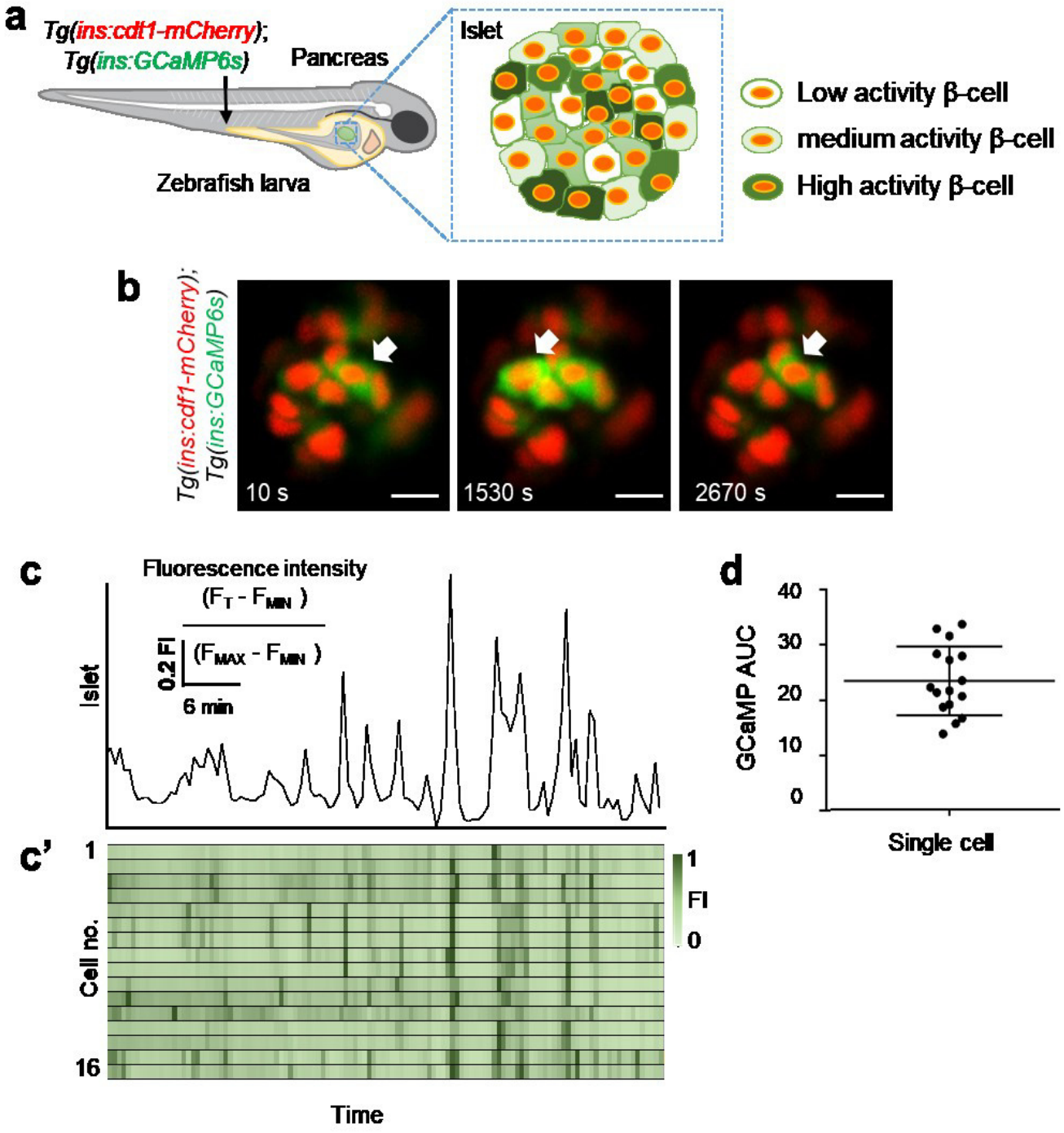

Figure 3. β-cell present endogenous spontaneous Ca^{2+} transients in the living zebrafish. a. Cartoon representing a transgenic zebrafish larva expressing the genetically-encoded Ca^{2+} indicator GCaMP6s (green) and the nuclear marker cdt1-mCherry (red) under the insulin promoter. GCaMP6s allows the examination of glucose-induced Ca^{2+}-influx in β-cells reported by changes in the green fluorescence in a Ca^{2+} concentration-dependent fashion. **b.** Snapshots from time-lapse recordings of the primary islet from a

larva mounted in agarose and imaged using a confocal microscope every 30 s. Arrows indicate cells exhibiting an increase in GCaMP6 signal at a given time. The images represent maximum intensity projections. **c.** The top panel shows the trace of cumulative normalized fluorescent intensity over time for the cells shown in b. **c'.** Normalized fluorescence intensity over time for each cell. Each cell is represented by a square. The normalized GCaMP6 fluorescence is displayed as a heat-map, showing the degree of cell activity in individual cells, **d.** Graph showing the activity of individual cells. The graph depicts the GCaMP6 area under covering the whole imaging recording of the islet shown in b for individual cells. Each cell is represented by a dot. Scale bars = 10 μm.

2.2. Insulin injection reduces endogenous β-cell Ca^{2+} activity

Increases in glucose levels in the blood trigger cytoplasmic Ca^{2+} influx and promote insulin secretion from β-cells. As we detected endogenous Ca^{2+} oscillations in β-cell *in vivo*, we wondered if these Ca^{2+} spikes occur in response to the free circulating glucose present in the zebrafish larvae at this stage (Gut et al., 2013). To test this possibility, we developed a new protocol for simultaneous live Ca^{2+} imaging and pericardial injection of insulin (Figure 4). After insulin administration, the Ca^{2+} spikes were promptly abrogated (Figure 4a-c). We measured the glucose levels after insulin injection, corroborating the lowering of the free glucose in the zebrafish larvae. This suggests that the *in vivo* Ca^{2+} oscillations are influenced by glucose levels in the larvae.

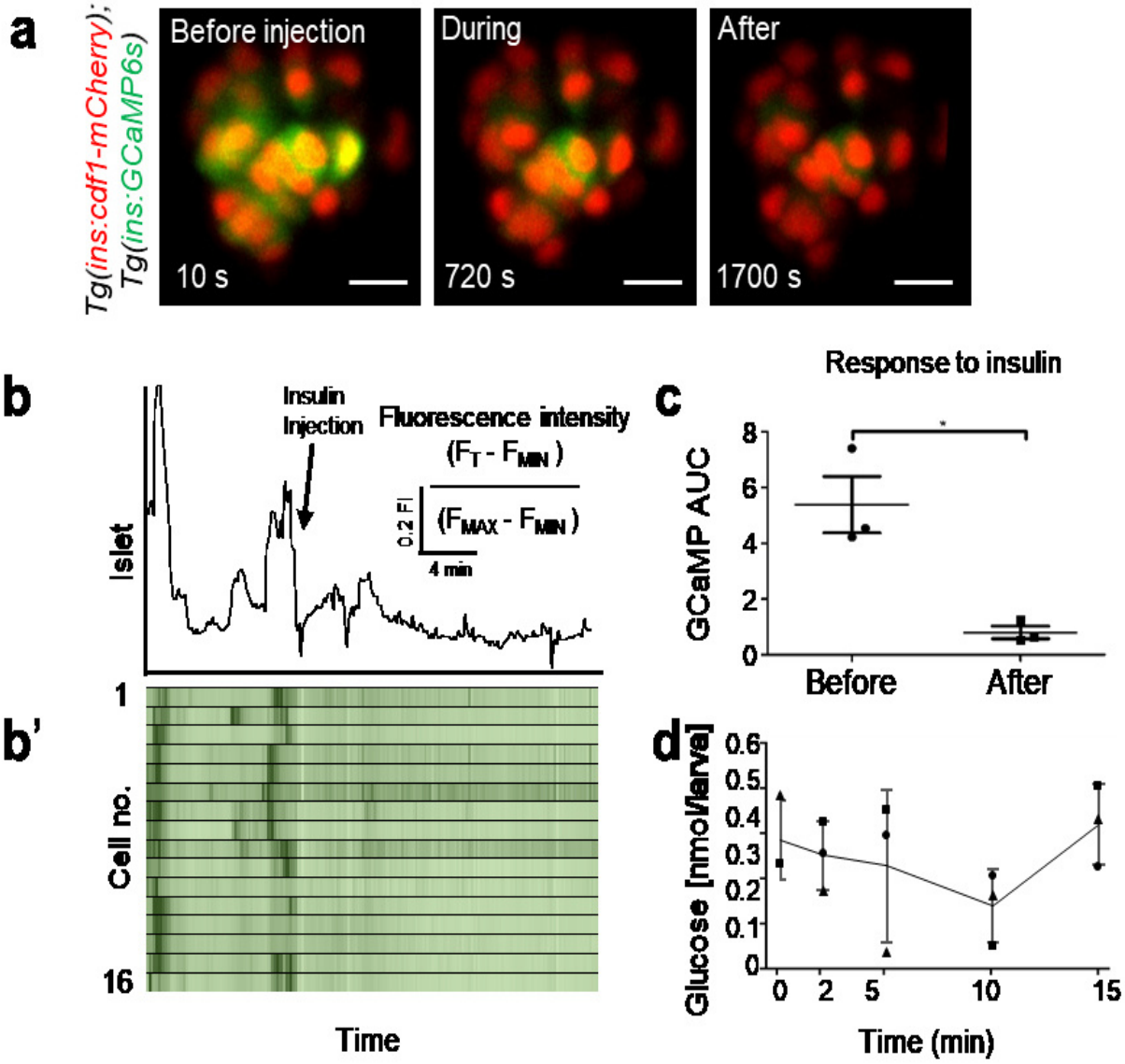

Figure 4. ***In vivo*** **β-cell endogenous Ca^{2+} transients are suppressed by insulin. a.** Snapshots from time-lapse recordings of the primary islet imaged before, during and after the intra-cardiac injection of 5nL of insulin (100 insulin-units/ml). The imaging and insulin administration were performed simultaneously with a frame rate acquisition every 15 s. **b.** A trace of cumulative normalized fluorescent intensity over time for the cells shown in A. The black arrow marks the instance of insulin injection1q1. **b'.** Normalized fluorescence intensity over time for each individual cell. (*n*=10, not graphically represented here) **c.** Quantification of the islet activity before and after the insulin injection. The graph depicts the GCaMP6 area under the curve covering 100 seconds before and 100 seconds after the insulin injection. The injection of insulin led to a reduction in GCAMP fluorescence intensity

(*n*=3 animals, paired two-tail t-test, P= 0,0476). Data are means ± SD. **f.** Changes in measured free glucose concentration in larvae following insulin injection as in **a**. Each dot represents a pool of 10 injected larvae. (*n*=3 for each time point, one-tailed ANOVA (with Tukey's multiple comparisons test), P=0,3587). Data are means ± SD. Scale bars = 10 μm.

2.3. Pharmacological inhibition of β-cell Ca^{2+} spikes interferes with glucose control

We observed that lowering the glucose levels via insulin administration into the zebrafish larvae decreases the calcium oscillations in the β-cell *in vivo* with concomitant lowering of glucose levels. This suggested that calcium oscillations are induced by the free glucose levels present in the zebrafish larvae (Gut et al., 2013). However, it is not clear if the calcium spikes contribute to glucose control or not.

To test if the Ca^{2+} spikes detected *in vivo* are necessary for glucose control, we blocked the β-cell membrane depolarization by using the well-known K_{ATP} channel opener diazoxide (Mariot et al., 1998). As previously reported, a 12 hours incubation of zebrafish larvae in 300μM diazoxide caused a significant increase in free glucose levels (Figure 5 a-b) (Li et al., 2014). In addition, whereas glucose incubation (130mM) alone did not rise significantly the glucose levels of zebrafish larvae, the co-incubation of glucose and diazoxide led to a ~3 fold increase of free glucose levels as compared to the DMSO controls (Figure 5b). To corroborate that diazoxide inhibits the endogenous calcium spikes, we performed live imaging following 12hrs of incubation in diazoxide. We detected GCaMP signal changes in β-cells over time in zebrafish incubated with diazoxide. However, Ca^{2+} spikes in β-cells were disturbed as compared to the controls. While in the controls there are clear spikes of high and low GCaMP signal, in the fluorescent traces of diazoxide treated zebrafish, we detected small, if not absent, spikes in fluorescence (Figure 5c-e). Altogether, these results suggest that the endogenous calcium oscillations are associated with proper glucose control in zebrafish.

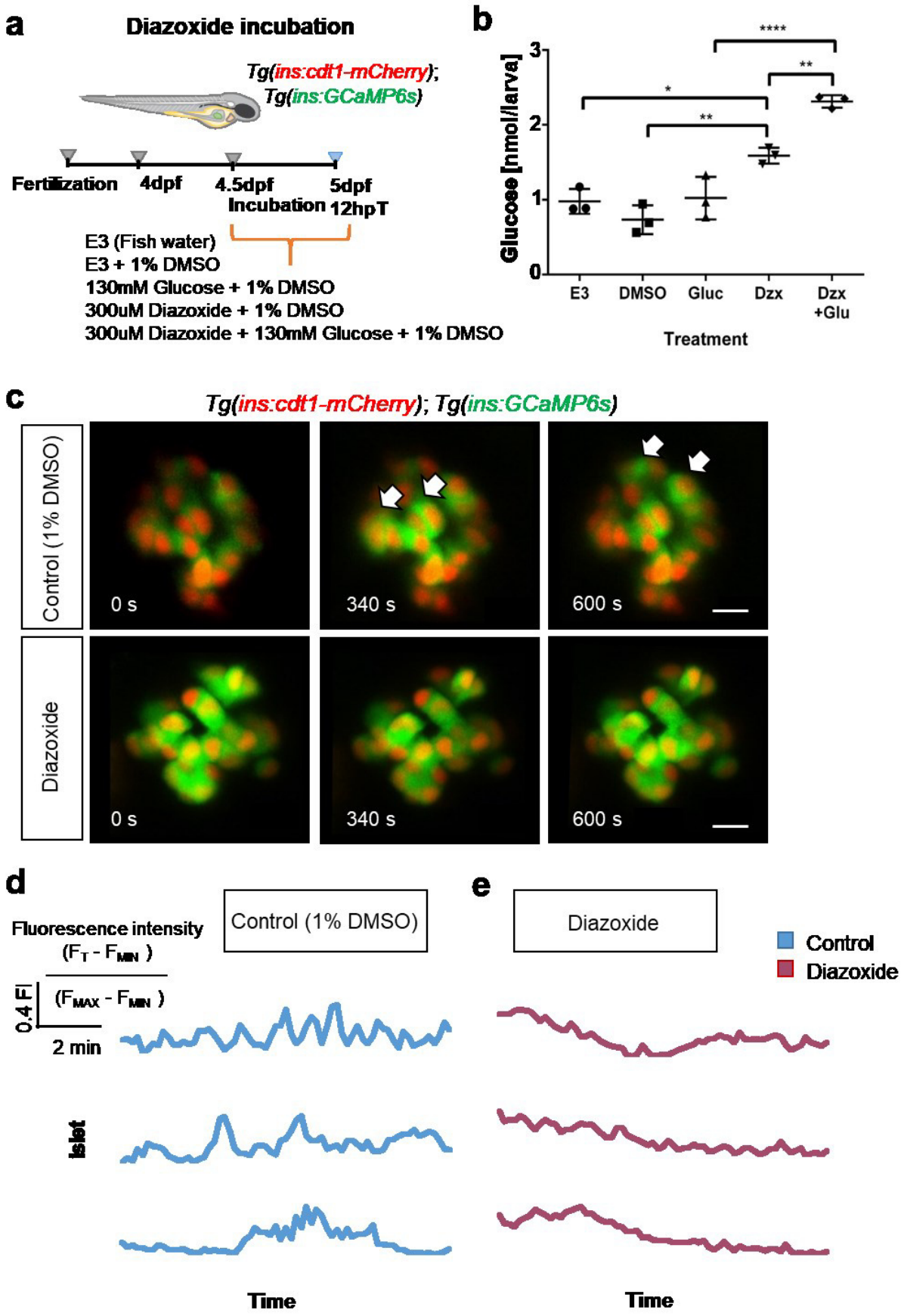
a
Diazoxide incubation
Tg(ins:cdt1-mCherry);
Tg(ins:GCaMP6s)
Fertilization
4dpf
4.5dpf
5dpf
Incubation 12hpT
E3 (Fish water)
E3 + 1% DMSO
130mM Glucose + 1% DMSO
300uM Diazoxide + 1% DMSO
300uM Diazoxide + 130mM Glucose + 1% DMSO
b
Glucose [nmol/larva]
E3
DMSO
Gluc
Dzx
Dzx +Glu
Treatment
c
Tg(ins:cdt1-mCherry); Tg(ins:GCaMP6s)
Control (1% DMSO)
Diazoxide
0 s
340 s
600 s
d
Fluorescence intensity
(FT - FMIN)
(FMAX - FMIN)
0.4 FI
2 min
Control (1% DMSO)
Islet
Time
e
Diazoxide
Control
Diazoxide
Time

(Figure text is in the next page)

Figure 5. Pharmacological inhibition of β-cell membrane depolarization. a. Cartoon model showing the design for testing the effects of β-cell membrane depolarization blockage by diazoxide in zebrafish larvae. The test consisted of incubating the larvae in 5 different solutions: E3 (Fish water), E3 + 1% DMSO as control, 130mM Glucose + 1% DMSO, 300μM Diazoxide + 1% DMSO and 300μM Diazoxide + 130mM Glucose + 1% DMSO. The larvae were incubating for 12 hrs in each solution at 4.5 dpf and the glucose was measured at 5 dpf. **b.** Plot showing glucose concentration for each condition. Glucose levels were similar in the E3 and DMSO treated fish. 130mM glucose incubation did not increase significantly the glucose levels in zebrafish as compare to the controls. Diazoxide incubation alone was sufficient to increase significantly the glucose levels in the larvae. The co-incubation of 130mM glucose and diazoxide led to a ~ 3-fold increase in free glucose compared to DMSO controls. **c.** Snapshots from time-lapse recordings of the primary islet imaged after 12hrs diazoxide incubation and DMSO control. The imaging was performed with a frame rate acquisition every 10 s. **d.** Traces of cumulative normalized fluorescent intensity over time for three different islets for DMSO controls and diazoxide incubated fish. The fluorescent traces shown on top correspond to the islets shown in c.

2.4 Transient blood flow interruption decreases β-cell calcium spikes

Previous studies on islet vasculature in zebrafish reported that at 6 days post fertilization (dpf), the zebrafish islet presents endothelial cells but no blood flow, suggesting that systemic insulin action might not be present (Moss et al., 2013). This would argue against the possibility that zebrafish β-cells can sense the systemic glucose levels through the blood flow. Hence, the endogenous calcium spikes might derive most probably from glucose diffusion. To address this question, we decided to explore if the β-cells in larvae are perfused by blood. For this purpose, we performed live imaging using triple transgenic *Tg(ins:GCaMP6s);Tg(ins:cdt1-mCherry);Tg(gata1a:DsRed) larvae in* which the gata1 promoter expresses DsRed in red blood cells (erythroid lineage). Thus, in order to capture the blood flow, we focused on a single

plane and the videos were recorded at a frame rate of 1 frame/155 milliseconds (~6.4 Hz). Contrary to the previous literature, we detected active blood flow through the islet in our recordings (*n*=10) (Figure 6a). Thus, the fact that we detected active blood flow, suggest that beta-cells are systemically connected and that the endogenous Ca^{2+} spikes in β-cells might be in response to glucose changes.

To determine if the blood flow is influencing the endogenous Ca^{2+} spikes in the β-cells, we temporally stopped the blood flow in the whole larvae while performing Ca^{2+} imaging. By using a blunt capillary, we exerted a direct pressure over the zebrafish heart; this led to the blockage of blood flow (Figure 6b). As expected, Ca^{2+} dynamics were decreased after a transient suppression of blood flow and recovered after heart release (Figure 6d).

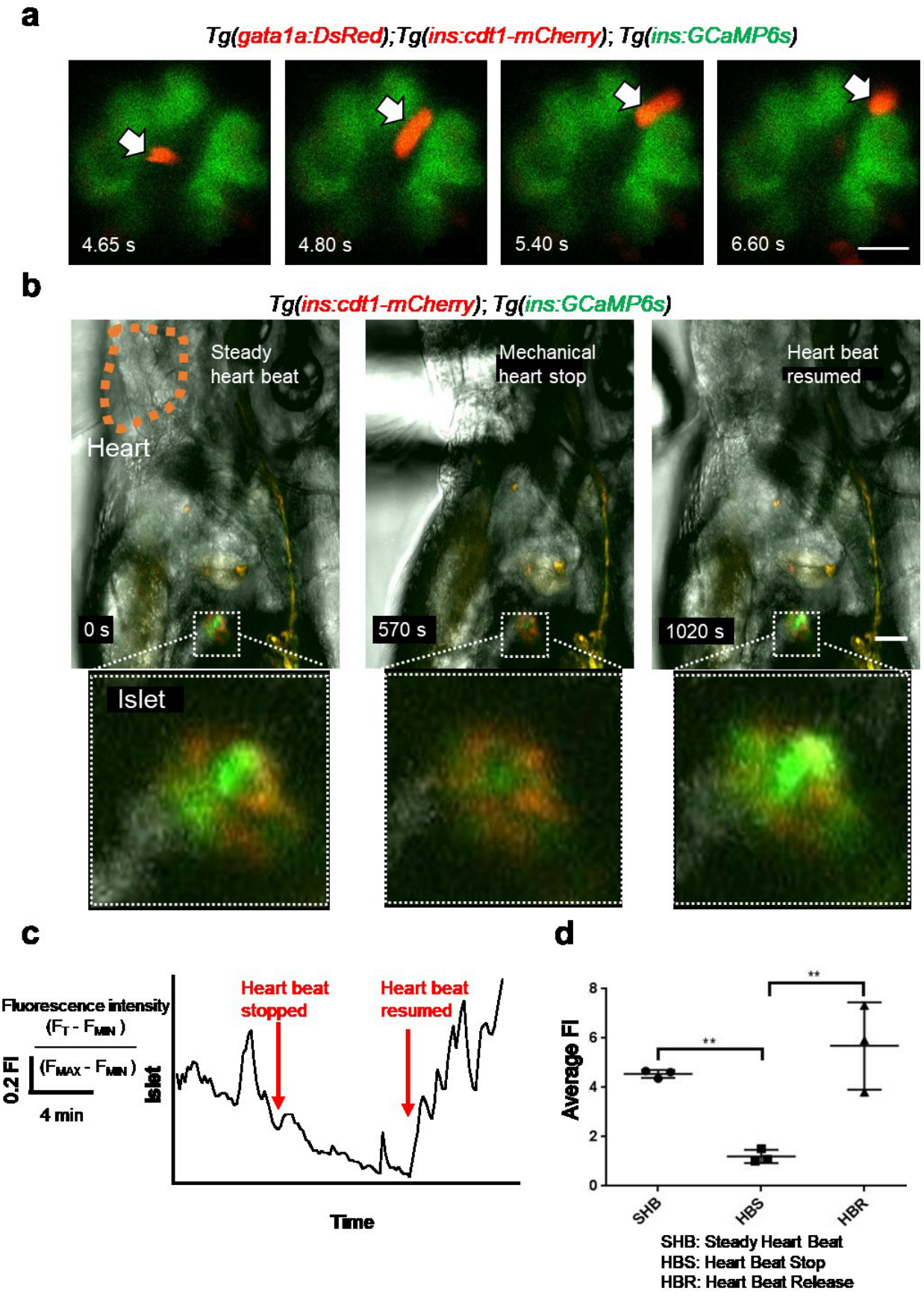

(Figure text is in the next page)

Figure 6. Blood flow interruption by mechanical controlled heart blockage. a. Snapshots from time-lapse recordings of the zebrafish triple transgenic islet *Tg(ins:GCaMP6s);Tg(ins:cdt1-mCherry);Tg(gata1a:DsRed)* imaged at 1 frame/155 milliseconds (*n*=10). Arrows shows a blood cell circulating through the islet. **b.** Snapshots from time-lapse recordings of the larvae, and zoom of the primary islet imaged before, during and after the mechanical heart stopping. The heart blockage and live imaging were performed simultaneously with a frame rate acquisition every 10 s. **c.** A trace of cumulative normalized fluorescent intensity over time for the islet shown in b. The red arrows mark the instance of heart blockage and heart release. **d.** Quantification of the islet activity before, during and after the heart blockage. The graph depicts the GCaMP6 average area under the curve covering 100 seconds before, 100 seconds during and 100 seconds after the heart blockage. The heart stopping decreased the GCAMP fluorescence intensity (*n*=3 animals, paired two-tail t-test, P= 0.0476).

2.5 Glucose bolus leads to a synchronous response of β-cells

The observations that stopping the blood flow or lowering the glucose levels via insulin injection decrease Ca^{2+} spikes of β-cell *in vivo* suggested that glucose levels and β-cell Ca^{2+} activity might be correlated. Therefore, we tested the impact of increasing glucose in zebrafish circulation to β-cell Ca^{2+} activity. To this end, we conducted live imaging and simultaneous pericardial glucose injection in the double transgenic *Tg(ins:GCaMP6s);Tg(ins:cdt1-mCherry)* larvae. This maneuver allows rapid entry of the sugar into the circulation (Figure 7a). The glucose injection led to a rapid (within ~20-50s) and statistically significant increase in cytosolic Ca^{2+} concentrations in β-cells across the islet, as revealed by the comparison of the changes in GCaMP fluorescence before and after the glucose injection (Figure 7b-c). At a single-cell level, a strong coordinated response is detected in all the cells imaged, with the GCaMP6 signal increasing to more than 25% above baseline during the whole recording (Figure 7b'). This activity corresponded to the time-dependent increases in whole animal glucose concentrations assessed separately after the glucose injection (Figure 7d).

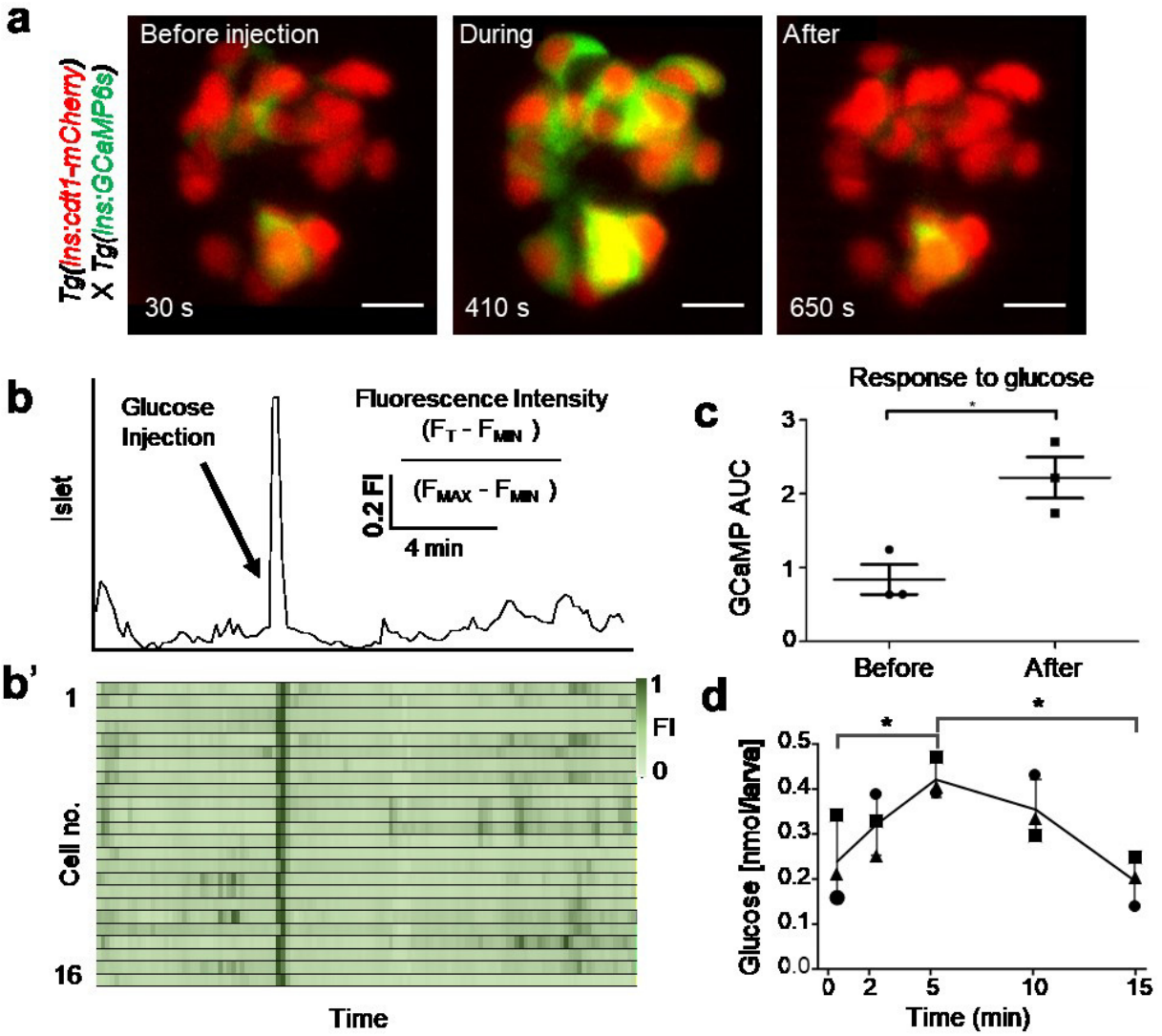

Figure 7. Glucose-stimulated Ca^{2+} influx imaged *in vivo* in zebrafish embryos. a. Snapshots from of an islet imaged before, during and after the intra-cardiac injection of 5 nL of 25 mM glucose solution. The images represent maximum intensity projections from the 3D volumes. Imaging and glucose stimulation were performed simultaneously. Note the near-synchronous increase in GCaMP6 fluorescence intensity across all the β cells in the islet upon glucose injection. **b.** A trace showing cumulative normalized fluorescent intensity over time for the cells shown in a. The black arrow marks the instance of the glucose injection. **b'**. Normalized fluorescence intensity over time for each individual cell. Each cell is represented by a. The normalized GCaMP6 fluorescence is displayed as a heat-map, showing the degree of cell activity (n=10 animals, not graphically represented here). **c.** Quantification of the islet response to glucose stimulation. The graph depicts the GCaMP6 area under the curve covering 100 seconds before and 100 seconds after the

glucose stimulation (*n*=3, paired two tail t-test, P=0.0108, data are means ± SD). The injection of glucose led to a dramatic increase in GCaMP6 fluorescence intensity. **d.** Changes in measured free glucose concentration in larvae following glucose injection as in a. Each dot represents a pool of 10 injected larvae. (n=3 for each time point, one-tailed ANOVA (with Tukey's multiple comparisons test, P= 0.0488 for 0 vs. 5min and P= 0.0152 for 5 vs.15min). Data are means ± SD Scale bars = 10 μm.

3. Leader β-cells coordinates Ca^{2+} dynamics *in vivo*

Sections of this chapter have been adapted from the following publication:

Victoria Salem, Luis Delgadillo Silva, Kinga Suba, Eleni Georgiadou, S. Neda Mousavy Gharavy, Nadeem Akhtar, Aldara Martin-Alonso, David C. A. Gaboriau, Stephen M. Rothery, Theodoros Stylianides, Gaelle Carrat, Timothy J. Pullen, Sumeet Pal Singh, David J. Hodson, Isabelle Leclerc, A. M. James Shapiro, Piero Marchetti, Linford J. B. Briant, Walter Distaso, Nikolay Ninov & Guy A. Rutter (2019). Leader β-cells coordinate Ca^{2+} dynamics across pancreatic islets *in vivo*. Nature Metabolism.

3.1. High speed 2D and 3D imaging reveals "leader" β-cells

Pulsatile insulin secretion relies in synchronous β-cell activity. This pattern of synchronicity is responsible for proper first phase and second phase of insulin secretion (Head et al., 2012; Nadal et al., 1999). Particularly, *in vitro* studies have suggested that the coordinated behavior of the islet is achieved by a special subpopulation of β-cells, termed hub cells. The calcium activity of hub cells is reported to precede the rest of the β-cells (Johnston et al., 2016). Yet, it is unknown if the zebrafish islet exhibits β-cells that precede the activation of the rest of the β-cells. As we found that glucose injection in zebrafish larvae at relatively low acquisition speed (0.1Hz) triggers a synchronous Ca^{2+} response across the islet, we decided to explore in more detail whether this apparent synchronous response was initiated faster by some of the islet cells, or if all cells activated simultaneously. Thus, in order to properly monitor the time of response for each individual cell, we adapted our live imaging to record a single plane of the islet taking 3 frames per second while simultaneously performing glucose injections in the double transgenic *Tg(ins:GCaMP6s);Tg(ins:cdt1-mCherry)* larvae. At this speed of acquisition, the cumulative response of all the cells in plane showed a time delay (assessed as the time it takes to achieve a GCaMP6 signal increase greater than >25% above baseline) of 11.6s (11.6s ± 8s SD, *n*=5). We

also monitored the individual time of response for each cell. We found that one or two cells (1.5 cells ± 0.53 SD, *n*=8) would show first an increase in fluorescence upon glucose injection, while other cells would take longer to respond. The average difference in the time of response for individual cells taken between the first and the last cell to respond upon glucose-injection was 6.3s (6.3s ± 3.9s SD, *n*=5). We call the cells that are the first to respond to glucose injection "leaders" (Figure 8). Interestingly, the R-square (coefficient of determination) between the time of response for individual cells and their physical distance from the leader cell showed a mild positive correlation of an R^2 =0.57 (0.57 ± 0.2 SD *n*=5). These observations suggest that the islet response is initiated in the leader cells and is then followed by the rest of the β-cells.

The finding of the presence of first responder β-cells might point to a functional heterogeneity of β-cells. However, we cannot exclude the possibility that the differences in time of response might be due to other reasons, for example, due to different levels of GCaMP expression by individual cells. To test this possibility, we used double transgenic *Tg(neuroD1:GCaMP6f);Tg(ins:cdt1-mCherry)* larvae, and applied our Ca^{2+} imaging protocol (Samarut et al., 2018). The *neuroD1* promoter drives uniform expression of GCaMP6f in all the endocrine cells of the zebrafish pancreas. Since the GCaMP6f has a half-decay of ~140 ± 20 ms, we focused on a single plane and acquire 6 frames per second (150ms per frame). Thus, we were able to monitor the individual time of response for each cell. In this setup, we found that the cumulative time of response for all cells was 8.8s after glucose injection (8.8s ± 0.45s SD, *n*=3). Similar to the transgenic line *Tg(ins:GCaMP6s)*, we found that in each islet, one or two cells in plane would respond first to the glucose injection, while other cells would take longer to reach a GCaMP signal greater than 25%. We found that the average delay from the first cell to respond to the last one was 2.2s (2.2s ± 2.25s SD, *n*=3). The difference in time compared to our recordings using GCaMP6s (6.3s vs 2.2s) could be explained by the fact that GCaMP6f has a relatively lower Ca^{2+} affinity (375nM) in comparison to the GCaMP6s (144nM), and thereby, the GCaMP6f signal would increase when more than double of calcium is present in the cytosol of the cell, in comparison to the GCaMP6s. Theoretically, in the β-cells the GCaMP6f would need double of calcium

to show a fluorescence increase as compared to GCaMP6s. This difference in the sensitivity of the two sensors might explain the changes in the overall time of response. For the islet shown in figure 9, the analysis of time of response and the distance from the leader cell showed an R^2=0.9. Calculating the average R-square between the time of response for each individual cell to its physical distance from the leader cell for three distinct samples gave us an R^2=0.6 (0.6 ± 0.27 SD, *n*=3) (Figure 9). Thus, using two different promoters to drive GCaMP expression in β-cells, we found a mild positive correlation between the time of response of each cell and their distance to the leader β-cell. Importantly, both transgenic reporters showed the presence of leader cells, thereby, indicating that the presence of the leader cell is not the result of using the insulin promoter to drive the calcium reporter expression.

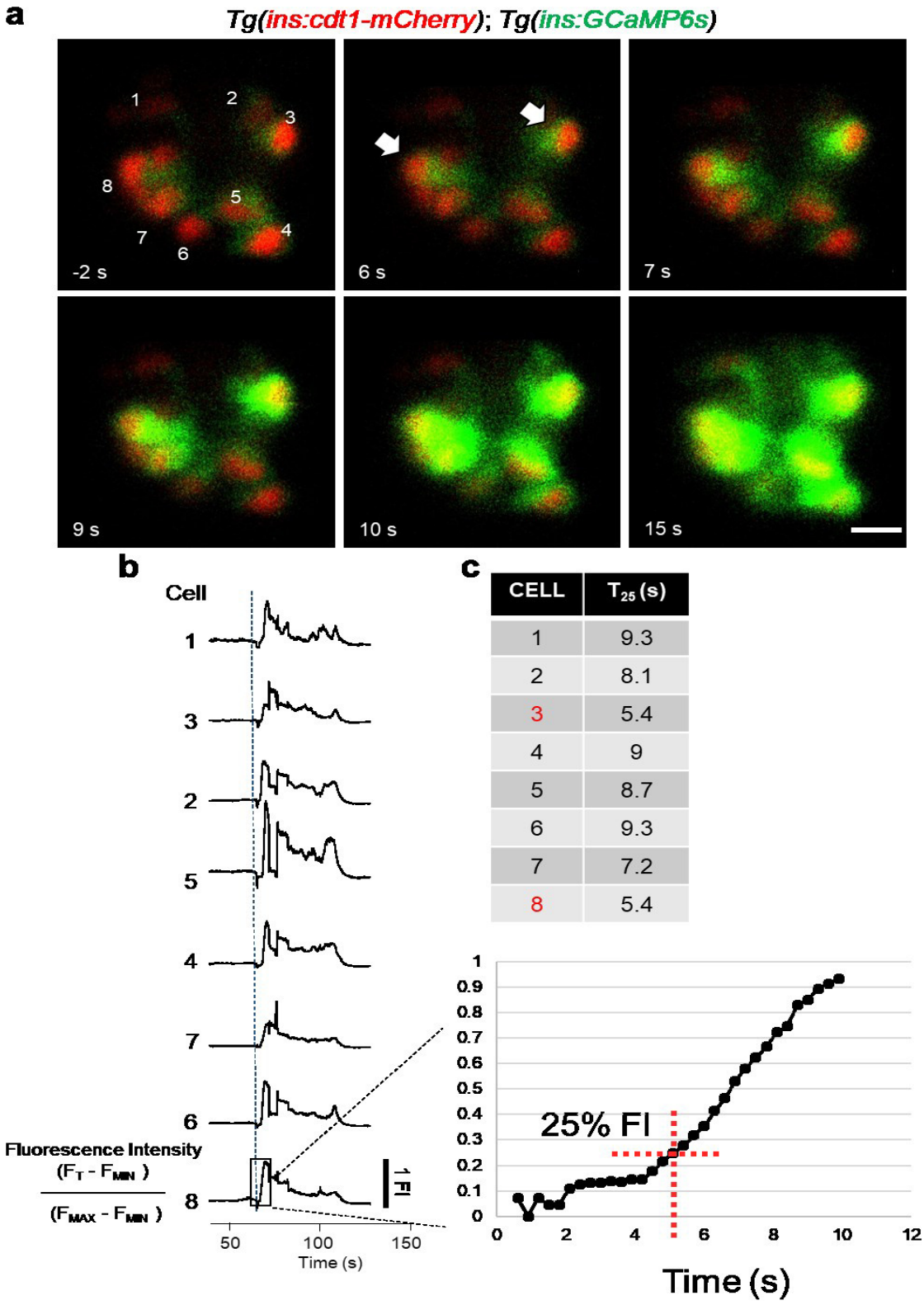

Figure 8. First responder β-cells are present in the zebrafish islet. a. Snapshots from time-lapse recordings of the primary islet from a larva at 1 frame / 300milliseconds. The

time indicates the relative time to the glucose injection. The white arrows show two β-cells that responded first to the glucose stimulus in terms of calcium influx, the next frames show the response of the other β-cells. **b.** Cumulative normalized fluorescent intensity over time for individual cells shown in “a”, also a zoom of the cell number 8 trace, which was one of the first cells to respond. **c.** table showing the time of response after the glucose injection with a rise of GCaMP6 signal >25% above baseline. In red the cells that responded first to the glucose injection.

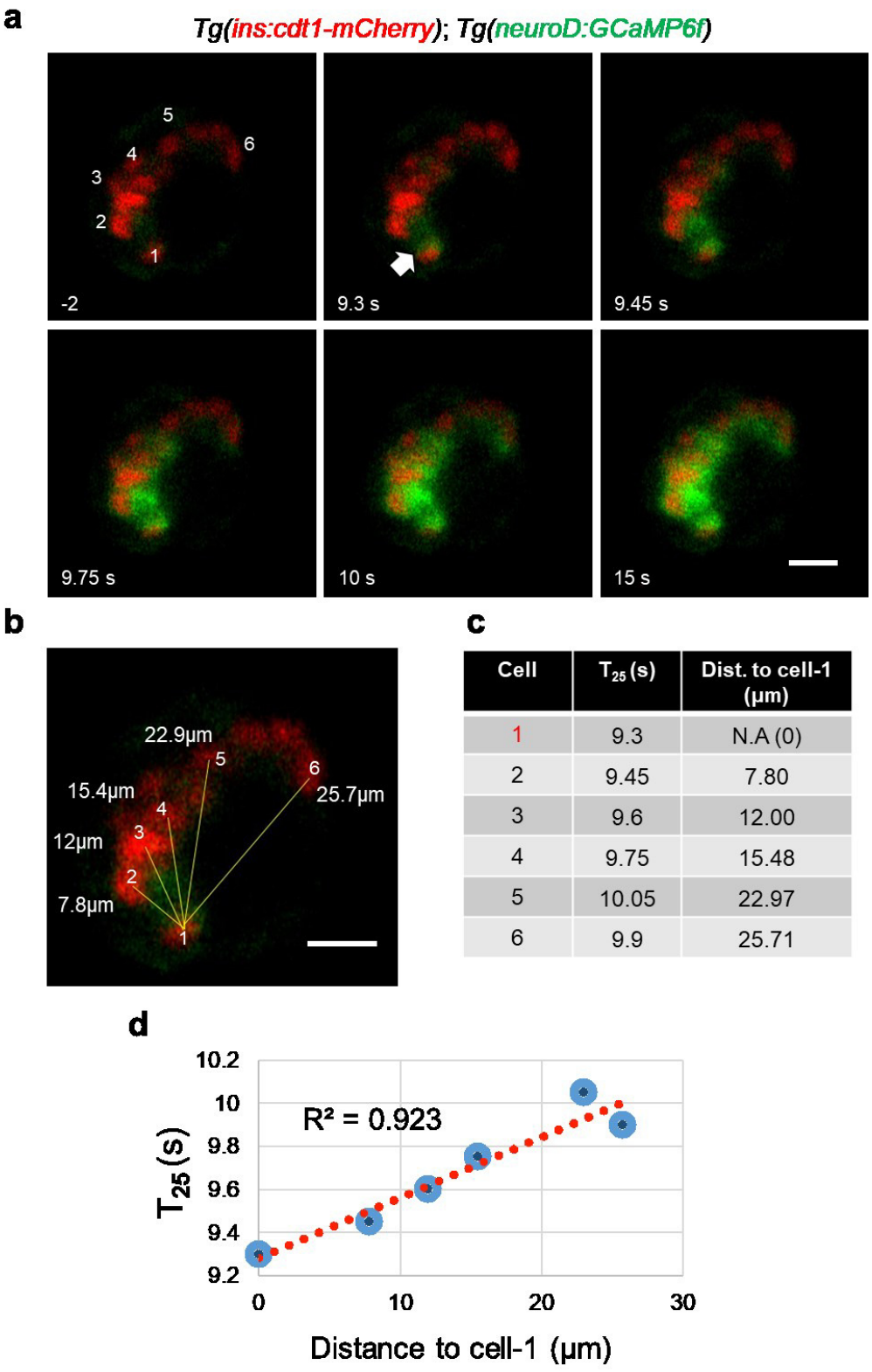

Figure 9. First responder β-cells are detected using GCaMP6f expressed under the *neuroD1* promoter. The *neuroD1* promoter labels with GCaMP6f all the endocrine cells

present in the islet and the cdt1-mCherry, labels the nuclei of individual β-cells. The Snapshots from time-lapse recordings of the primary islet from a larva at 1 frame / 150milliseconds. The time indicates the relative time to the glucose injection. The white arrow points to the a β-cell that responded first to the glucose stimulus. Scale bar = 10μm **b.** Distance measured from the nuclei of the first responder cell to the rest of the cells shown in "a" **c.** table showing the distance in micrometers to the first responder cell and the individual time of response after the glucose injection as the GCaMP6 signal >25% above baseline. **d.** Graph plotting the time of response to each cell vs the distance relative to the first cell to respond. The dotted line shows a linear regression and the associated R^2. Each dot represents one cell.

We found that the first responder β-cells are present in two different transgenic lines expressing Ca^{2+} reporters. This suggests that there might be a functional heterogeneity of β-cells. However, the delay in response might also reflect differences in glucose access among individual cells. To address how fast glucose distributes in the zebrafish islet, we performed an *in vivo* injection of the fluorescence glucose analogue 2-NBDG (2-(N-(7-Nitrobenz-2-oxa-1,3-diazol-4-yl)Amino)-2-Deoxyglucose). We conducted recording in a single plane of the islet, taking 6 frames per second (1 frame/150ms). In this setup, we found that the time it takes for the first cell to increase its normalized fluorescence intensity by 25% in comparison to the last one was <500ms (n=5). This implies that the diffusion rate through the islet can be as fast as 500ms and that the cells have comparable access to glucose (Figure 10a-d).

Next we tested if the 2D data is representative of the whole islet response in zebrafish. To this end, we applied fast confocal microscopy using a resonant scanner. The resonant scanner is a set of two galvanometric mirrors used to raster (line-scan) the sample, in X and Y positions at frequencies up to 12,000 Hz. This translates to scanning 12,000 lines per second, meaning that an image of 512px (lines) can be acquired in around 40ms. We achieved whole islet live-imaging at acquisition rate of 0.8Hz covering ~700μm^3, while applying our method for glucose injection. We resolved around 20 cells, which constitute the majority of the primary islet cells and analyzed the time of response for individual cell in the whole islet. The fast 3D recording showed that one

or two cells (1.6 ± 0.57 SD, *n*=3) responded first to the glucose injection (GCaMP6 signal >25% above baseline) and the rest of cells followed these cells with an average lag of 7.7s (7.7s ± 3.6s SD, *n*=3) (Figure 10 e-f). As in the 2D recordings, we found a mild positive correlation (R^2=0.46; ± 0.28 STD, *n*=3) between the time of response for each individual cell and the distance to the leader cell. Therefore, our 2D data, is representative of the islet behavior.

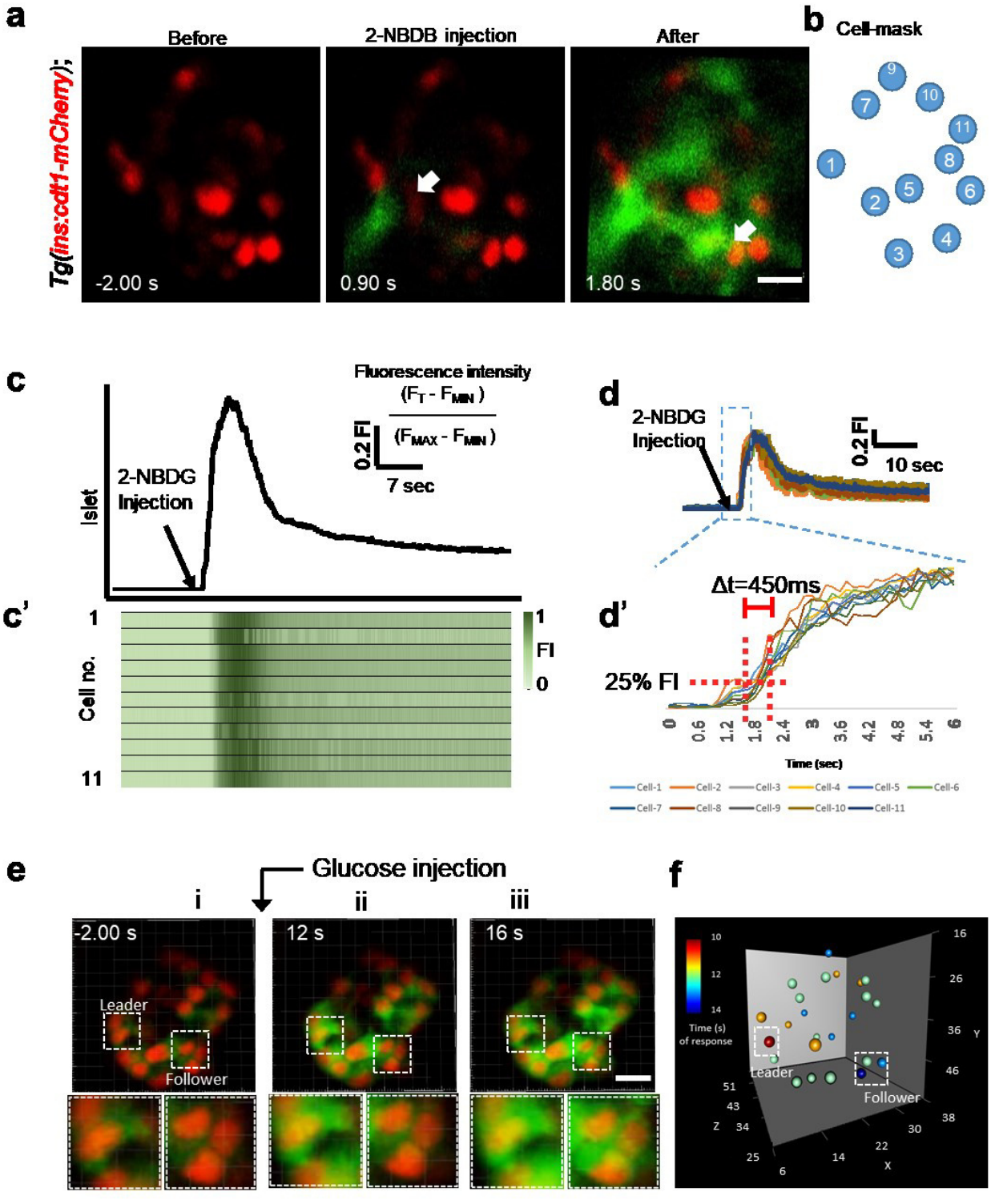

Figure 10. ***In vivo*** **injection of the fluorescence glucose analogue 2-NBDG and 3D whole islet imaging. a.** Snapshots of an islet imaged before, during and after intra-cardiac injection of 5 nL of 300μM 2-NBDG. White arrows indicate the first cell and the last cell to achieve a fluorescence increase of >25%. Scale bar = 10μm. **b.** Cell mask used to extract

the 2-NBDG signal of every cell. **c.** Trace of the cumulative normalized fluorescence intensity of all the cells shown in a. The Black arrow marks the time when the 2-NBDG injection took place. **c'**. Heatmap of normalized fluorescence intensity over time for individual cells corresponding to the cells shown in a. **d.** Fluorescence traces for all the cells imaged in a. **d'.** A close up for the fluorescence traces of all the cells imaged in A. It took 450ms from the first cell (Cell-1) to the last one (Cell-4) to register an increase of 25% of the normalized fluorescence intensity (*n*=5 animals, not graphically represented here). **e.** 3D islet projections acquired at 0.8 Hz before and during glucose injection. **f.** Associated 3D map showing the time of response in a colour-key fashion (the red colour represents the fastest response whereas dark blue represents the slowest). (*n*=3 animals, not graphically represented here).

3.2. Pan-islet response to glucose is impaired after leader β-cells ablation

We found that the islet response to glucose starts in one or two cells (leader), which are then followed by the rest of the β-cells. This behavior is reminiscent of previously defined *in vitro* hubs cells. Thus, we decided to test if these leader β-cells (leader), cells have functional role in the islet (Johnston et al., 2016). To this end, we developed a method for single-cell *in vivo* ablation through two-photon laser irradiation (Figure 11). Animals were challenged with three separate pulses of intracardiac glucose introduced before and after ablation of either leader (n=20) or follower cells (*n*=20). The leader cell was identified *in situ* by "eye" observation during the experiment. We found that ablation of leader cells led to a significant reduction in the glucose response in terms of the total islet AUC GCaMP signal (Figure 11c) whereas ablation of follower did not lead to a statistically significant decrease.

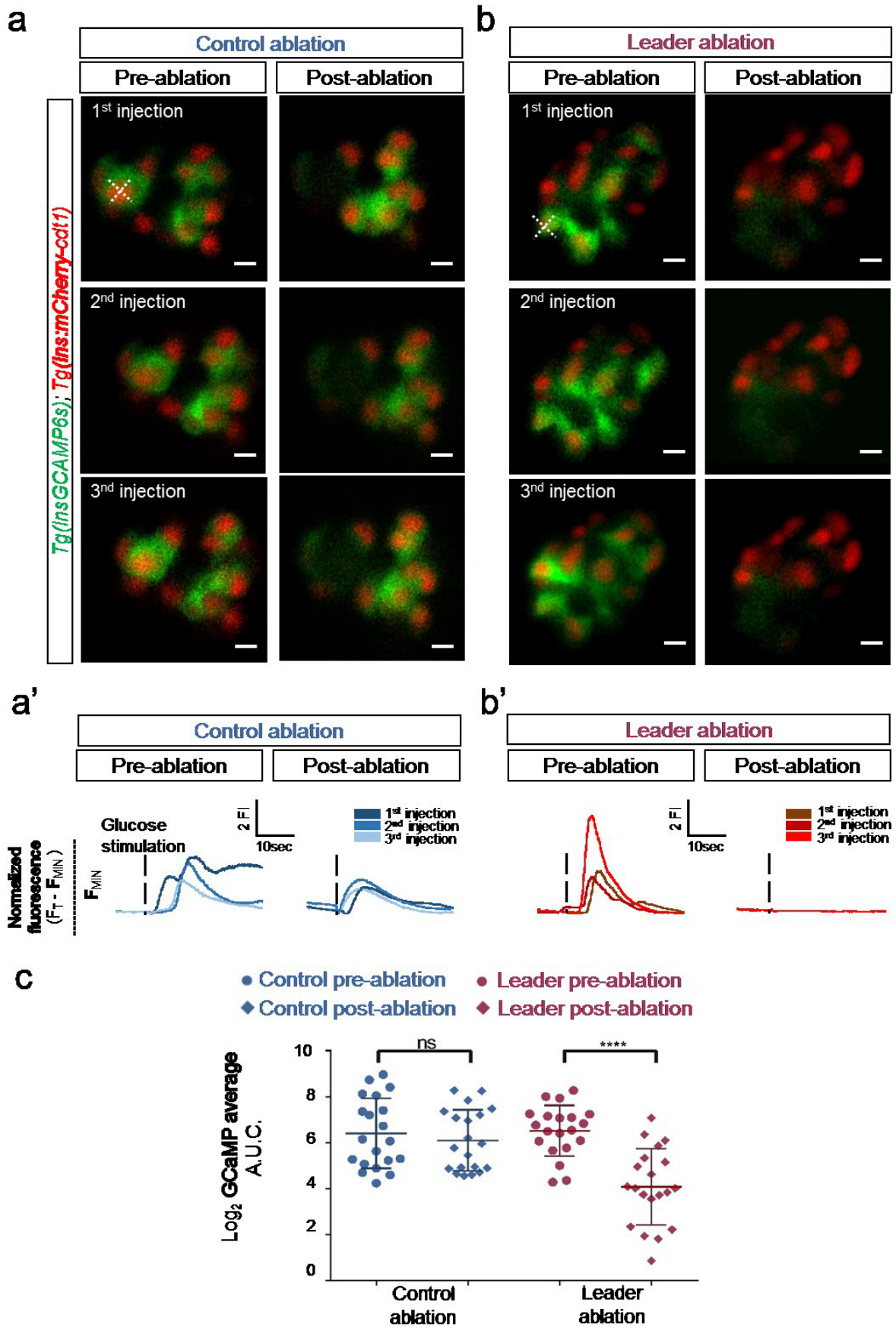

(Figure text is in the next page)

Figure 11. Ablation of temporally defined 'leader' cells (but not 'follower' cells) alters islet responsivity to glucose *in vivo* in zebrafish. a, b, Images from the time-lapse recording (6 frames s–1, single plane) of the islet after three consecutive glucose stimulations before and after 'leader' or 'follower' (control) cell ablation. Glucose was injected at 5-min intervals while the Ca^{2+} dynamics were monitored. After the identification of presumptive 'follower' or 'leader' cells, these cells were ablated using a two-photon laser ablation via roi-scan (see Methods). The letter X indicates the targeted cells. The top panels show representative frames from the movies before and after the ablation of a 'follower' (**a**) or a 'leader' cell (**b**). The lower traces (**a'**,**b'**) show the normalized GCaMP6 fluorescence traces and the peak in Ca^{2+} influx after glucose injection pre- and post-ablation. FI, fluorescence intensity. **c**, Quantification of the AUC reflecting 200 frames of normalized GCaMP6 fluorescence before and after the ablation of a 'follower' or a 'leader' cell ($n = 20$ islets each) (paired, two-tailed, Student's *t*-test, $P = 3.43 \times 10\text{-}5$, NS, not significant). The ablation of 'leader', but not 'follower', cells led to a significant reduction in the total islet GCaMP response. Each data-point represents the average AUC from three glucose injections in individual larvae. Data are mean ± s.d. The experiments were performed eight independent times with several samples showing similar results.

To ensure that, as expected from this approach, the laser ablation technique was highly localized to a single cell, we fixed islets immediately after the laser cell-ablation (<10 min) and performed TUNEL assay and immunohistochemistry using anti-mCherry and DAPI. Only targeted cells revealed evidence of DNA damage as revealed by the TUNEL signal, while the neighboring cells showed no obvious damage (Figure 12). Moreover, we show that islet blood flow remains unaltered following the ablation of the cells using bright-field imaging before and after the ablation.

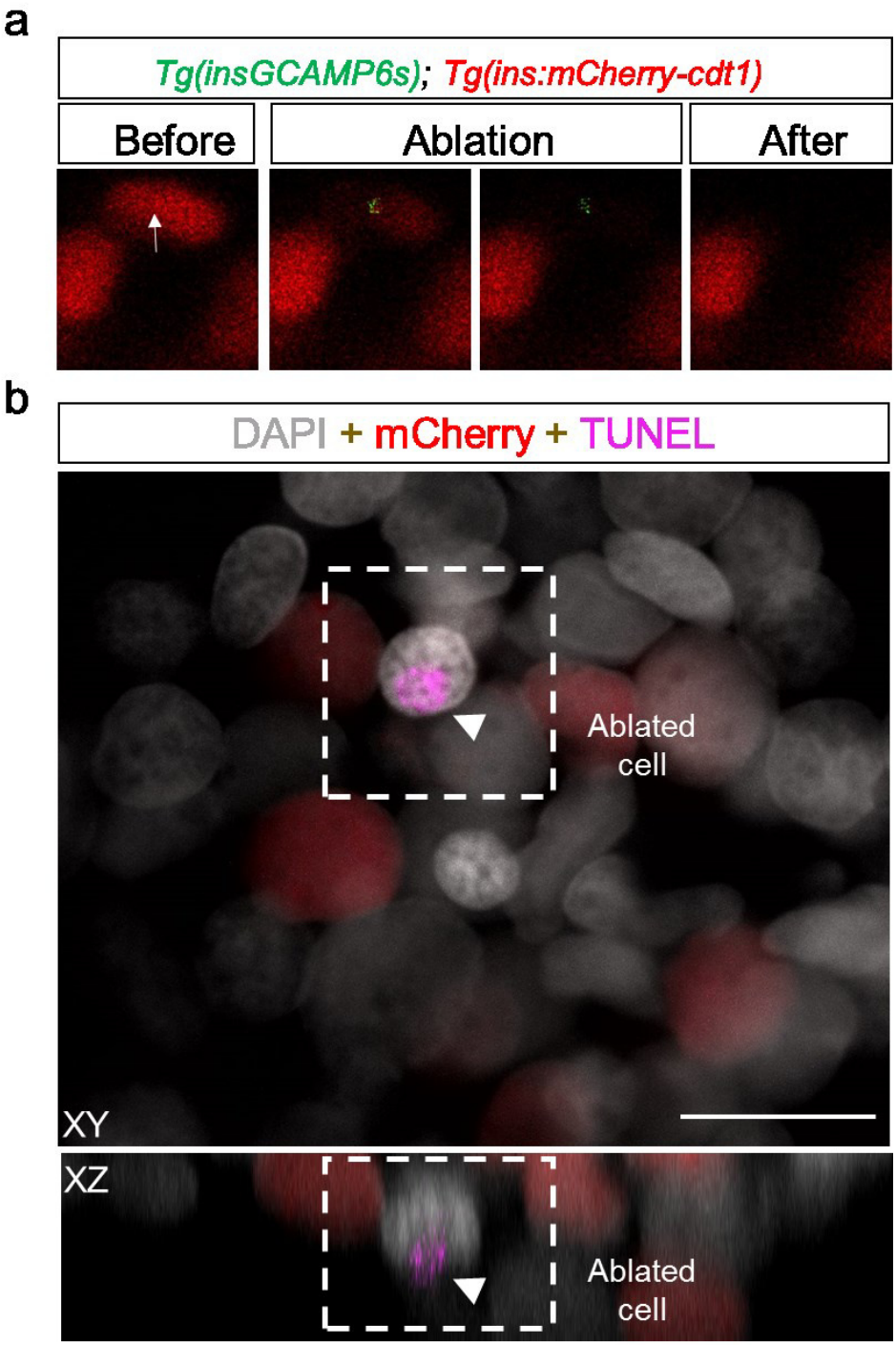

Figure 12. 2-Photon laser ablation achieves highly targeted single cell destruction. a. Images of a time-lapse recording in a single plane of a cell undergoing laser ablation (arrow). The snapshots show the nuclei of β-cells marked using *Tg(ins:mCherry-cdt1)* before, during and after the ablation of the targeted cell. **b**. Confocal image corresponding to the islet showed in a, following fixation, TUNEL assay and immunohistochemistry against

mCherry. Arrow marks the damaged nucleus of the ablated cell. The TUNEL assay revealed DNA damage only in the ablated cell, and showed no discernible damage to neighbour cells. Scale bar = 10μm.

4. Optically orthogonal toolset for *in vivo* optogenetics and Ca^{2+} imaging

4.1. Development of optogenetics actuators systems in zebrafish β-cells

The calcium reporter GCaMP allowed us to record for the first time the Ca^{2+} dynamics of the pancreatic β-cells in the living zebrafish. After a glucose injection, we found that one or two cells respond first (on, average=1.5, n=8, STD= 0.53), which are then followed by the rest of the β-cells. We tested the function of these leader β-cells by laser ablation and we found that their ablation led to a significant reduction in the total islet GCaMP response to a glucose stimulus. Therefore, we decided to functionally dissect the role of individual β-cells in islet coordination *in vivo*. An ideal *in vivo* strategy should allow highly targeted, yet reversible activation or silencing of the β-cells. To this end, we created several transgenic lines including red genetically-encoded calcium indicators (GECIs) in order to combine them with optogenetic actuators with different optical spectra and capabilities (Table 3-4).

Table 3. Generated transgenic lines expressing optogenetic actuators.

ACTUATORS

Name	Founders	Excitation	Peak current	Desensitization*	Comments from the thesis author
ChR2[1]	2	470nm	~0.7nA	~0.22	Not evaluated *in vivo* yet
CheRiff[2]	2	460nm	~2nA	~0.665	Works in combination with jRCaMP1a and K-GECO1
ChrimsonR[3]	3	590nm	~0.7nA	~0.58	Present around 10-20% activation under 488nm laser light illumination
eNPHR3.0[4]	3	589nm	~(outward) 0.74nA	N.R.	Works *in vivo*, but it desensitizes in around 20s of constant illumination

*Referred as the steady-state current divided by peak current

N.R. not reported.

[1]Values obtain from Boyden, *et al.* 2005

[2]Values obtain from Hochbaum, *et al*. 2015

[3]Values obtain from Oda, *et al.* 2018

[4]Values obtain from F. Zhang *et al*. 2007

4.2. Red fluorescent calcium reporters in zebrafish β-cells

The red genetically-encoded calcium indicators (GECIs) have the inherent advantage of possessing a longer excitation-wavelength as compared to green GECIs. Therefore, during *in vivo* imaging they present reduced phototoxicity and light scattering in the tissues. Furthermore, they can be combined with multicolor imaging in the blue, cyan and green channels without spectral crosstalk. Thus, we decided to clone under the zebrafish insulin promoter the three most promising red calcium indicators to date in order to establish complementary tools for *in vivo* Ca^{2+} imaging (Table 4, Figure 13) (Molina et al., 2019).

Table 4. Generated transgenic lines expressing red Ca^{2+} indicators

RED CALCIUM INDICATORS

PROTEIN	Founders	Excitation	Dynamic range (F_{max}/F_{min})	Ca^{2+} K_d	Comments from this thesis author
jRCaMP1a[1]	3	570nm	3.2± 0.1	214 nM	Low ΔF *in vivo*
jRGECO1a[1]	6	561nm	11.6 ± 0.4	148 nM	Did not worked *in vivo*
K-GEKO1[2]	4	565nm	~12	165 nM	Good ΔF and response times *in vivo*

[1]Values obtain from Dana, *et al.* 2006 (Dana et al., 2016)

[2]Values obtain from Shen, *et al.* 2018 (Shen et al., 2018)

The jRGECO1a was the most promising of the red-GECIs with a dynamic range of >11(F_{max}/F_{min}) and response times of 300ms to a single AP (Dana et al., 2016). Thus, we created a transgenic line *Tg(ins:jRGECO1a;cryaa:mCherry),* expressing JRGECO1a under the zebrafish insulin promoter. However, in all the transgenic founders that we evaluated, we detected what appeared to be cellular aggregation of jRGECO1a in the β-cells (Figure 13b, white arrows). Besides this uneven expression patterns, the injection of 25mM glucose in the stable transgenic lines did not result in fluorescent changes under our live imaging protocol (Figure 13b'). Aside from these undesirable effects of jRGECO1a expression in the β-cells, the jRGECO1a presents photoconversion under blue light exposure (λ ≤ 488). Therefore, we discarded further investigation and usage of jRGECO1a.

We also developed transgenic lines expressing the red GECIs jRCaMP1a and K-GECO1 under the zebrafish insulin promoter. These two transgenic lines *Tg(ins:jRCaMP1a;cryaa:mCherry)* and *Tg(ins:K-GECO1a;cryaa:mCherry)* showed uniform expression in the β-cells and under our protocol for glucose injection and live imaging, both showed detectable changes in red fluorescence (Figure 13c-d). These preliminary data confirmed that it is possible to use the red-GECIs to study β-cell Ca^{2+} dynamics *in vivo*.

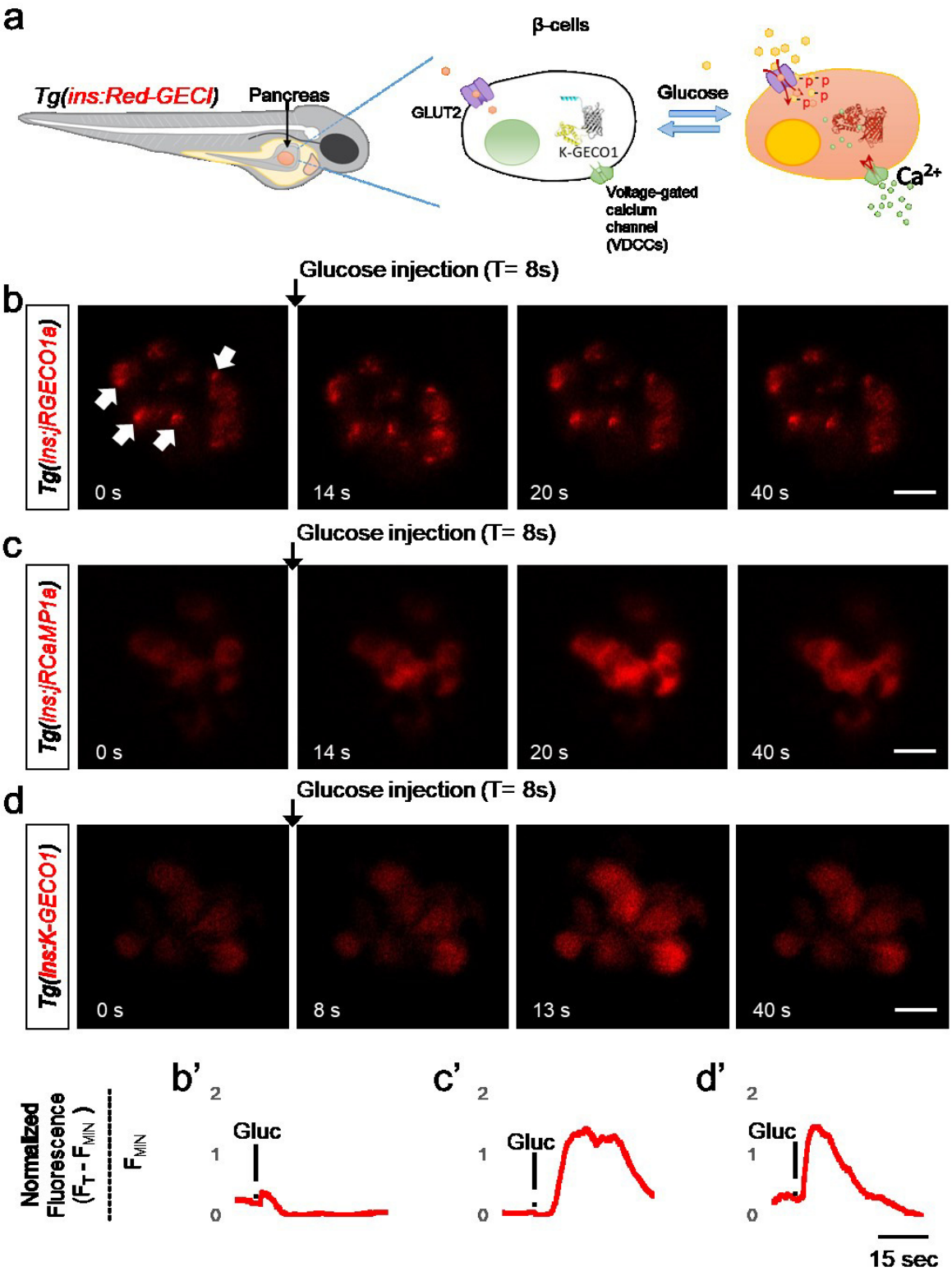

Figure 13. *In vivo* β-cell response to a glucose injection using the red-GECIs. **a.** Cartoon representing a transgenic zebrafish larvae, expressing a red Genetically-Encoded Calcium Indicator under the insulin promoter. In presence of high glucose, the β-cells

present influx of Ca^{2+}, increasing the fluorescence of the red-GECIs. Images from the time-lapse recording (6 frames/s, single plane) of the islet before and after a glucose stimulation with 5nL of 25mM glucose in three different transgenic lines: **b.** *Tg(ins:jRGECO1a)*, **c.** *Tg(ins:jRCaMP1a)* and, **d.** *Tg(ins:K-GECO1)*. The lower traces (**b'**,**c'**,**d'**) show the normalized red fluorescence intensity traces after glucose injection for each transgenic line. FI, fluorescence intensity. The white arrows points to jRGECO protein aggregations in the β-cells. Scale bar = 10μm.

4.3. *In vivo* temporal optogenetic silencing of β-cells

The laser ablation is an irreversible system for β-cell interrogation. Thus, in order to overcome this limitation, we created the transgenic line *Tg(ins:eNpHR3.0-mCherry;cryaa:CFP)* to perform reversible silencing of β-cells. The NpHR is a light-gated chloride pump, which is activated by red light (λ = 560–590 nm) and can inhibit robustly cell depolarization. Theoretically, if we activate the NpHR during a glucose stimulus, the electrical silencing of the β-cells should inhibit the glucose-induced influx of Ca^{2+}. To test if this approach can be applied *in vivo*, we performed simultaneously live imaging, pericardial glucose injection and optogenetic silencing of the β-cells in the double transgenic larvae *Tg(ins:GCaMP6s);Tg(ins:eNpHR3.0-mCherry)*. In these experiments, we gave first a pulse of glucose and then recorded the normal Ca^{2+} response of the β-cells. Subsequently, we gave another pulse of glucose and simultaneously activated the NpHR by illumination with the red laser (λ = 561) while recording the Ca^{2+} dynamics. Finally, we gave a third glucose bolus to examine if β-cells were silenced in a reversible manner. Notably, we were able to temporally inhibit the glucose-induced influx of Ca^{2+}, as reported by a reduction in the GCaMP signal (Figure 14), indicating that NpHR-excitation effectively blocks depolarization and calcium influx even in the presence of high glucose.

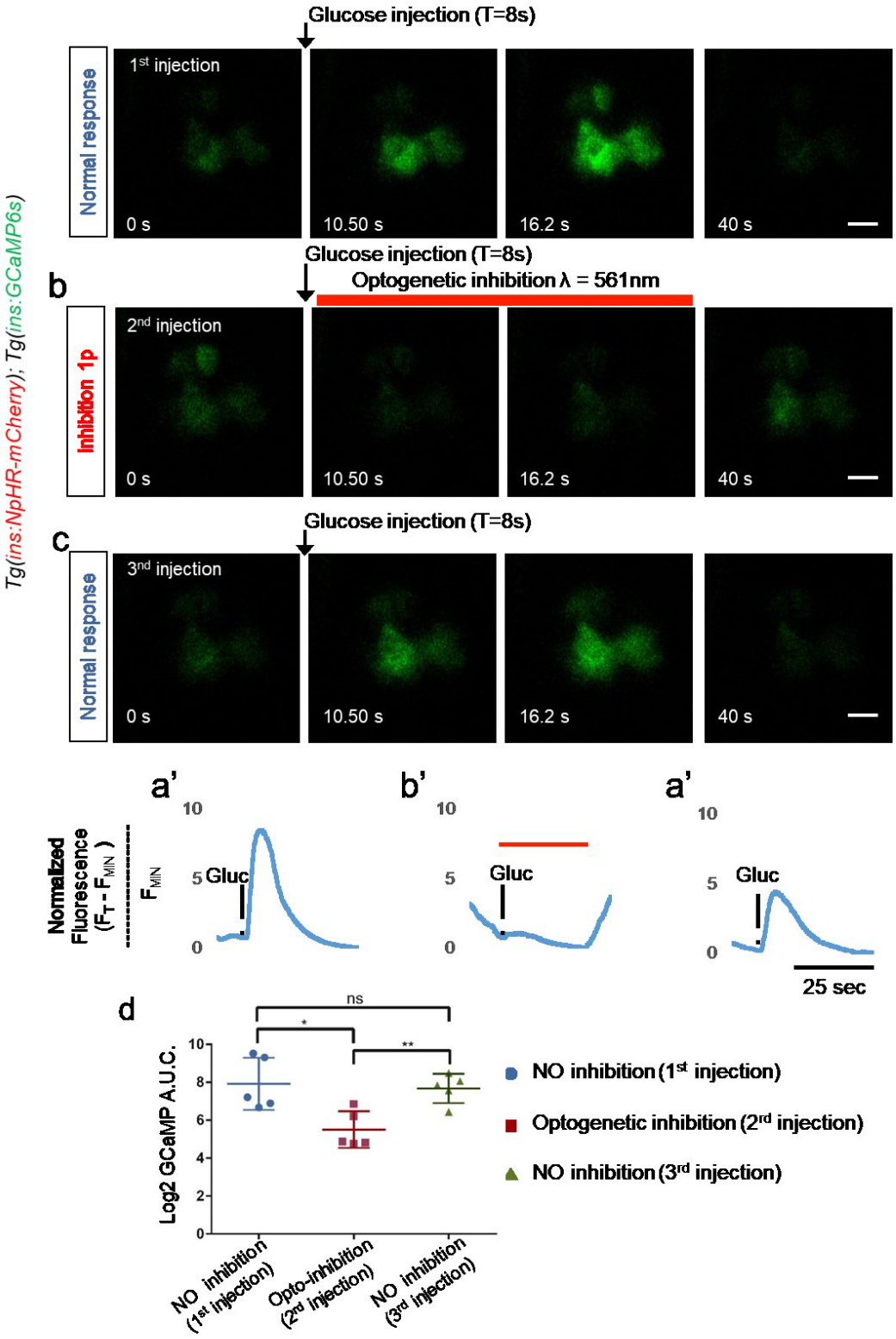

Figure 14. 1-Photon *in vivo* temporal inhibition of all β-cell decreases significantly the islet GCaMP signal during a glucose stimulation in zebrafish. a. Images from the time-lapse recording (6 frames/s, single plane) of the islet before and after a glucose

stimulation with only blue laser (λ = 488). **b.** images from the same islet shown in a, during the second glucose injection and simultaneous *in vivo* optogenetic inhibition with a red laser (λ = 561). The optogenetic inhibition was done by activating the red laser after 7s of imaging with a simultaneous glucose bolus. The optogenetic inhibition was stopped after 30s of constant red laser illumination. **c.** Images from the time-lapse recording of the islet as in "a" and "b", before and after the third glucose stimulation with only green laser (λ = 488). The lower traces (**a'**,**b′**,**c′**) show the normalized GCaMP6 fluorescence traces after glucose injection under normal conditions and upon light-mediated inhibition of β-cell depolarization. FI, fluorescence intensity. The red bar, indicates the time of red laser exposure. **d.** Quantification of the AUC reflecting 200 frames of normalized GCaMP6 fluorescence for each condition ($n = 5$ islets each) (1-way paired ANOVA, Tukey's correction *p-value* = 0.0114, NS, not significant). Each data-point represents the AUC of GCaMP in an individual sample. This experiment was performed 1 time with 5 samples showing similar results. Scale bar, 10 μm.

4.4. *In vivo* temporal optogenetic silencing of a subset of β-cells can inhibit the islet response

Since we were able to inhibit the whole islet response to a glucose stimulus *in vivo* via NpHR optogenetics, we decided to functionally dissect the role of individual β-cells in islet coordination. For this purpose, we exploited the already established ROI (Region Of Interest) scan technology to shine light on individual cells while recording glucose-stimulated calcium influx. The ROI-scan is used for FRAP (Fluorescence Recovery After Photobleaching) experiments in which a ROI is scanned with a particular laser light and intensity. We used this method to perform calcium imaging and optogenetics by targeting individual cells using a manually defined ROI to activate a particular laser light only inside this area of illumination, while simultaneously performing Ca^{2+} imaging. We hypothesized that if we would silence a leader cell during the glucose-induced influx of Ca^{2+}, its inhibition should diminish the response of the islet. In contrast, if a follower cells is temporally silenced, we should detect a normal response to glucose in the rest of the β-cells (Figure 15a). In the preliminary data presented in Figure 15, we gave a first pulse of glucose

to identify the putative leader-cell. Subsequently, we gave another pulse of glucose and simultaneously activated the NpHR by illumination with the red laser (λ = 561), targeting either the presumptive leader cell or a follower cell. We found that as expected, the inhibition of the follower cell did not prevent the Ca^{2+} in the rest of the β-cells. In contrast, the inhibition of the putative leader-β-cell produced the silencing of a majority of the cells. Interestingly, a small cluster of cells still showed an increase in GCaMP6s signal upon leader cell inactivation (Figure 14c). This result suggests that this islet might contain two leader cells, each controlling a different group of cells (Figure 15c-c´).

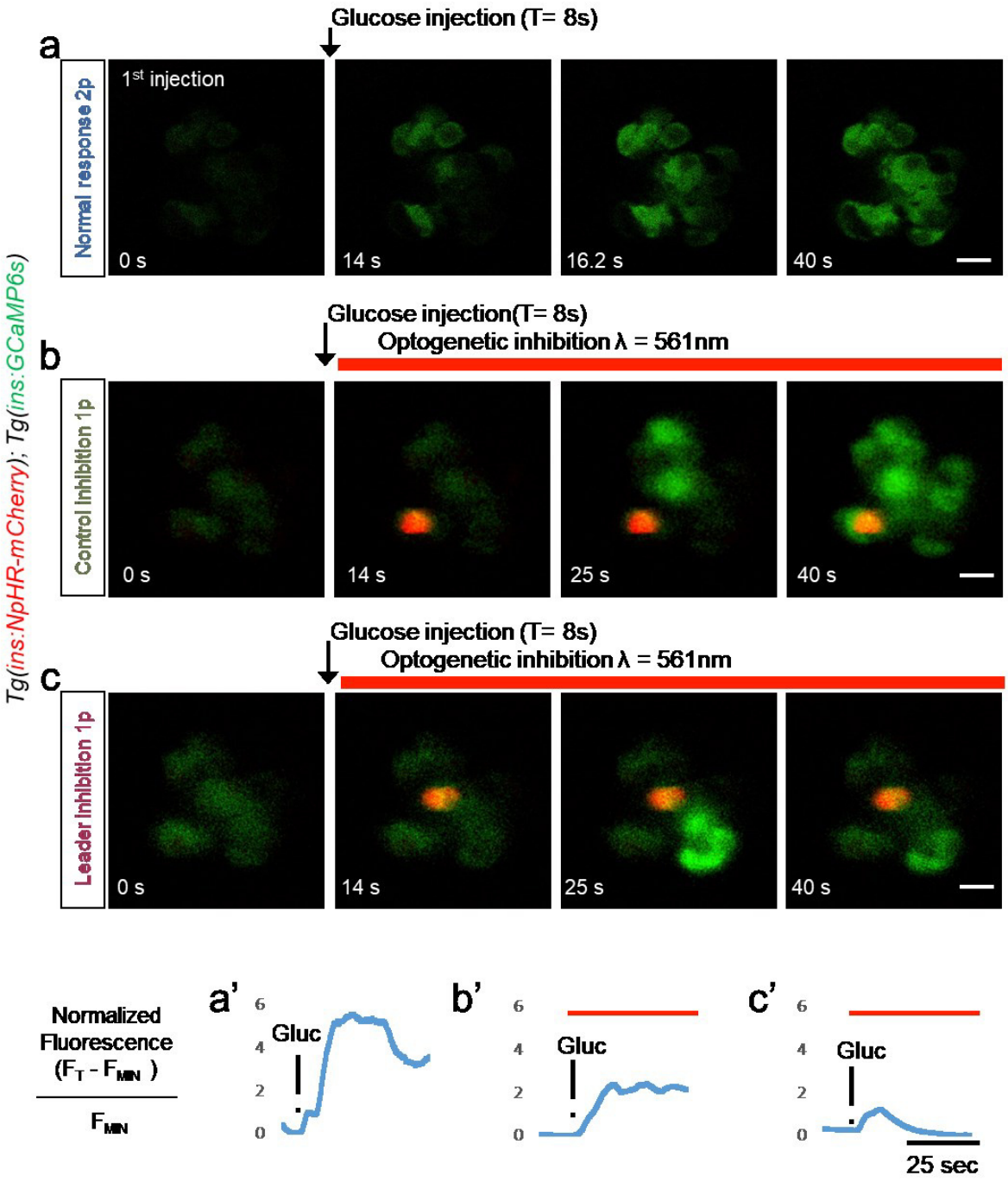

Figure 15. 1-Photon (1p) *in vivo* temporal inhibition of leader-β-cell decreases significantly the islet GCaMP glucose response in zebrafish. a. Images from the time-lapse recording (6 frames/s, single plane) of the islet after a glucose stimulation in a 2-photon (2p) imaging (λ = 900). **b,c,** images from the same islet shown in a, in 1p imaging with green laser (λ = 488) after a glucose injection and simultaneous *in vivo* optogenetic inhibition with a red laser (λ = 561). The optogenetic inhibition was done with the ROI-scan encompassing the area of one follower or putative leader-β-cell. Glucose was injected at 5-

min intervals. The red signal correspond to the mCherry fluorescence as the NpHR is fused to mCherry. The lower traces (**a'**,**b'**,**c'**) show the normalized GCaMP6 fluorescence traces and the peak in Ca^{2+} influx after glucose stimulation and upon the light-mediated inhibition of a control or a leader-β-cell. FI, fluorescence intensity. The red bar, indicates the time of red laser exposure. Scale bar, 10 μm.

4.5. *In vivo* temporal optogenetic activation of β-cells

We wondered if the leader β-cells can actively recruit follower cells. Previous reports on β-cells expressing the light-gated cation pump channelrhodopsin-2 (ChR2) in mouse islets had shown the possibility to trigger Ca^{2+} influx and insulin secretion from β-cells after blue light exposure (Reinbothe et al., 2014). Thus, it is reasonable to assume that the β-cells can be activated *in vivo* via channelrhodopsin optogenetics. However, the light-inducible activators ChR2 and CheRiff have their maximum spectrum activation at ≈460-470nm light, leading to an incompatibility with the GCaMP imaging (Table 2 and 3). A possible solution is the usage of the red-light-sifted channelrhodopsin from *Chlamydomonas noctigama* (ChRimson), which presents a maximum spectrum activation at ≈590 nm light. Thus, theoretically, ChRimson would allow for optogenetic activation of β-cells and simultaneous recording of Ca^{2+} activity (Oda et al., 2018).

In order to test if β-cells can co-activate other β-cells *in vivo*, we generated a transgenic line expressing the optogenetic activator of depolarization ChRimsonR (ChRimsonR fused to mRuby2) under the zebrafish insulin promoter (Table 3). Theoretically, if a leader β-cell can activate directly the follower cells, if we artificially depolarize such a "leader" cell in absence of a glucose stimulus, its activation should be enough to trigger influx of Ca^{2+} in the rest of the β-cells. With this in mind, we performed a preliminary Ca^{2+} live imaging experiment and optogenetic activation via ChRimsonR to interrogate β-cell coordination *in vivo.* To this end, we used *Tg(nrd:GCaMP6f);Tg(ins:ChRimsonR-mRuby2)* double

transgenic larvae. In these experiments, we first gave a pulse of glucose to identify *in situ* by "eye" the putative leader β-cell. Subsequently, we activated the ChRimsonR by illumination with the red laser (λ = 561nm), targeting either a first responder or a follower cell while recording the GCaMP signal. In the particular example shown in Figure 16, we found congruency with an activation model: the activation of the putative leader-β-cell led to a significant increase in GCaMP signal, similar to the one produced by a glucose stimulus, and co-activation of several cells. In contrast, follower cells showed lower potential to co-activate the cells outside the area of laser Illumination (Figure 16b-c). Despite the fact that the ChRimsonR presents a maximum spectrum activation at ≈590 nm, during the evaluation of the ChRimsonR and GCaMP optogenetic system, we detected an activation of around 10%-20% of ChRimsonR. This activation was present even at very low laser powers and using a non-optimal laser line (λ=470nm) for GCaMP excitation, thereby lowering the quality of the images. Hence, we only present one sample, since this system is far from optimal and we decided to explore other more rigorous approaches.

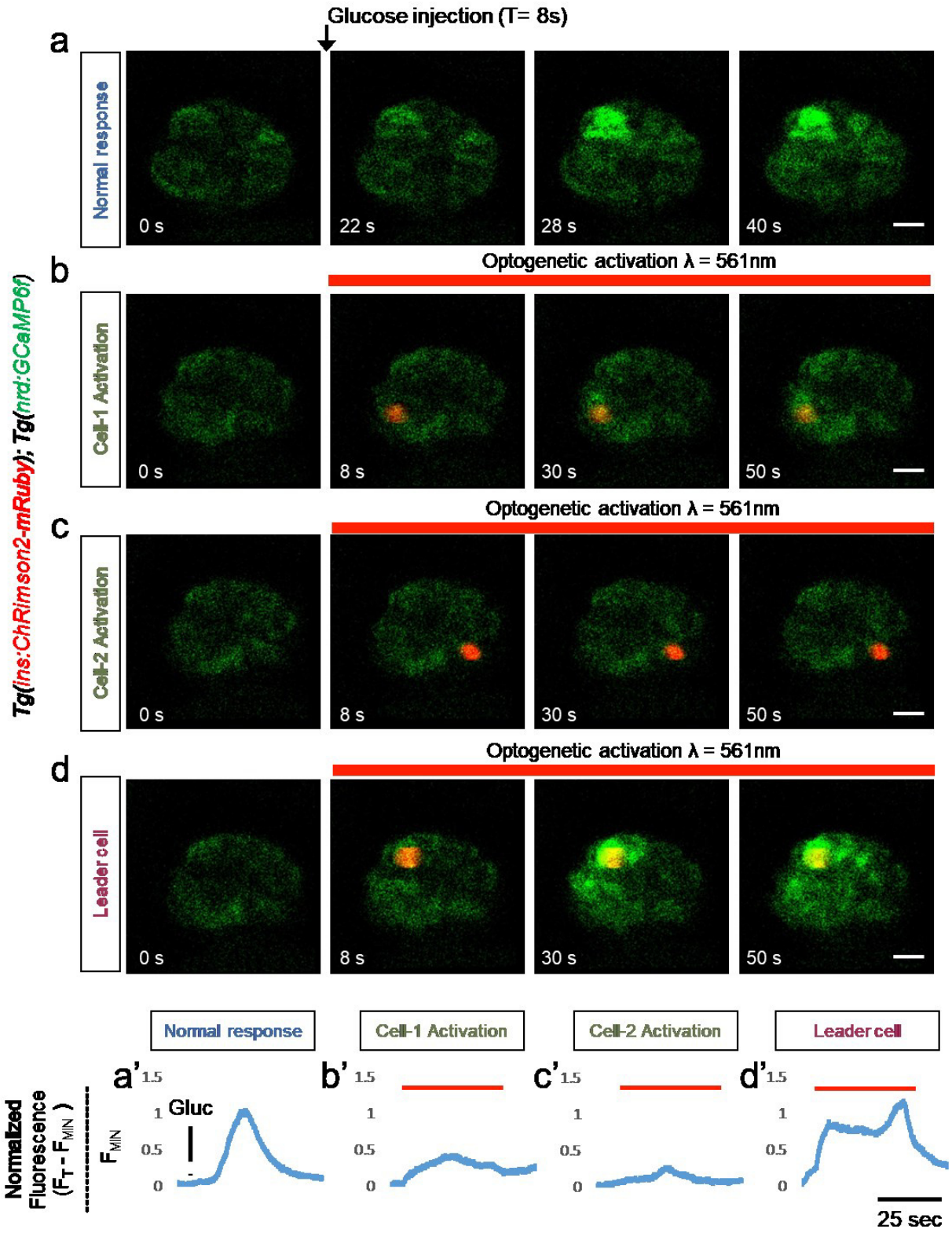

Figure 16. 1-Photon *in vivo* temporal activation of leader-β-cell promotes islet GCaMP response similar to a glucose stimulation. a. Images from the time-lapse recording (6 frames s–1, single plane) of the islet after a glucose stimulation in 1-photon (1p) imaging.

b,c, images from the same islet shown in a, in 1p imaging with green laser (λ = 488) and simultaneous *in vivo* optogenetic activation with a red laser (λ = 561). The optogenetic activation was done with the ROI-scan encompassing the area of one follower or putative leader-β-cell. The red signal corresponds to the mRuby fluorescence as the ChRimson2 is fused to mRuby. The lower traces (**a'**,**b'**,**c'**) show the normalized GCaMP6 fluorescence traces and the peak in Ca^{2+} influx after glucose injection and upon the light-mediated activation of a control or a leader-β-cell. FI, fluorescence intensity. The red bar, indicates the time of red laser exposure. Scale bar 10μm

Due to the optical crosstalk presented by the ChRimsonR and GCaMP systems, we cannot guarantee that β-cells are not pre-activated by simply exciting the GCaMP reporter. Thus, we decided to try our newly developed transgenic lines bearing the red GECIs K-GECO1 in combination with the blue actuator CheRiff. First, we probed if β-cell influx of Ca^{2+} was possible via CheRiff optogenetic activation. For this purpose, we merged our red Ca^{2+} live imaging ROI-scan technology and optogenetic activation via CheRiff. To this end, we used *Tg(ins:K-GECO1;cryaa:mCherry);Tg(ins:CheRiff-GFP;cmcl2:GFP)* double-transgenic larvae. If the CheRiff is operational *in vivo*, during blue illumination we should detect an increase in Ca^{2+} by the K-GECO1. In case that the CheRiff is not operational *in vivo*, we should not detect any significant increase in red signal in the β-cells upon blue illumination. Thus, in this experiment, we first imaged the islet for 7.5s and then we activated the CheRiff by illuminating with blue laser (λ = 470nm) for 30s while simultaneously recording the Ca^{2+} dynamics in the red channel. We found that it was possible to trigger a significant influx of Ca^{2+} upon pan-islet optogenetic activation *in vivo* (Figure 17). Similarly to the ChRimson results, we found that single cell activation of different cells leads to variable levels of recruitment of the neighbor cells. Notably, whereas most illuminated cells only activating themselves and immediate neighbors, the illumination of cell number 3 shown in Figure 17c led to co-activation of a majority of the imaged cells in the islet.

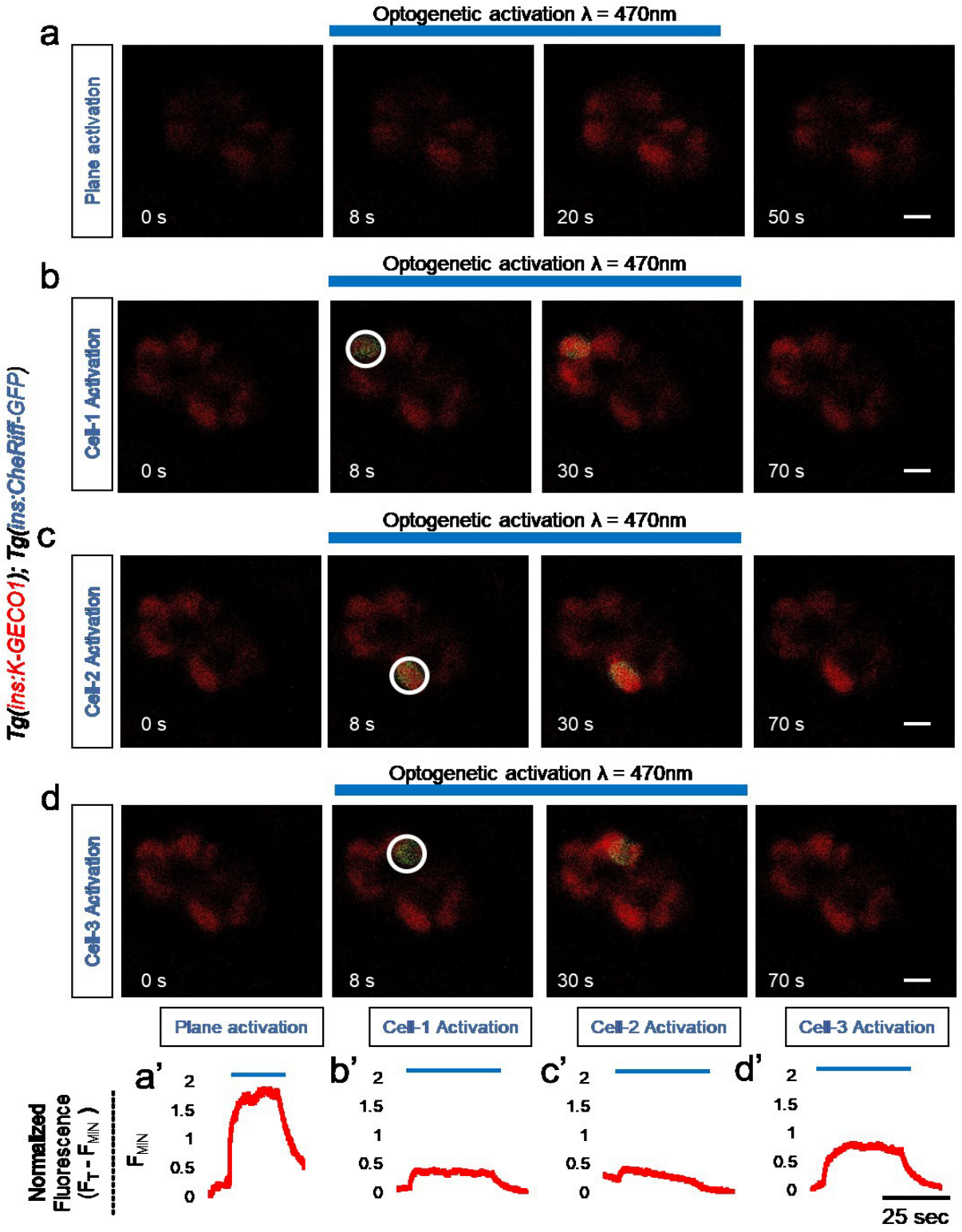

Figure 17. 1-Photon (1p) *in vivo* temporal optogenetic activation of β-cells via CheRiff promotes calcium influx in zebrafish. a. Images from the time-lapse recording (6 frames/s, single plane) of the islet before, during and after blue illumination in 1-photon

(1p) (λ = 470) in double transgenic *Tg(ins:K-GECO1);Tg(ins:CheRiff-GFP)* zebrafish larvae. **b,c,** images from the same islet shown in a, in 1p imaging with red laser (λ = 561) and simultaneous *in vivo* optogenetic activation with a red laser (λ = 470). The optogenetic activation was done with the ROI-scan encompassing the area of one cell. The green signal correspond to the GFP fluorescence, as the CheRiff is fused to GFP. The lower traces (**a**′,**b**′,**c**′) show the normalized K-GECO1 fluorescence traces for all the imaged β-cells. FI, fluorescence intensity. The blue bar, indicates the time of blue laser exposure. White circles labels the targeted cell. Preliminary data from 1 animal. Scale bar 10μm

5. Discussion and future directions

5.1. β-cell calcium spikes are systemically influenced

In this thesis, we explored the Ca^{2+} dynamics of the β-cell in their native unaltered microenvironment. To this end, we developed high-resolution and high-speed protocols for β-cell imaging *in vivo*. We simultaneously stimulated the zebrafish β-cells with glucose while recording their Ca^{2+} dynamics in 2D and 3D. The three main advances made in this thesis are: 1) we show that β-cells present constant Ca^{2+} activity *in vivo*, which is systemically influenced; 2) during a glucose stimulus *in vivo*, the β-cells coordinate their function through temporally defined leader cells; 3) we developed and implemented systems for *in vivo* optogenetic interrogation, which in preliminary evaluation show that individual β-cells present variable capabilities for islet coordination.

In the past, the β-cells have been seen rather as a uniform population, and often termed as a functional syncytium (Nadal et al., 1999). However, our observations together with imaging of islets in the anterior eye chamber of the eye directly suggest different functional roles among the β-cells, i.e. leader and follower β-cells in generating multicellular islet dynamics (Salem et al., 2019). This is congruent with the emerging literature addressing the sub-population of β-cells based on differential cell-surface markers, gene expression profiles, topological location, embryonic origin and functional heterogeneity *in vitro* (Ackermann et al., 2016; Bader et al., 2016; Ellenbroek et al., 2013; Johnston et al., 2016; Katsuta et al., 2012; Li et al., 2016; Singh et al., 2017; Smukler et al., 2011; Xin et al., 2016).

Discussion and future directions

Previously, Singh *et al*. showed that zebrafish islets imaged in culture do not show significant Ca^{2+} activity in basal glucose (5mM) (Singh et al., 2017). In contrast, we found that the β-cells present frequent Ca^{2+} spikes *in vivo*. These likely occur in response to spikes of systemic sugar levels, as lowering glucose levels stopped this activity. Consistent with our findings, Jacob *et al*. recently reported the presence of fast and faint Ca^{2+} oscillation in the β-cells from mice that were fasted for 4 hrs and imaged following transplantation in the anterior chamber of the mouse eye (ACE) (Jacob et al., 2020). This suggests that β-cells are active not only after a feeding, but constantly. This finding is relevant since previous literature has shown that mice, dogs and humans present pulsatile insulin secretion under fasting conditions (Anderson et al., 1967; Head et al., 2012; Lang et al., 1979; Satin et al., 2015). Pulsatile insulin secretion is believed to be more efficient for glucose control as compared to a steady increase in insulin due the kinetics of insulin receptor and insulin signaling activation, especially in the liver where ~80% of insulin is cleared (Goodner et al., 1988; Matthews et al., 1983; Meier et al., 2005; Paolisso et al., 1988). Moreover, Matveyenko *et al.* showed that insulin delivery at a constant, as opposed to a pulsatile pattern, via the portal vein in rats led to an impaired activation of the hepatic insulin receptor substrate (IRS-1 and IRS-2) and aberrant downstream signaling via AKT and Foxo1 (Matveyenko et al., 2012). Hence, an important question to be addressed in the future is if the presence of endogenous Ca^{2+} oscillations in β-cells might be driving insulin secretion and if there is a pulsatile pattern in the zebrafish as well. For this purpose the generation for a reliable and quantitative method for zebrafish insulin assessment needs to be developed such as custom zebrafish insulin ELISA or and insulin secretion reporter in combination with *in vivo* calcium imaging.

The presence of endogenous Ca^{2+} spikes in the β-cells is likely to derive from the free glucose circulating in the zebrafish (Gut et al., 2013). Indeed, we found that lowering the glucose levels via insulin injection, decreased the Ca^{2+} spikes *in vivo* (Figure 4). This suggests a correlation between glucose levels and the endogenous Ca^{2+} activity of the β-cell *in vivo*. Supporting the concept that β-cells endogenous Ca^{2+} are involved in glucose control, we found that the pharmacological inhibition of β-cell depolarization using the K_{ATP} channel opener diazoxide provoked

hyperglycemia and glucose intolerance in zebrafish larvae (Figure 5 a-b) (Mariot et al., 1998). However, while aberrant in nature, we still detected GCaMP signal changes in the zebrafish islets incubated with diazoxide. This, suggest that proper endogenous Ca^{2+} oscillations might be associated to the proper glucose control *in vivo*.

Contrary to a previous report, which claimed that there is no blood flow in the islets of zebrafish larvae (Moss et al., 2013), we found that the islets present proper blood perfusion (Figure 6a). This highlights a key difference between the *in vitro* models to study islet biology and our *in vivo* zebrafish model in which blood flow is preserved. In addition, the presence of perfusion suggests that the endogenous Ca^{2+} oscillations of the β-cells might derive from glucose levels present in the blood. Indeed, we found that the temporal blockage of the blood flow decreased the Ca^{2+} signal of the β-cells (Figure 6). Our findings are aligned well with studies showing that lowering blood perfusion to the islet also reduces endogenous Ca^{2+} oscillations. Mullapudi *et al.* recently studied the effects of β-cell specific overexpressing of the soluble isoform of Vegf receptor 1 (sFlt1), a potent angiogenic inhibitor. They found that larvae from *Tg(ins:sflt1)* zebrafish showed an apparently normal islet and β-cells architecture, except for the lack of islet vasculature and blood perfusion. In this model, only around 2% of the β-cells presented endogenous Ca^{2+} activity as revealed by the GCaMP5 imaging. Additionally, glucose measurements in basal conditions from these larvae showed a threefold increase in free glucose levels in comparison to WT controls (Mullapudi et al., 2019). Altogether these data suggest that blood perfusion is key for endogenous Ca^{2+} activity of the β-cells *in vivo*. Similarly to the fish, mouse models with islet or pancreatic specific VEGF-A knock-out present glucose intolerance possibly as they lack rapid insulin release due to poor blood perfusion and a 30% reduction in islet vasculature (D'Hoker et al., 2013; Reinert et al., 2013). It is well established that oxygen is key for proper β-cell function. However, none of the experiments mentioned above can guarantee if lowering the blood flow might induce mild hypoxia and hence directly decrease the Ca^{2+} oscillations, yet, it reinforces the importance of proper blood flow for β-cell function (Gerber and Rutter, 2017). Hence, these results are to be considered, for example, during the rational design of tissue-engineered devices to encapsulate β-cells, where

proper blood supply and oxygen might be a limiting factor for β-cell function (Coronel et al., 2019).

5.2. First responder β-cells are present *in vivo*

Our study together with work done in parallel by Lorincz *et al.* converge on showing that zebrafish β-cells show a synchronized response to glucose stimulation *in vivo* (Delgadillo-Silva et al., 2019; Lorincz et al., 2018; Salem et al., 2019). This coordinated behavior resembles previous studies showing that upon glucose stimulation, isolated islets show a typical synchronous train of Ca^{2+} oscillations. These synchronous Ca^{2+} oscillations are suggested to be responsible for proper first phase and second phase of insulin secretion. Indeed, these Ca^{2+} oscillation patterns are lost in pathological conditions such as diabetes (Cohrs et al., 2020; Head et al., 2012; Nadal et al., 1999). Thus, future or subsequent studies should address if zebrafish present the typical mammal first-phase and second phase insulin secretion.

We also found that the average time of response from the time of glucose injection to the time of islet activation was 4.34s (4.34s ± 4.40s SD, *n*=40). This is much shorter than previous *in vitro* studies. For example, isolated mouse islets show an average time of response of 301.2s ± 42.1s SD, to peak after stimulatory glucose is added (from 0mM to 10mM glucose) (Zhang et al., 2003). Similarly, in pancreatic tissue slice-recordings, it has been reported that the median time of delay from the time the stimulatory glucose is added to the first cell to respond is 93s (from 6mM to 12mM glucose) (Stozer et al., 2013). As expected, our results matches more closely *in vivo* models with active blood flow, such as the calcium dynamics recorded in islets transplanted in the anterior chamber of the mouse eye (ACE). Indeed, using the ACE *in vivo* system, Jacob *et al.*, reported that mouse islets present a time of response of 12 seconds after a glucose injection into the tail vein (0.4g of glucose per mouse kg) (Jacob et al., 2020).

Upon glucose stimulation, the islet response seemed to be initiated

in one or two β-cells (average=1.5 cells, *n*=8, STD=0.53). We refer to these β-cells as “leaders”. In support to the idea that the response is initiated in leader β-cells, we found a mild positive correlation between the time of response for individual cells and their distance from the leader (*n*=5, R^2 =0.57 ± 0.2 STD) (Figure 8). Also, we found similar results employing the *neuroD1* promoter, which drives the expression of GCaMP6f uniformly in all endocrine cells of the zebrafish pancreas. In this model, we also observed a mild positive correlation between the time of response for individual cells and their distance from the first responder (*n*=3, R^2 =0.6 ± 0.2 STD) (Figure 9). Finally, similarly to our 2D data, 3D recording of glucose injection showed the presence of initiating cells: one or two cells (average=1.6 cells, *n*=3, STD=0.57) responded first to the glucose injection with an average time lag from the first to the last cell of 7.7s (*n*=3, mean = 7.7s ± 3.6s STD) (Figure 10 e-f). The 3D analysis also revealed a positive correlation between the time of response and the Euclidean distance calculated from the centroid of the nuclei from the leader cell (*n*=3, R^2=0.46 ± 0.28 STD). In the case that two leader cells were present, the cells were divided in two groups based on the nearest leader cell, then we plotted the time of response vs the distance and calculated the R^2 for each group. To compare the islets having two leader cells with those having only one, we averaged the R^2 values of the former and compared them to the latter. Since our measurements from both 2D and 3D imaging are very consistent with each other, we concluded that our data is representative of the overall islet behavior.

We assessed whether the difference in time of response of individual β-cells could be due to differences in glucose access, rather than a genuine functional heterogeneity. However, by monitoring the glucose diffusion rate using the fluorescence glucose analogue 2-NBDG, we found that it takes less than 500 milliseconds to cover all the cells on a plane (*n=5*) (Figure 10) (Zou et al., 2005). This rapid diffusion seems to be comparable to mouse islets imaged in the ACE where, after a tail vein injection of 2-NBDG, it takes 2 seconds to cover completely the islet, while the glucose response in terms of the calcium peak takes around 12s. Thereby, in both models the glucose diffusion into the islet occurs faster than the calcium response (Jacob et al., 2020). Still, remains open the critical question whether the first responder cells are the cells to be

exposed first to glucose. Due to the vast overlap in the fluorescent spectra of GCaMP and 2-NBDG, we could not co-inject glucose and 2-NBDG while simultaneously recording the Ca^{2+} response and the pattern of glucose diffusion into the islet. This question might be better addressed using a combination of our new transgenic line expressing the red calcium indicator K-GECO1 and 2-NBDG. If the cells follow the same pattern as the glucose diffusion through the islet, it would suggest that blood flow is the key factor dictating the Ca^{2+} response pattern. On the other hand, if they do not follow the glucose pattern of islet diffusion, it would suggest a functional heterogeneity. Indeed, we already started such experiments and the preliminary data indicate that the pattern of glucose diffusion into the islet visualized by the 2-NBDG injection does not seem to match the pattern of β-cell activation, as visualized with the calcium indicator K-GECO1 (data not shown).

5.3. Leader β-cells coordinate Ca^{2+} influx *in vivo*

Previous studies of β-cell coordination in the mouse showed the existence of a subpopulation of β-cells referred to as hub-cells. These hub cells tend to present calcium activity before the rest of the population, serving as pacemakers, which dictate the glucose response of the rest of the β-cells (Johnston et al., 2016). To evaluate if the first responders found in our model might mirror the hub β-cell function to coordinate the rest of the β-cells, we performed *in vivo* single-cell laser ablation, employing 2-photon ablation (Figure 11). We found that the laser-ablation of follower cells had no significant effect on the subsequent Ca^{2+} spikes, while the ablation of leader cells reduced significantly the Ca^{2+} response (Figure 11c). It must be noted that not in all cases the ablation of a presumptive leader cell led to a silencing of the rest of the imaged cells. In some cases (7/20), only one region on the islet was silenced, showing activity in another area, whereas in a few cases (3/20), there was no reduction in the response. This could be due to several reasons: a) there are more than one cell that may coordinate the islet response; b) in our 2D recording, we were in the wrong plane and did not find the true the leader cell; c) we targeted the wrong cell since we identified the

presumptive leader *in situ* by “eye” observation.

Similarly to the zebrafish, mouse islets imaged in the ACE of mice present β-cells, which fire first during Ca^{2+} pulses across the islet. These first responders β-cells in the mouse were always the first to fire when a second or third burst was detected, but not always in the fourth or fifth burst. Interestingly, using Granger causality analysis it was shown that these first responders were always the most highly connected. The Granger causality analysis was developed in the field of econometrics and is a statistical tool to define the causality of the events (Stokes and Purdon, 2017). This suggests that those β-cells that fired first are causally linked to the activity of the rest of the β-cells, i.e. they coordinate the rest of the β-cells. These first responders in the case of mouse islets might be an analogous population to the leader β-cells found in the zebrafish islet and both subpopulation resemble the *in vitro* identified hub-cells due to their capacity to coordinate the calcium dynamics of the rest of the β-cells (Salem et al., 2019).

Since our laser ablation experiments were performed in a relative short window of time (<30min) after the cell ablation, a very important question remains to be answered. Specifically, we need to define how long it takes for the islet to recover its normal response to a glucose stimulus in terms of Ca^{2+} influx after leader cell ablation. If the islet recovers within a few hours, it would mean that the leader β-cell can be replaced by other cells. On the other hand, if the islet requires days to recover, this would imply that leader β-cells might be a critical subpopulation of β-cells.

Another important open question is to define how stable the leader cell is under unperturbed conditions. To be able to address this question, a strategy for lineage tracing is required. Instead of general methods such as Cre-loxp system which label most of the cells, a more spatially precise system is needed. The mEos2 is a green-to-red photoconvertible protein and can be fused to the histone H2B, targeting the nucleus, and making the labeling very stable even after cell division (McKinney et al., 2009). Thus, the generation a transgenic zebrafish lines, expressing the mEos2-H2B under the insulin promoter could be an excellent tool to precisely

photo-label any β-cell *in vivo*. Theoretically, Ca^{2+} imaging and photo-labelling of the leader cell, followed by repeated evaluation through several days would allow to answer the question if the leader cell is stable or not. If the leader cell is not stable and other cells take over this role during this time, it would suggest that this phenomenon might reflect a non-cell autonomous property driven by the immediate microenvironment, for example by the innervation, blood flow or glucose access. On the other hand, if the leader cell remains stable over several days even as the islet grows and the number of β-cells increases, it would suggest that this phenotype reflects a cell-autonomous mechanism. Thus, a combination of functional and longitudinal studies is required to answer this important question.

5.4. β-cell optogenetic interrogation shows heterogeneous potential of individual β-cells for islet coordination

Optogenetics, or "light-driven" actuators allow functional interrogation with high temporal and spatial precision. These tools can target genetically defined cell populations, thus, allowing precise cellular interrogation. The archaeal inhibitory chloride pump halorhodopsin (NpHR), which is activated by yellow light (λ = 560–590 nm) has been successfully applied for optical manipulation of neuronal activity and β-cells (Johnston et al., 2016; Nagel et al., 2003; Zhang et al., 2007). Thus, we generated a transgenic zebrafish line expressing the eNpHR3.0 under the insulin promoter and we showed that it is possible to inhibit the β-cell response to a glucose bolus *in vivo* (Figure 14).

After showing that it is possible to reversibly silence the β-cells *in vivo*, we performed single-cell optogenetic interrogation. We tested if the inhibition of first responders would be sufficient to silence the rest of the β-cells. Since we only recently developed this system, we have so far collected only a limited number of good quality movies from which we can derive preliminary results. In one of these few examples (1/3), we found that leader-cell optogenetic inhibition silenced most but not all of the β-cells. In contrast, the optogenetic silencing of a follower cell had no major

effect in the response of the rest of the β-cells. This variability shows that in some islets there could be more than one leader-cell capable of coordinating other β-cells. However, we propose that the "secondary" leader might be less capable of coordination the islet response as compared to the "primary" leader cell (Figure 15c). Alternatively, in the presence of two or more leader cells in an islet, each cell might be responsible for coordinating a group of cells, such that the inhibition of one cells does not completely shut down the whole islet. Besides this, the silencing of follower cells via NpHR did not interfere with the response of the rest of the β-cells.

The next question we addressed was if the leader β-cells can directly activate follower cells. One possibility to answer this question is using the light-sensitive cation pump channelrhodopsin-2 (ChR2). Theoretically, the ChR2 could trigger depolarization under blue illumination (λ = 488) of the leader cells, allowing us to evaluate if the leader cells can effectively recruit follower cells. However, the activation spectra of ChR2 and GCaMP overlap, therefore, we opted to use the red-light channelrhodopsin from Chlamydomonas noctigama (ChRimson). We generated a transgenic zebrafish line expressing ChRimsonR under the insulin promoter. In our preliminary results, the activation of follower cells produced an increase in the GCaMP signal in the targeted cell but poor activation outside of the illuminated area (Figure 16b). Meanwhile, the optogenetic activation of the leader-β-cell led to an increase in GCaMP signal similar to the one produced by a glucose stimulus by co-activating most other cells in the plane (Figure 16c). It must be noted that combining the ChRimson activation system with the GCaMP sensor presents a caveat: the ChRimson presents around 10% activity in blue light (λ = 488) (Oda et al., 2018). A cleaner system, i.e. a system without wavelength crosstalk of activation and imaging will be more desirable to rigorously probe this model of activation.

Indeed, in this thesis, we developed another system for β-cell interrogation via optogenetic activation. Since the most sensitive and well-characterized channelrhodopsins occupied the blue-green spectra, we generated transgenic lines expressing Red-based GECIs jRGECO1a, JRCaMP1a and K-GECO1 under the zebrafish insulin promoter. We

evaluated each transgenic line *in vivo* and we found that the jRCaMP1a and K-GEKO1 presented detectable changes in fluorescence after glucose injection, while the jRGECO1a did not work *in vivo* (Figure 13). Next, we cloned the blue shifted channelrhodopsin CheRiff. The CheRiff channelrhodopsin requires 9-fold lower light intensities in comparison to ChR2, and does not present activation in light above of 550 nm (Hochbaum et al., 2014). Thus, we combined the optically orthogonal system of the red-GECI K-GECO1 and the blue actuator CheRiff. As expected, the optogenetic activation of the β-cells via CheRiff showed a substantial influx of Ca^{2+} into the β-cells recorded (Figure 17a). Thus, the K-GECO1/CheRiff system can be used for *in vivo* single-β-cell optogenetic interrogation.

After corroborating the possibility to activate the β-cells *in vivo,* we interrogated individual β-cells. Interestingly, we found heterogeneous capability of the β-cells to activate neighbor cells. In the example shown in Figure 17c, one of the interrogated β-cell was capable to activate all the rest of the β-cells (Figure 17c). This suggests a possible hierarchy in leader β-cells: while most of these cells can only recruit few cells, a special subpopulation of β-cells might have the potential to activate most of the β-cells in the zebrafish in plane.

The preliminary results using eNpHR, ChRimson and CheRiff single β-cell interrogation suggest that individual β-cells present heterogeneous capabilities to coordinate other β-cells *in vivo.* This is congruent with previous reports using the optogenetic inhibitor eNPHR in isolated islets from mouse. Johnston *et al.* showed that optogenetic electrical silencing via halorhodopsin (NpHR) of a particular subpopulation of β-cells was enough to impair Ca^{2+} coordination across the mouse isolated islets. The hub cells, in comparison to other β-cells, were characterized by high levels of glucokinase (GCK), two to fivefold lower expression of insulin, Pdx1 and Nkx-6.1, reduced expression of sarcoplasmic reticulum Ca2+/ATPase (SERCA2) and hyperpolarized mitochondria (Johnston et al., 2016). Along similar lines, Westacott *et al.,* using the optogenetic activator ChR2, reported that optogenetic activation in around 5% of β-cells triggered substantial activation of the islet outside the area used to activate single cells. They even suggest that areas of β-

cells with the highest oscillatory frequencies of NAD(P)H could be playing a major role governing the oscillatory frequencies and matching to the areas of initiating Ca^{2+} waves propagation (Westacott et al., 2017). Whether the herein identified leader cells are an analogous entity to the *in vitro* identified hub cell subpopulations needs to be addressed. Therefore, the next steps in the characterization of the leader β-cells could comprise a careful topological/immunohistochemistry characterization. For this purpose, the mEos2 photoconvertible tools could be implemented to photo-label the leader β-cell and then quantify the expression of different proteins. This would address if the leader β-cell is defined by the cell neighborhood, blood flow access, and axonal innervation from the peripheral nervous system.

Our study does not address the question on how the crosstalk between leader and follower cells is achieved. One tentative explanation is that leader β-cells activate the follower cells through Connexin-mediated Gap junctions. In support to this idea, it has been shown that isolated islet from $Cx36^{-/-}$ mice, show very low and irregular Ca^{2+} oscillations, without the characteristic synchronicity upon glucose stimulation (Ravier et al., 2005). Indeed, $Cx36^{-/-}$ mice were shown to lack a proper first and second phase of insulin secretion (Head et al., 2012). It is not unrealistic that Gap junctions might be involved in zebrafish β-cell coordination. Interestingly, specific connexin combinations in zebrafish neuronal networks can drive polarization in cell coupling. Fasciani, *et al.* showed that the heterotypic channel formed by the connexins Cx47 and Cx43 had selective directional cationic permeability and voltage-gating properties and allowed for unidirectional flow of ions and larger molecules between coupled oligodendrocyte and astrocyte cells (Fasciani et al., 2018). Interestingly, from zebrafish β-cells mRNA sequencing experiments, we have detected the expression of several Cx36-like proteins, particularly the expression of the *gjd2/cx35.5* and *gjd1a/cx34.1*, that share ≥85% amino acid identity to themselves and to the mammalian Cx36 proteins (Delgadillo-Silva et al., 2019; Miller et al., 2017). Thus, it is plausible that the leader β-cells might activate the follower β-cells by Gap junction-mediated mechanisms. For exploring the possibility whether the leader β-cells actively coordinate the follower cell through Gap junctions, and whether homo and heterotypic channels might play a role in

directionality of activation, the generation of *gjd2a/cx35.5* and *gjd1a/cx34.1* knock-out lines and reporters is required.

Finally, during this work, the most important limitation is that we have no genetic signature or marker to label the leader β-cells. To define markers, single-cell sequencing might be employed after labeling the leader β-cells, employing for example the mEos2 photoconvertible tool. The mRNA profile can be used to establish specific markers for leader β-cells. However, this approach is impractical since such maneuver would require the in-situ identification of the leader β-cells and then their retrieval for cell sequencing. A feasible alternative would be to evaluate different possible markers such as glucokinase expression, insulin content, or NAD(P)H levels (Johnston et al., 2016; Westacott et al., 2017). So far, we were limited to inject glucose and detect *in situ* by "eye" observation which cells were the first to respond to a glucose stimulus. Thus, if a reliable marker is established, new questions can be addressed. Furthermore, we were restrained to early stages of zebrafish development. Therefore, we do not know if the β-cells present these characteristics at later stages of the zebrafish. We are currently initiating imaging in much older and feeding animals, in which the islet has a comparable size to medium-sized mouse or human islets.

Several questions are now open: Is the leader β-cell a cell autonomous property? Are the Ca^{2+} waves propagated through connexins similarly to mouse islets? What is the relationship of the leader cell position relative to nerves, blood vessels and other islet cell types? Further studies are also required to determine whether leader β-cells function is altered under metabolic stress or in pathogenic conditions such as diabetes.

In summary, our data shows that β-cells present constant Ca^{2+} activity *in vivo*, and that this activity is systemically influenced and required for proper glucose control. Also, our data suggest that *in vivo*, the β-cells coordinate their function through temporally defined leader cells. The leader cell serves as an initiating point, and seems to help propagate the calcium wave through the islet by recruiting follower cells in response to a glucose stimulus (Figure 18). Moreover, we introduced new

methodologies for *in vivo* silencing of the β-cells via NpHR. We also presented preliminary results showing that the optically orthogonal system of the red calcium indicator K-GEKO1 and the blue-shifted channelrhodopsin CheRiff can be used *in vivo*. Altogether, our preliminary data provides a new frame of work and insights into the labor division within the islet *in vivo*, reinforcing the importance of β-cell heterogeneity for islet function. The paradigm here developed, to study the roles of individual cells in terms of Ca^{2+} coordination within the functioning islet may be applicable for other tissues where coordination is crucial for proper function.

(Figure text is in the next page)

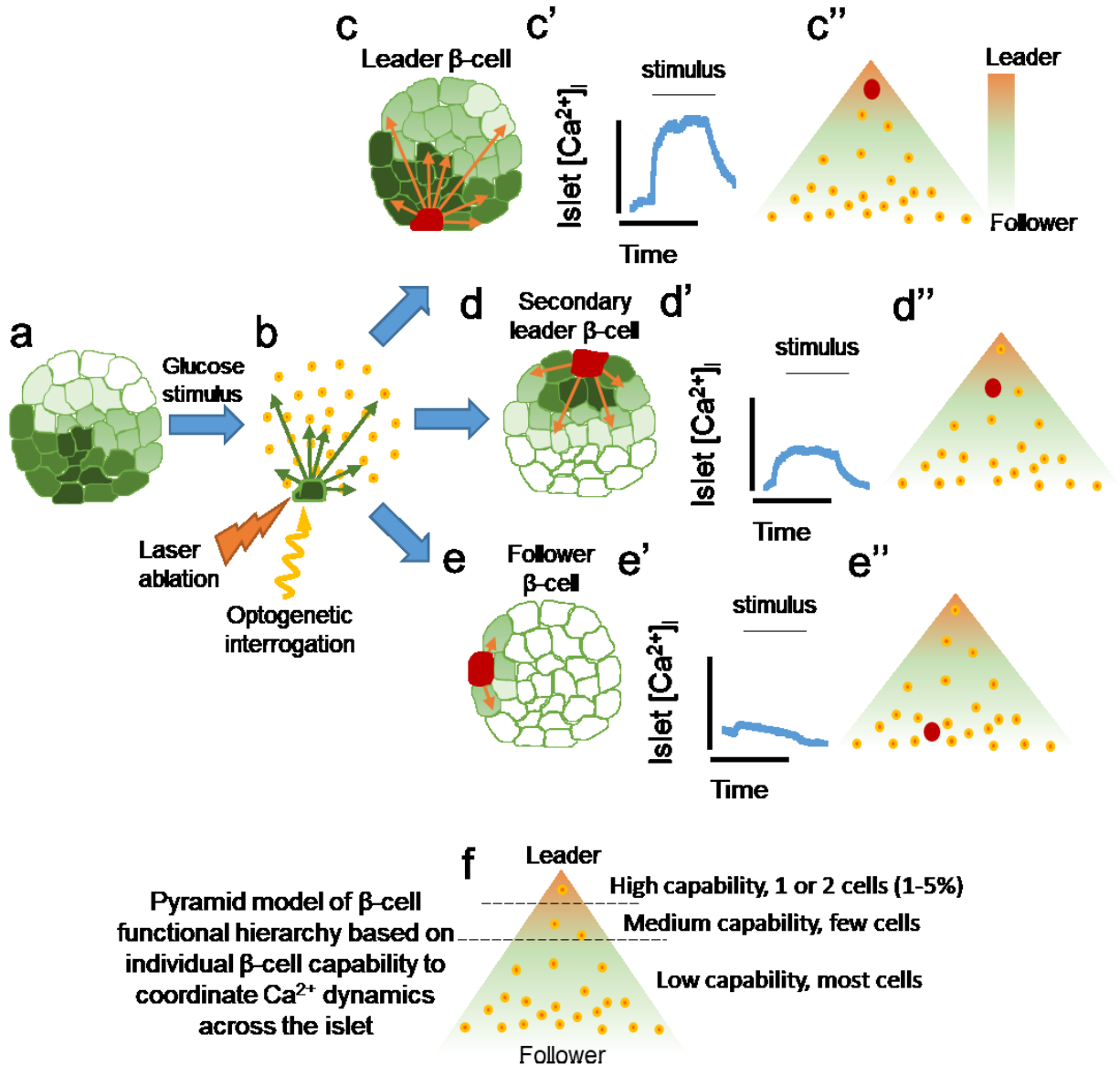

Figure 18. Model of β-cell Leader-to-follower coordination of Ca^{2+} dynamics *in vivo*. **a.** The islet must coordinate its activity to secrete the proper amounts of insulin. **b** The functional characterization via laser-ablation and optogenetic interrogation led us to propose a hierarchical model of β-cell coordination. The coordination involves primary and secondary leader cells at the top of the hierarchy, as well as follower cells at the bottom. **c**. The primary leader β-cell occupies the highest rank in the functional hierarchy, as being capable to coordinate Ca^{2+} activity across many cells. **d**. Secondary leader β-cells present medium to low capability to coordinate other β-cells. **e**. Most of the β-cells are followers since they present low capability to recruit other β-cells. (**c'**,**d′**,**e′**) Proposed theoretical traces of Ca^{2+} influx after activation of a primary leader, secondary leader and follower β-cells. (**c''**,**d″**,**e''**). Pyramid model showing the position into the hierarchy as expected from a leader, secondary and follower β-cells. **f**. Pyramid model illustrating the descending hierarchy model with one or two leader β-cell on the top level, few secondary leader β-cells in the second level, and most of the β-cells on the bottom level as follower β-cells.

6. Materials and methods

Sections of this chapter have been adapted from the following publication:

Victoria Salem, Luis Delgadillo Silva, Kinga Suba, Eleni Georgiadou, S. Neda Mousavy Gharavy, Nadeem Akhtar, Aldara Martin-Alonso, David C. A. Gaboriau, Stephen M. Rothery, Theodoros Stylianides, Gaelle Carrat, Timothy J. Pullen, Sumeet Pal Singh, David J. Hodson, Isabelle Leclerc, A. M. James Shapiro, Piero Marchetti, Linford J. B. Briant, Walter Distaso, Nikolay Ninov & Guy A. Rutter (2019). Leader β-cells coordinate Ca^{2+} dynamics across pancreatic islets *in vivo*. Nature Metabolism.

6.1. Zebrafish strains and husbandry

Zebrafish wild type (WT) AB, WIK and TL were used in all the experiments. Zebrafish were raised in standard conditions at 28 °C. The previously established transgenic lines used in this study were *Tg(ins:GCaMP6s;cryaa:mCherry)* (Singh et al., 2017), *Tg(ins:cdt1-mCherry;cryaa:GFP)* (Ninov et al., 2013), *Tg(gata1a:DsRed)* (Traver et al., 2003) and *Tg(nrd:GCaMP6f)* (Rupprecht et al., 2016). We utilized the *Tg(ins:cdt1-mCherry)* in preference of a pan β-cell marker such as *Tg(ins:mKO-nls),* this allowed a clear separation of the spectra and simultaneous signal recordings from the GCaMP and mCherry channels, which was particularly important during fast imaging. All experiments were carried out in compliance with European Union and German laws (Tierschutzgesetz) and with the approval of the TU Dresden and the Landesdirektion Sachsen Ethics Committees (approval nos: AZ 24D-9168,11-1/2013-14, TV38/2015, T12/2016, and T13/2016, TVV50/2017, TVV 45/2018, and TVV33-2019). In this study, all live imaging in vivo, compound and glucose injections, as well as experimental procedures were performed with zebrafish larvae that did not exceed the 5-dpf stage, as stated in the animal protection law (TierSchVersV §14). According to the EU directive 2010/63/EU, the use of these earlier zebrafish stages reduces the number of experimental animals, according to the principles of the 3Rs.

6.2. Transgenic lines generation

For the construction of the *Tg(ins:eNPHR3.0-mCherry; cryaa:CFP)* and *Tg(ins:ChRimsonR-mRuby2;cryaa:CFP)* lines, we used PCR amplification with primers designed to introduce 5' EcoRI and 3' PacI restriction enzymes sites in the cDNAs for eNPHR3.0-mCherry and ChRimsonR-mRuby2. A previously established plasmid backbone containing ins:mKO2-zCdt1; cryaa:CFP (Ninov et al., 2013) was digested with EcoRI/PacI and eNPHR3.0-mCherry and ChRimsonR-mRuby2 were ligated using the EcoRI/PacI sites.

For the construction of ins:jGECO1a;cryaa:mCherry, ins:jRCaMP1a;cryaa:mCherry and ins:K-GECO1;cryaa:mCherry plasmids, we used PCR amplification with primers designed to introduce 5' EcoRI and 3' PacI restriction enzymes sites in the cDNAs. The established plasmid backbone containing ins:mAG-zGeminin; cryaa:mCherry (Ninov et al., 2013) was digested with EcoRI/PacI and jGECO1a, jRCaMP1a and K-GECO1 were ligated using the EcoRI/PacI sites.

For the construction of ins:ChR2-GFP;cmcl2:GFP, and ins:CheRiff-GFP;cmcl2:GFP plasmids, we used PCR amplification with primers designed to introduce 5' EcoRI and 3' PacI restriction enzymes sites in the cDNAs. First, the established plasmid backbone, containing ins:mKO2-zCdt1; cryaa:CFP (Ninov et al., 2013) was digested with KpnI to remove the Cryaa promoter and the CFP. Then, we amplified the 244 minimal cmcl2 zebrafish heart promoter flanked with 5' KpnI and 3' HindIII (Huang et al., 2003), we also amplified GFP flanked with 5' HindIII and 3' SpeI, and also, we included the bGH poly(A) signal flanked with 5' SpeI and 3' KpnI. We ligated the 3 products in a single reaction, to create the plasmid containing ins:mKO2-zCdt1; cmcl2:GFP. Then the plasmid ins:mKO2-zCdt1; cmcl2:GFP, was digested with EcoRI/PacI and ChR2-GFP and CheRiff-GFP were ligated using the EcoRI/PacI sites.

All the constructs were flanked with I-SceI sites to facilitate transgenesis. Several founders were screening and founders with Mendelian segregation were selected for each transgenic line. These

lines were used in all further experiments.

6.3. Glucose measurements

For glucose measurements, groups of 10 anesthetized larvae were pooled together in a 1.5mL capped tube, then all liquid removed and snap frozen in liquid nitrogen. The larvae were stored at -80°C until used. Following thawing on ice, 250 µL of PBS were added, and then the larvae were sonicated with an ultrasonic homogenizer (Bandelin, SONOPLUS). Glucose concentration was determined using the BioVision Glucose Assay Kit (Biovision Inc, California, US) according to the manufacturer's instructions.

6.4. Pericardial injection of glucose and insulin

Injections were performed using pulled glass pipettes with a 5nL tip volume calibrated microscopically (3.5'' Drummond #3-000-203-G/X, Sutter pipette puller P-1000). A pneumatic pico-pump (FemtoJet, Eppendorf) was employed with the following parameters: injecting pressure 500 hPa and compensation pressure of 0 hPa, 1 second injection. The capillary was introduced into the pericardial cavity in the agarose-mounted larva, assisted by a micromanipulator (InjectMan N2, Eppendorf). Doses were 5 nL of 25 mM glucose and 5 nL insulin at 100 units/ml.

6.5. Live imaging

Embryos were treated with 0.003% (200 µM) 1-phenyl 2-thiourea (PTU) to inhibit pigmentation from 24hpf onwards. At 4.5 dpf, the larvae were anaesthetized using 0.4g/L Tricaine. The larvae were mounted in glass-bottomed microwell dishes (MatTek corporation) using 1% low-melting agarose containing 0.4g/L Tricaine. After the agarose was solidified, the dishes were filled with embryonic fish water and 0.4g/L Tricaine. Live imaging was performed on an inverted laser scanning confocal system ZEISS LSM 780 inverted with a C-Apochromat 40X/N.A. 1.2 water correction lens. In the *Tg(ins:GCaMP6s);Tg(ins:cdt1-mCherry)*

double-transgenic animals, we acquired the GCaMP6s and mCherry signals simultaneously using the 488nm and 561nm laser lines. The GCaMP6s signal was rendered in green and the nuclear signal in red. Videos were recorded at a 10 s/image (0.1 Hz) frame rate, unless indicated otherwise, with a Z-step thickness of 1.2 µm, covering on average 35 µm, and an XY resolution of 0.12 µm per pixel (512x512 pixels). Laser power was maintained as low as possible (<1.5%) to decrease phototoxicity. For faster imaging, we focused on a single plane, recording a frame every 150 milliseconds with an XY resolution of 0.08 µm per pixel (512x512 pixels).

6.6. Fast whole islet live imaging

Embryos were mounted as described in Live imaging section. Videos were recorded at ~0.8 Hz per Z-stack (~700µm3), with a Z-step thickness of 4.5 µm, covering on average 70 µm in depth, and an XY resolution of 0.24 µm per pixel (256x256 pixels). This imaging speed and volume was achieved using the resonant scanner technology with an inverted laser scanning confocal system (Leica SP5 MP), using an IRAPO L 25X/N.A. 0.95 water lens. The resonant scanner was set at 8,000 Hz with a bidirectional line scanning in order to achieve maximum speed.

6.7. Selective two-photon laser ablation of leader cells in the zebrafish islet.

Live imaging and intra-cardiac glucose injections were performed as described above using *Tg(ins:gCaMP6s;cryaa:mCherry), Tg(ins:cdt1-mCherry;cryaa:GFP)* larvae. Images were captured across a single confocal plane at an imaging acquisition rate of 6 frames/second (6Hz) or 150miliseconds per image. We performed three independent injections of glucose, separated by 5 min. intervals. The “leader cell” (that is the temporally-defined first responder) was identified by eye based on the changes in gCaMP6s-fluorescence after each glucose-injection. The larvae were then transferred to a Leica SP5 MP confocal microscope, equipped with a two-photon laser and 25×/0.95 N.A objective. A region of interest was selected encompassing the center of the nucleus of the cell

to be ablated, covering a circle with an approximate diameter of 0.5 μm. The cell of interest was then exposed to two-photon laser irradiation at the output power of 2.0 W (λ = 800 nm) for 5 s to minimize possible damage to other areas. We then performed live imaging and intra-cardiac injection again, using the protocol described above. All procedure was done within 20 min after the laser irradiation, to record the response following cell ablation. Control cells that were not the temporally-defined leader ("followers") were ablated with the same methodology as leader cells.

6.7. Selective one-photon optogenetic interrogation of β-cells in the zebrafish islet.

Live imaging and intra-cardiac glucose injections were performed as described above using the following *Tg(ins:gCaMP6s;cryaa:mCherry); Tg(ins:eNpHR3.0-mCherry;cryaa:CFP)*, *Tg(nrd:GCaMP6f); Tg(ins:ChRimsonR-mRuby2;cryaa:CFP)* and *Tg(ins:K-GECO1;cryaa:mCherry);Tg(ins:CheRiff-GFP;cmcl2:GFP)* double transgenic larvae. Images were captured across a single confocal plane at an imaging acquisition rate of 6 frames/second (6Hz) or 150miliseconds per image. We performed 1 injection of glucose to record the response to a glucose stimulus for each animal. The "leader cell" (that is the temporally-defined first responder) was identified by eye based on the changes in GCaMP6-fluorescence after the glucose-injection. The larvae were imaged into a Leica SP5 MP confocal microscope, equipped with a roi-scan and 25×/0.95 N.A objective. A region of interest was selected encompassing the center of the nucleus with an approximate diameter of 10 μm. A baseline for GCaMP signal was acquired in the first 7.5s or (50 frames) before the optogenetic interrogation was performed. The cell of interest was then exposed to a 1-photon laser with 5% of laser power (λ = 561 nm) for about 45s (300frames), while the Ca^{2+} dynamic were simultaneously recorded. After the laser was turn off, another 22.5 s (150frames) were recorded. Control cells that were not the temporally-defined leader ("followers") were ontogenetically interrogated with the same methodology as leader cells. For whole islet activation, the laser line (λ=561) for the *Tg(ins:gCaMP6s;cryaa:mCherry); Tg(ins:eNpHR3.0-*

mCherry;cryaa:CFP), and (λ=470) for the *Tg(ins:K-GECO1;cryaa:mCherry);Tg(ins:CheRiff-GFP;cmcl2:GFP)* double transgenic larvae was activated in the whole plane with a lase intensity of 1%.

6.8. Islet blood flow imaging

Imaging of islet blood flow was performed using triple transgenic larvae *Tg(ins:GCaMP6s);Tg(ins:cdt1-mCherry);Tg(gata1a:DsRed)*. *Tg(gata1a:DsRed)* reporter was used as a marker of red blood cells. Live imaging was performed on a ZEISS LSM 780 confocal microscope equipped with a C-Apochromat 40X/1.2 NA water correction lens. The GCaMP6s and mCherry signals from β cells, and DsRed signals from blood cells, were simultaneously acquired using the 488nm and 561nm laser lines. The GCaMP6s signal was rendered in green. The blood cells and the nuclear signal of β cells were rendered in red. We focused on a single plane and the videos were recorded at a frame rate of 1 frame/150 milliseconds (6 Hz).

6.9. Mechanical heart stop

To stop the blood flow in zebrafish larvae, a glass-pulled pipette (3.5'' Drummond #3-000-203-G/X, Sutter pipette puller P-1000), with a manually blunted end, was used to exert a direct pressure into the heart. The heart was blocked for around 400s. The mechanical heart stopping was executed simultaneously to live Ca^{2+} imaging in the *Tg(ins:GCaMP6s);Tg(ins:cdt1-mCherry)* double-transgenic larvae, as described above. Videos were recorded at a 10 s frame rate (0.1 Hz), and a Z-step thickness of 2.8 µm, covering on average 50 µm, with a resolution of 0.83 µm per pixel (512x512 pixels).

6.10. Immunostaining

Larvae fixed in 4% PFA overnight were permeabilized in 1% PBT (Triton-X-100) and blocked for 2hrs in 4% PBTB (BSA). Skin were dissected to expose the pancreas. Primary and secondary antibody

staining's were performed overnight at 4 °C. Primary antibodies were anti-Insulin (Guinea Pig from DAKO 1:200), anti-mCherry (Rabbit abcam ab167453, 1:200). Secondary antibodies were Alexa Fluor 488 anti-guinea pig (1:200); Alexa Fluor 561 anti-rabbit (1:200). Nuclear staining was performed using DAPI 1:1000. Samples were mounted in Vectashield. Images were acquired using Z-Stacks on a LSM-780 Zeiss confocal microscope.

6.11. TUNEL assay

After the live imaging was performed, and the leader cells were ablated, the larvae were immediately fixed in 4% PFA overnight. In order to detect DNA damage, we employed Click-iT® TUNEL Alexa Fluor 647 kit (Invitrogen: C10247). Briefly, larvae were dissected to expose the pancreas, then the larvae were permeabilized with 1% PBT (Triton-X-100) for 1hr. Larvae were dehydrated using serial incubations of 5min with 25%, 50%, 75% and 100% MetOH in PBT. Then placed at -20°C for 1hr. The larvae were rehydrated following 5min serial incubations of 75%, 50%, 25% and 0% MetOH in PBT. Larvae were treated using 1µg/mL proteinase K at room temperature for 1hr. The proteinase K was neutralized by washing the larvae with PBTB (PBT 4%BSA and 1%DMSO) and then PBT (3X20min). Larvae were then fixed again with 4% PFA for 30min at RT, then washed with PBT and incubated in acetone/ethanol (1:2) at -20°C for 1hr. We performed terminal deoxynucleotidyl transferase dUTP nick end labeling (TUNEL) to detect β-cell DNA damage using the Click-iT® TUNEL Alexa Fluor 647 kit (Invitrogen: C10247). TUNEL detection was performed according to the kit protocol. To detect insulin and mCherry signal, which are quenched following the Click-iT®reaction, we performed antibody staining using anti-mCherry and anti-insulin as described in the immunostaining section. Nuclear staining was performed using DAPI 1:1000. After the immunostaining, the samples were mounted in Vectashield. Images were acquired using Z-Stacks on a LSM-780 Zeiss confocal microscope. For image analysis, the nuclei of the β cells were segmented using the DAPI channel.

6.12 Image analysis of GCaMP6s fluorescence intensity from *in vivo* imaging.

The cumulative population response of β cells was quantified from maximum intensity projections (MIP) of the z-stack. In the MIP, the islet area was delimited manually using the Region of Interest (Johnston et al.) Manager in ImageJ (https://imagej.net/Fiji). Using the ROI, the fluorescence intensity of GCaMP6s was extracted. The fluorescence intensity was normalized for the whole imaging time using the following formula:

$$(F_T – F_{MIN}) / (F_{MAX} – F_{MIN}),$$

were F_T is the fluorescence intensity at a given time while F_{MAX} and the F_{MIN} are the maximum and minimum values recorded during the live imaging session, respectively.

Single-cell signal analysis of GCaMP signal was performed either from single-confocal slices covering a majority of imaged β cells (2D) or by segmenting the nuclei from the Z-stacks using the nuclear mCherry signal in 3D images. For nuclear segmentation, we utilized the 3D image suite in Image J, and the 3D iterative thresholding plugin (Ollion et al., 2013). The following parameters were set based on the estimated approximate nuclear size of β cells: minimum volume = 100 pixels; maximum volume = 1200 pixels; criteria method = “volume”; threshold method = “volume”; value method = 10 units. This generated a voxel covering the nuclei of β cells. Using the 3D ROI manager plugin, we extracted the fluorescence intensity from each voxel over time (Schindelin et al., 2012). Plots, we first extracted the centroids from each voxel and then plotted them using the R software and the package “rgl”. Single-cell heat-maps based on 2D analysis were created using Excel and conditional formatting setting the colors in a gradient from 0 to 1.

6.13 Quantification of GCaMP6s fluorescence intensity

For the quantification of changes in GCaMP6 fluorescence upon glucose or insulin injection, the cumulative response of all imaged β-cells

to glucose injection was quantified. To this end, we compared the area under the curve based on the normalized fluorescence intensity 10 frames before and after the injections of glucose or insulin (covering 200 seconds of imaging) using the formula:

$$(F_T – F_{MIN}) / (F_{MAX} – F_{MIN}),$$

For the quantification of changes in GCaMP6 fluorescence upon laser-cell ablation (Figure 4), the cumulative response of all imaged β cells to glucose injection was quantified. In this case, the maximum value (F_{MAX}) was not used for normalization since such normalization could mask the effect of loss of response following cell ablation due to normalization to background fluorescence. Instead, we only subtracted the background from the imaging session using the following formula:

$$(F_T – F_{MIN}) / F_{MIN},$$

The larvae were injected with three separate pulses of glucose before and after the ablation. For each injection the GCaMP area under the curve was calculated covering 200 frames after the glucose injection. The average area under the curve was calculated before and after the ablation and plotted as log2.

6.14 Spatial drift correction images.

The red channel (cdt1-mCherry) signal from the β cell nuclei was used to correct for spatial drift in the green GCaMP6s channel. A maximum projection of each Z-stack in the time series was entered into the FIJI plugin “Descriptor-based series registration (2d/3d + t)” (https://imagej.net/Descriptor-based_registration (2d/3d)), applying the model “Rigid (2d)”, with “3-dimensional quadratic fit” (Schindelin et al., 2012). A sigma of 13 and threshold of 0.03 was applied to the detection of nuclear signal, with a minimum number of three neighbors, redundancy of 1 and a random sample consensus (Ransac) error of 5. Matching across time series was achieved using global optimization, unless indicated otherwise. Stabilization in the Z dimension was achieved using the Fiji “Reslice” command. The “Descriptor-based series registration

(2d/3d + t)" plugin was used with nuclei detection sigma set to 5 and with a threshold of 0.03.

6.15 Statistical analysis

Statistical significance between two conditions was assessed using paired or unpaired Student's t-test. Interactions between multiple conditions were determined using one- or two-way ANOVA (with Tukey's or Bonferroni posthoc tests). Analyses were performed using Graph Pad Prism (GraphPad Software version 7.0) and significant p-values are described in each relevant section. Values are plotted as mean ± STD, unless otherwise stated.

7. References

Ackermann, A.M., and Gannon, M. (2007). Molecular regulation of pancreatic beta-cell mass development, maintenance, and expansion. J Mol Endocrinol *38*, 193-206.
Ackermann, A.M., Wang, Z., Schug, J., Naji, A., and Kaestner, K.H. (2016). Integration of ATAC-seq and RNA-seq identifies human alpha cell and beta cell signature genes. Mol Metab *5*, 233-244.
Ahmed, A.M. (2002). History of diabetes mellitus. Saudi Med J *23*, 373-378.
Akerboom, J., Carreras Calderon, N., Tian, L., Wabnig, S., Prigge, M., Tolo, J., Gordus, A., Orger, M.B., Severi, K.E., Macklin, J.J.*, et al.* (2013). Genetically encoded calcium indicators for multi-color neural activity imaging and combination with optogenetics. Front Mol Neurosci *6*, 2.
Anderson, G.E., Kologlu, Y., and Papadopoulos, C. (1967). Fluctuations in postabsorptive blood glucose in relation to insulin release. Metabolism *16*, 586-596.
Ashcroft, F.M., and Rorsman, P. (2012). Diabetes mellitus and the beta cell: the last ten years. Cell *148*, 1160-1171.
Bader, E., Migliorini, A., Gegg, M., Moruzzi, N., Gerdes, J., Roscioni, S.S., Bakhti, M., Brandl, E., Irmler, M., Beckers, J.*, et al.* (2016). Identification of proliferative and mature beta-cells in the islets of Langerhans. Nature *535*, 430-434.
Barrett, K.E., Barman, S.M., Boitano, S., Brooks, H.L., Weitz, M., Kearns, B.P., and Ganong, W.F. (2010). Ganong's Review of Medical Physiology.
Bastidas-Ponce, A., Scheibner, K., Lickert, H., and Bakhti, M. (2017). Cellular and molecular mechanisms coordinating pancreas development. Development *144*, 2873-2888.
Bell, G.I., and Polonsky, K.S. (2001). Diabetes mellitus and genetically programmed defects in beta-cell function. Nature *414*, 788-791.
Boyden, E.S., Zhang, F., Bamberg, E., Nagel, G., and Deisseroth, K. (2005). Millisecond-timescale, genetically targeted optical control of neural activity. Nat Neurosci *8*, 1263-1268.
Chen, C., Chmelova, H., Cohrs, C.M., Chouinard, J.A., Jahn, S.R., Stertmann, J., Uphues, I., and Speier, S. (2016). Alterations in beta-Cell Calcium Dynamics and Efficacy Outweigh Islet Mass Adaptation in Compensation of Insulin Resistance and Prediabetes Onset. Diabetes *65*, 2676-2685.
Chen, T.W., Wardill, T.J., Sun, Y., Pulver, S.R., Renninger, S.L., Baohan, A., Schreiter, E.R., Kerr, R.A., Orger, M.B., Jayaraman, V.*, et al.* (2013). Ultrasensitive fluorescent proteins for imaging neuronal activity. Nature *499*, 295-300.
Cohrs, C.M., Chen, C., Jahn, S.R., Stertmann, J., Chmelova, H., Weitz, J., Bahr, A., Klymiuk, N., Steffen, A., Ludwig, B.*, et al.* (2017). Vessel Network Architecture of Adult Human Islets Promotes Distinct Cell-Cell Interactions In Situ and Is Altered After Transplantation. Endocrinology *158*, 1373-1385.
Cohrs, C.M., Panzer, J.K., Drotar, D.M., Enos, S.J., Kipke, N., Chen, C., Bozsak, R., Schöniger, E., Ehehalt, F., Distler, M.*, et al.* (2020). Dysfunction of Persisting β Cells Is a Key Feature of Early Type 2 Diabetes Pathogenesis. Cell Reports *31*, 107469.
Collombat, P., Hecksher-Sorensen, J., Broccoli, V., Krull, J., Ponte, I., Mundiger, T., Smith, J., Gruss, P., Serup, P., and Mansouri, A. (2005). The simultaneous loss of Arx and Pax4 genes promotes a somatostatin-producing cell fate specification at the expense of the alpha- and beta-cell lineages in the mouse endocrine pancreas. Development *132*, 2969-2980.
Collombat, P., Mansouri, A., Hecksher-Sorensen, J., Serup, P., Krull, J., Gradwohl, G., and Gruss, P. (2003). Opposing actions of Arx and Pax4 in endocrine pancreas development. Genes Dev *17*, 2591-2603.
Coronel, M.M., Liang, J.P., Li, Y., and Stabler, C.L. (2019). Oxygen generating biomaterial improves the function and efficacy of beta cells within a macroencapsulation device. Biomaterials *210*, 1-11.
D'Hoker, J., De Leu, N., Heremans, Y., Baeyens, L., Minami, K., Ying, C., Lavens, A., Chintinne, M., Stange, G., Magenheim, J.*, et al.* (2013). Conditional hypovascularization and hypoxia in islets do not overtly influence adult beta-cell mass or function. Diabetes *62*, 4165-4173.

References

Dana, H., Mohar, B., Sun, Y., Narayan, S., Gordus, A., Hasseman, J.P., Tsegaye, G., Holt, G.T., Hu, A., Walpita, D*., et al.* (2016). Sensitive red protein calcium indicators for imaging neural activity. Elife *5*.

Delgadillo-Silva, L.F., Tsakmaki, A., Akhtar, N., Franklin, Z.J., Konantz, J., Bewick, G.A., and Ninov, N. (2019). Modelling pancreatic beta-cell inflammation in zebrafish identifies the natural product wedelolactone for human islet protection. Dis Model Mech *12*.

Eames, S.C., Philipson, L.H., Prince, V.E., and Kinkel, M.D. (2010). Blood sugar measurement in zebrafish reveals dynamics of glucose homeostasis. Zebrafish *7*, 205-213.

El'tseva, T.V., Adamskaia, E.I., Peryshkova, T.A., and Babichev, V.N. (1992). [Disorder of neuroendocrine regulation of sexual behavior of male rats with streptozotocin-induced diabetes]. Probl Endokrinol (Mosk) *38*, 46-50.

Ellenbroek, J.H., Tons, H.A., de Graaf, N., Loomans, C.J., Engelse, M.A., Vrolijk, H., Voshol, P.J., Rabelink, T.J., Carlotti, F., and de Koning, E.J. (2013). Topologically heterogeneous beta cell adaptation in response to high-fat diet in mice. PLoS One *8*, e56922.

Fasciani, I., Pluta, P., Gonzalez-Nieto, D., Martinez-Montero, P., Molano, J., Paino, C.L., Millet, O., and Barrio, L.C. (2018). Directional coupling of oligodendrocyte connexin-47 and astrocyte connexin-43 gap junctions. Glia *66*, 2340-2352.

Gerber, P.A., and Rutter, G.A. (2017). The Role of Oxidative Stress and Hypoxia in Pancreatic Beta-Cell Dysfunction in Diabetes Mellitus. Antioxid Redox Signal *26*, 501-518.

Giordano, E., Bosco, D., Cirulli, V., and Meda, P. (1991). Repeated glucose stimulation reveals distinct and lasting secretion patterns of individual rat pancreatic B cells. J Clin Invest *87*, 2178-2185.

Goodner, C.J., Sweet, I.R., and Harrison, H.C., Jr. (1988). Rapid reduction and return of surface insulin receptors after exposure to brief pulses of insulin in perifused rat hepatocytes. Diabetes *37*, 1316-1323.

Gradwohl, G., Dierich, A., LeMeur, M., and Guillemot, F. (2000). neurogenin3 is required for the development of the four endocrine cell lineages of the pancreas. Proc Natl Acad Sci U S A *97*, 1607-1611.

Grapengiesser, E., Gylfe, E., and Hellman, B. (1988). Glucose-induced oscillations of cytoplasmic Ca2+ in the pancreatic beta-cell. Biochem Biophys Res Commun *151*, 1299-1304.

Grienberger, C., and Konnerth, A. (2012). Imaging calcium in neurons. Neuron *73*, 862-885.

Grodsky, G.M., Bennett, L.L., Smith, D.F., and Schmid, F.G. (1967). Effect of pulse administration of glucose or glucagon on insulin secretion in vitro. Metabolism *16*, 222-233.

Gut, P., Baeza-Raja, B., Andersson, O., Hasenkamp, L., Hsiao, J., Hesselson, D., Akassoglou, K., Verdin, E., Hirschey, M.D., and Stainier, D.Y.R. (2013). Whole-organism screening for gluconeogenesis identifies activators of fasting metabolism. Nat Chem Biol *9*, 97-104.

Harz, H., and Hegemann, P. (1991). Rhodopsin-Regulated Calcium Currents in Chlamydomonas. Nature *351*, 489-491.

Head, W.S., Orseth, M.L., Nunemaker, C.S., Satin, L.S., Piston, D.W., and Benninger, R.K. (2012). Connexin-36 gap junctions regulate in vivo first- and second-phase insulin secretion dynamics and glucose tolerance in the conscious mouse. Diabetes *61*, 1700-1707.

Hochbaum, D.R., Zhao, Y., Farhi, S.L., Klapoetke, N., Werley, C.A., Kapoor, V., Zou, P., Kralj, J.M., Maclaurin, D., Smedemark-Margulies, N*., et al.* (2014). All-optical electrophysiology in mammalian neurons using engineered microbial rhodopsins. Nat Methods *11*, 825-833.

Huang, C.J., Tu, C.T., Hsiao, C.D., Hsieh, F.J., and Tsai, H.J. (2003). Germ-line transmission of a myocardium-specific GFP transgene reveals critical regulatory elements in the cardiac myosin light chain 2 promoter of zebrafish. Dev Dyn *228*, 30-40.

Ivanova, A., Kalaidzidis, Y., Dirkx, R., Sarov, M., Gerlach, M., Schroth-Diez, B., Muller, A., Liu, Y., Andree, C., Mulligan, B*., et al.* (2013). Age-dependent labeling and imaging of insulin secretory granules. Diabetes *62*, 3687-3696.

Jacob, S., Kohler, M., Troster, P., Visa, M., Garcia-Prieto, C.F., Alanentalo, T., Moede, T., Leibiger, B., Leibiger, I.B., and Berggren, P.O. (2020). In vivo Ca(2+) dynamics in single pancreatic beta cells. FASEB J *34*, 945-959.

Janjuha, S., Pal Singh, S., and Ninov, N. (2018). Analysis of Beta-cell Function Using Single-cell Resolution Calcium Imaging in Zebrafish Islets. J Vis Exp.

Johnston, N.R., Mitchell, R.K., Haythorne, E., Pessoa, M.P., Semplici, F., Ferrer, J., Piemonti, L., Marchetti, P., Bugliani, M., Bosco, D*., et al.* (2016). Beta Cell Hubs Dictate Pancreatic Islet Responses to Glucose. Cell Metab *24*, 389-401.

Kahn, S.E., Cooper, M.E., and Del Prato, S. (2014). Pathophysiology and treatment of type 2 diabetes: perspectives on the past, present, and future. Lancet *383*, 1068-1083.

Katsarou, A., Gudbjornsdottir, S., Rawshani, A., Dabelea, D., Bonifacio, E., Anderson, B.J., Jacobsen, L.M., Schatz, D.A., and Lernmark, A. (2017). Type 1 diabetes mellitus. Nat Rev Dis Primers *3*, 17016.

References

Katsuta, H., Aguayo-Mazzucato, C., Katsuta, R., Akashi, T., Hollister-Lock, J., Sharma, A.J., Bonner-Weir, S., and Weir, G.C. (2012). Subpopulations of GFP-marked mouse pancreatic beta-cells differ in size, granularity, and insulin secretion. Endocrinology *153*, 5180-5187.

Kimmel, R.A., Dobler, S., Schmitner, N., Walsen, T., Freudenblum, J., and Meyer, D. (2015). Diabetic pdx1-mutant zebrafish show conserved responses to nutrient overload and anti-glycemic treatment. Sci Rep *5*, 14241.

Kinkel, M.D., and Prince, V.E. (2009). On the diabetic menu: zebrafish as a model for pancreas development and function. Bioessays *31*, 139-152.

Lang, D.A., Matthews, D.R., Peto, J., and Turner, R.C. (1979). Cyclic oscillations of basal plasma glucose and insulin concentrations in human beings. N Engl J Med *301*, 1023-1027.

Li, J., Klughammer, J., Farlik, M., Penz, T., Spittler, A., Barbieux, C., Berishvili, E., Bock, C., and Kubicek, S. (2016). Single-cell transcriptomes reveal characteristic features of human pancreatic islet cell types. EMBO Rep *17*, 178-187.

Li, M., Maddison, L.A., Page-McCaw, P., and Chen, W. (2014). Overnutrition induces beta-cell differentiation through prolonged activation of beta-cells in zebrafish larvae. Am J Physiol Endocrinol Metab *306*, E799-807.

Lin, J.Y. (2011). A user's guide to channelrhodopsin variants: features, limitations and future developments. Exp Physiol *96*, 19-25.

Lorincz, R., Emfinger, C.H., Walcher, A., Giolai, M., Krautgasser, C., Remedi, M.S., Nichols, C.G., and Meyer, D. (2018). In vivo monitoring of intracellular Ca(2+) dynamics in the pancreatic beta-cells of zebrafish embryos. Islets *10*, 221-238.

Marciniak, A., Cohrs, C.M., Tsata, V., Chouinard, J.A., Selck, C., Stertmann, J., Reichelt, S., Rose, T., Ehehalt, F., Weitz, J.*, et al.* (2014). Using pancreas tissue slices for in situ studies of islet of Langerhans and acinar cell biology. Nat Protoc *9*, 2809-2822.

Marciniak, A., Selck, C., Friedrich, B., and Speier, S. (2013). Mouse pancreas tissue slice culture facilitates long-term studies of exocrine and endocrine cell physiology in situ. PLoS One *8*, e78706.

Mariot, P., Gilon, P., Nenquin, M., and Henquin, J.C. (1998). Tolbutamide and diazoxide influence insulin secretion by changing the concentration but not the action of cytoplasmic Ca2+ in beta-cells. Diabetes *47*, 365-373.

Mast, S.O. (1916). The process of orientation in the colonial organism, Gonium pectorale, and a study of the structure and function of the eye-spot. The journal of experimental zoology.

Matthews, D.R., Naylor, B.A., Jones, R.G., Ward, G.M., and Turner, R.C. (1983). Pulsatile insulin has greater hypoglycemic effect than continuous delivery. Diabetes *32*, 617-621.

Mattis, J., Tye, K.M., Ferenczi, E.A., Ramakrishnan, C., O'Shea, D.J., Prakash, R., Gunaydin, L.A., Hyun, M., Fenno, L.E., Gradinaru, V.*, et al.* (2011). Principles for applying optogenetic tools derived from direct comparative analysis of microbial opsins. Nat Methods *9*, 159-172.

Matveyenko, A.V., Liuwantara, D., Gurlo, T., Kirakossian, D., Dalla Man, C., Cobelli, C., White, M.F., Copps, K.D., Volpi, E., Fujita, S.*, et al.* (2012). Pulsatile portal vein insulin delivery enhances hepatic insulin action and signaling. Diabetes *61*, 2269-2279.

McKinney, S.A., Murphy, C.S., Hazelwood, K.L., Davidson, M.W., and Looger, L.L. (2009). A bright and photostable photoconvertible fluorescent protein. Nat Methods *6*, 131-133.

Meier, J.J., Veldhuis, J.D., and Butler, P.C. (2005). Pulsatile insulin secretion dictates systemic insulin delivery by regulating hepatic insulin extraction in humans. Diabetes *54*, 1649-1656.

Miller, A.C., Whitebirch, A.C., Shah, A.N., Marsden, K.C., Granato, M., O'Brien, J., and Moens, C.B. (2017). A genetic basis for molecular asymmetry at vertebrate electrical synapses. Elife *6*.

Molina, R.S., Qian, Y., Wu, J., Shen, Y., Campbell, R.E., Drobizhev, M., and Hughes, T.E. (2019). Understanding the Fluorescence Change in Red Genetically Encoded Calcium Ion Indicators. Biophys J *116*, 1873-1886.

Moss, L.G., Caplan, T.V., and Moss, J.B. (2013). Imaging beta cell regeneration and interactions with islet vasculature in transparent adult zebrafish. Zebrafish *10*, 249-257.

Mullapudi, S.T., Boezio, G.L.M., Rossi, A., Marass, M., Matsuoka, R.L., Matsuda, H., Helker, C.S.M., Yang, Y.H.C., and Stainier, D.Y.R. (2019). Disruption of the pancreatic vasculature in zebrafish affects islet architecture and function. Development *146*.

Murphy, R., Ellard, S., and Hattersley, A.T. (2008). Clinical implications of a molecular genetic classification of monogenic beta-cell diabetes. Nat Clin Pract Endocrinol Metab *4*, 200-213.

Nadal, A., Quesada, I., and Soria, B. (1999). Homologous and heterologous asynchronicity between identified alpha-, beta- and delta-cells within intact islets of Langerhans in the mouse. J Physiol *517 (Pt 1)*, 85-93.

Nagel, G., Ollig, D., Fuhrmann, M., Kateriya, S., Musti, A.M., Bamberg, E., and Hegemann, P. (2002). Channelrhodopsin-1: a light-gated proton channel in green algae. Science *296*, 2395-2398.

Nagel, G., Szellas, T., Huhn, W., Kateriya, S., Adeishvili, N., Berthold, P., Ollig, D., Hegemann, P., and Bamberg, E. (2003). Channelrhodopsin-2, a directly light-gated cation-selective membrane channel. Proc Natl Acad Sci U S A *100*, 13940-13945.

References

Nakai, J., Ohkura, M., and Imoto, K. (2001). A high signal-to-noise Ca(2+) probe composed of a single green fluorescent protein. Nat Biotechnol *19*, 137-141.

Nath, A.K., Ryu, J.H., Jin, Y.N., Roberts, L.D., Dejam, A., Gerszten, R.E., and Peterson, R.T. (2015). PTPMT1 Inhibition Lowers Glucose through Succinate Dehydrogenase Phosphorylation. Cell Rep *10*, 694-701.

Ninov, N., Hesselson, D., Gut, P., Zhou, A., Fidelin, K., and Stainier, D.Y. (2013). Metabolic regulation of cellular plasticity in the pancreas. Curr Biol *23*, 1242-1250.

Oda, K., Vierock, J., Oishi, S., Rodriguez-Rozada, S., Taniguchi, R., Yamashita, K., Wiegert, J.S., Nishizawa, T., Hegemann, P., and Nureki, O. (2018). Crystal structure of the red light-activated channelrhodopsin Chrimson. Nat Commun *9*, 3949.

Ollion, J., Cochennec, J., Loll, F., Escude, C., and Boudier, T. (2013). TANGO: a generic tool for high-throughput 3D image analysis for studying nuclear organization. Bioinformatics *29*, 1840-1841.

Paolisso, G., Sgambato, S., Torella, R., Varricchio, M., Scheen, A., D'Onofrio, F., and Lefebvre, P.J. (1988). Pulsatile insulin delivery is more efficient than continuous infusion in modulating islet cell function in normal subjects and patients with type 1 diabetes. J Clin Endocrinol Metab *66*, 1220-1226.

Paredes, R.M., Etzler, J.C., Watts, L.T., Zheng, W., and Lechleiter, J.D. (2008). Chemical calcium indicators. Methods *46*, 143-151.

Poretsky, L. (2010). Principles of Diabetes Mellitus.

Ravier, M.A., Guldenagel, M., Charollais, A., Gjinovci, A., Caille, D., Sohl, G., Wollheim, C.B., Willecke, K., Henquin, J.C., and Meda, P. (2005). Loss of connexin36 channels alters beta-cell coupling, islet synchronization of glucose-induced Ca2+ and insulin oscillations, and basal insulin release. Diabetes *54*, 1798-1807.

Reinbothe, T.M., Safi, F., Axelsson, A.S., Mollet, I.G., and Rosengren, A.H. (2014). Optogenetic control of insulin secretion in intact pancreatic islets with beta-cell-specific expression of Channelrhodopsin-2. Islets *6*, e28095.

Reinert, R.B., Brissova, M., Shostak, A., Pan, F.C., Poffenberger, G., Cai, Q., Hundemer, G.L., Kantz, J., Thompson, C.S., Dai, C.*, et al.* (2013). Vascular endothelial growth factor-a and islet vascularization are necessary in developing, but not adult, pancreatic islets. Diabetes *62*, 4154-4164.

Rorsman, P., and Renstrom, E. (2003). Insulin granule dynamics in pancreatic beta cells. Diabetologia *46*, 1029-1045.

Rukstalis, J.M., and Habener, J.F. (2009). Neurogenin3: a master regulator of pancreatic islet differentiation and regeneration. Islets *1*, 177-184.

Rupprecht, P., Prendergast, A., Wyart, C., and Friedrich, R.W. (2016). Remote z-scanning with a macroscopic voice coil motor for fast 3D multiphoton laser scanning microscopy. Biomed Opt Express *7*, 1656-1671.

Salem, V., Silva, L.D., Suba, K., Georgiadou, E., Neda Mousavy Gharavy, S., Akhtar, N., Martin-Alonso, A., Gaboriau, D.C.A., Rothery, S.M., Stylianides, T.*, et al.* (2019). Leader β-cells coordinate Ca2+ dynamics across pancreatic islets in vivo. Nature Metabolism *1*, 615-629.

Samarut, E., Swaminathan, A., Riche, R., Liao, M., Hassan-Abdi, R., Renault, S., Allard, M., Dufour, L., Cossette, P., Soussi-Yanicostas, N.*, et al.* (2018). gamma-Aminobutyric acid receptor alpha 1 subunit loss of function causes genetic generalized epilepsy by impairing inhibitory network neurodevelopment. Epilepsia *59*, 2061-2074.

Satin, L.S., Butler, P.C., Ha, J., and Sherman, A.S. (2015). Pulsatile insulin secretion, impaired glucose tolerance and type 2 diabetes. Mol Aspects Med *42*, 61-77.

Schindelin, J., Arganda-Carreras, I., Frise, E., Kaynig, V., Longair, M., Pietzsch, T., Preibisch, S., Rueden, C., Saalfeld, S., Schmid, B.*, et al.* (2012). Fiji: an open-source platform for biological-image analysis. Nat Methods *9*, 676-682.

Serre-Beinier, V., Le Gurun, S., Belluardo, N., Trovato-Salinaro, A., Charollais, A., Haefliger, J.A., Condorelli, D.F., and Meda, P. (2000). Cx36 preferentially connects beta-cells within pancreatic islets. Diabetes *49*, 727-734.

Shen, Y., Dana, H., Abdelfattah, A.S., Patel, R., Shea, J., Molina, R.S., Rawal, B., Rancic, V., Chang, Y.F., Wu, L.*, et al.* (2018). A genetically encoded Ca(2+) indicator based on circularly permutated sea anemone red fluorescent protein eqFP578. BMC Biol *16*, 9.

Singh, S.P., Janjuha, S., Hartmann, T., Kayisoglu, O., Konantz, J., Birke, S., Murawala, P., Alfar, E.A., Murata, K., Eugster, A.*, et al.* (2017). Different developmental histories of beta-cells generate functional and proliferative heterogeneity during islet growth. Nat Commun *8*, 664.

Smukler, S.R., Arntfield, M.E., Razavi, R., Bikopoulos, G., Karpowicz, P., Seaberg, R., Dai, F., Lee, S., Ahrens, R., Fraser, P.E.*, et al.* (2011). The adult mouse and human pancreas contain rare multipotent stem cells that express insulin. Cell Stem Cell *8*, 281-293.

Speier, S., Nyqvist, D., Kohler, M., Caicedo, A., Leibiger, I.B., and Berggren, P.O. (2008). Noninvasive high-resolution in vivo imaging of cell biology in the anterior chamber of the mouse eye. Nat Protoc *3*, 1278-1286.

Spooner, B.S., Walther, B.T., and Rutter, W.J. (1970). The development of the dorsal and ventral mammalian pancreas in vivo and in vitro. J Cell Biol *47*, 235-246.

References

Stokes, P.A., and Purdon, P.L. (2017). A study of problems encountered in Granger causality analysis from a neuroscience perspective. Proc Natl Acad Sci U S A *114*, E7063-E7072.

Stozer, A., Dolensek, J., and Rupnik, M.S. (2013). Glucose-stimulated calcium dynamics in islets of Langerhans in acute mouse pancreas tissue slices. PLoS One *8*, e54638.

Traver, D., Paw, B.H., Poss, K.D., Penberthy, W.T., Lin, S., and Zon, L.I. (2003). Transplantation and in vivo imaging of multilineage engraftment in zebrafish bloodless mutants. Nat Immunol *4*, 1238-1246.

Tsien, R.Y. (1980). New calcium indicators and buffers with high selectivity against magnesium and protons: design, synthesis, and properties of prototype structures. Biochemistry *19*, 2396-2404.

Vecchio, I., Tornali, C., Bragazzi, N.L., and Martini, M. (2018). The Discovery of Insulin: An Important Milestone in the History of Medicine. Front Endocrinol (Lausanne) *9*, 613.

Weitz, J.R., Makhmutova, M., Almaca, J., Stertmann, J., Aamodt, K., Brissova, M., Speier, S., Rodriguez-Diaz, R., and Caicedo, A. (2018). Mouse pancreatic islet macrophages use locally released ATP to monitor beta cell activity. Diabetologia *61*, 182-192.

Westacott, M.J., Ludin, N.W.F., and Benninger, R.K.P. (2017). Spatially Organized beta-Cell Subpopulations Control Electrical Dynamics across Islets of Langerhans. Biophys J *113*, 1093-1108.

Xin, Y., Kim, J., Okamoto, H., Ni, M., Wei, Y., Adler, C., Murphy, A.J., Yancopoulos, G.D., Lin, C., and Gromada, J. (2016). RNA Sequencing of Single Human Islet Cells Reveals Type 2 Diabetes Genes. Cell Metab *24*, 608-615.

Yang, Y.H.C., Kawakami, K., and Stainier, D.Y. (2018). A new mode of pancreatic islet innervation revealed by live imaging in zebrafish. Elife *7*.

Zhang, F., Wang, L.P., Brauner, M., Liewald, J.F., Kay, K., Watzke, N., Wood, P.G., Bamberg, E., Nagel, G., Gottschalk, A.*, et al.* (2007). Multimodal fast optical interrogation of neural circuitry. Nature *446*, 633-639.

Zhang, M., Goforth, P., Bertram, R., Sherman, A., and Satin, L. (2003). The Ca2+ dynamics of isolated mouse beta-cells and islets: implications for mathematical models. Biophys J *84*, 2852-2870.

Zhang, Q., Galvanovskis, J., Abdulkader, F., Partridge, C.J., Gopel, S.O., Eliasson, L., and Rorsman, P. (2008). Cell coupling in mouse pancreatic beta-cells measured in intact islets of Langerhans. Philos Trans A Math Phys Eng Sci *366*, 3503-3523.

Zhao, Y., Araki, S., Wu, J., Teramoto, T., Chang, Y.F., Nakano, M., Abdelfattah, A.S., Fujiwara, M., Ishihara, T., Nagai, T.*, et al.* (2011). An expanded palette of genetically encoded Ca(2)(+) indicators. Science *333*, 1888-1891.

Zou, C., Wang, Y., and Shen, Z. (2005). 2-NBDG as a fluorescent indicator for direct glucose uptake measurement. J Biochem Biophys Methods *64*, 207-215.

8. Annexes

(in the following pages)

Annexes

Dresden University of Technology **Annex 1**
Faculty of Medicine Carl Gustav Carus
Doctorate Regulations of 24th July 2011

Statements regarding the opening of doctorate proceedings

1. I herewith declare that I have produced this paper without the prohibited assistance of third parties and without making use of aids other than those specified; notions taken over directly or indirectly from other sources have been identified as such.

2. I received assistance from the following persons in conjunction with the selection and evaluation of materials and creation of the manuscript:

Dr. Nikolay Ninov

Prof. Dr. Stefan R. Bornstein

Prof. Stephan Speier

Dr. Anthony Gavalas

Prof. Guy Rutter

Dr. Victoria Salem

3. No further persons were involved in the intellectual creation of the presented work. I have in particular not taken recourse to the assistance of a commercial doctorate advisor. No third parties have received remuneration or payment in kind from me, neither directly nor indirectly, for work in connection with the contents of the presented thesis.

4. This paper has not previously been presented in identical or similar form to any other German or foreign examination board.

5. Contents of this thesis have been published in the following form:

Leader β-cells coordinate Ca^{2+} dynamics across pancreatic islets in vivo. Victoria Salem, **Luis Delgadillo Silva**, Kinga Suba, Eleni Georgiadou, S. Neda Mousavy Gharavy, Nadeem Akhtar, Aldara Martin-Alonso, David C. A. Gaboriau, Stephen M. Rothery, Theodoros Stylianides, Gaelle Carrat, Timothy J. Pullen, Sumeet Pal Singh, David J. Hodson, Isabelle Leclerc, A. M. James Shapiro, Piero Marchetti, Linford J. B. Briant, Walter Distaso, Nikolay Ninov & Guy A. Rutter. (2019). **Nature Metabolism 1, 615-629**

Modelling pancreatic β-cell inflammation in zebrafish identifies the natural product wedelolactone for human islet protection. Luis Fernando Delgadillo-

Silva, Anastasia Tsakmaki, Nadeem Akhtar, Zara J. Franklin, Judith Konantz, Gavin A. Bewick, Nikolay Ninov. **Disease Models & Mechanisms 2019 12: dmm036004 doi: 10.1242/dmm.036004**

6. I confirm that I accept the applicable Doctorate Regulations of the Faculty of Medicine Carl Gustav Carus of the Dresden University of Technology.

Place, date

Signature of the candidate

Technische Universität Dresden **Anlage 1**
Medizinische Fakultät Carl Gustav Carus
Promotionsordnung vom 24. Juli 2011

Erklärungen zur Eröffnung des Promotionsverfahrens

1. Hiermit versichere ich, dass ich die vorliegende Arbeit ohne unzulässige Hilfe Dritter und ohne Benutzung anderer als der angegebenen Hilfsmittel angefertigt habe; die aus fremden Quellen direkt oder indirekt übernommenen Gedanken sind als solche kenntlich gemacht.

2. Bei der Auswahl und Auswertung des Materials sowie bei der Herstellung des Manuskripts habe ich Unterstützungsleistungen von folgenden Personen erhalten:

Dr. Nikolay Ninov

Prof. Dr. Stefan R. Bornstein

Prof. Stephan Speier

Dr. Anthony Gavalas

Prof. Guy Rutter

Dr. Victoria Salem

3. Weitere Personen waren an der geistigen Herstellung der vorliegenden Arbeit nicht beteiligt. Insbesondere habe ich nicht die Hilfe eines kommerziellen Promotionsberaters in Anspruch genommen. Dritte haben von mir weder unmittelbar noch mittelbar geldwerte Leistungen für Arbeiten erhalten, die im Zusammenhang mit dem Inhalt der vorgelegten Dissertation stehen.

4. Die Arbeit wurde bisher weder im Inland noch im Ausland in gleicher oder ähnlicher Form einer anderen Prüfungsbehörde vorgelegt.

5. Die Inhalte dieser Dissertation wurden in folgender Form veröffentlicht:

Leader β-cells coordinate Ca^{2+} dynamics across pancreatic islets in vivo. Victoria Salem, **Luis Delgadillo Silva**, Kinga Suba, Eleni Georgiadou, S. Neda Mousavy Gharavy, Nadeem Akhtar, Aldara Martin-Alonso, David C. A. Gaboriau, Stephen M. Rothery, Theodoros Stylianides, Gaelle Carrat, Timothy J. Pullen, Sumeet Pal Singh, David J. Hodson, Isabelle Leclerc, A. M. James Shapiro, Piero Marchetti, Linford J. B. Briant, Walter Distaso, Nikolay Ninov & Guy A. Rutter. (2019). **Nature Metabolism 1, 615-629**

Modelling pancreatic β-cell inflammation in zebrafish identifies the natural product wedelolactone for human islet protection. Luis Fernando Delgadillo-

Silva, Anastasia Tsakmaki, Nadeem Akhtar, Zara J. Franklin, Judith Konantz, Gavin A. Bewick, Nikolay Ninov. **Disease Models & Mechanisms 2019 12: dmm036004 doi: 10.1242/dmm.036004**

6. Ich bestätige, dass es keine zurückliegenden erfolglosen Promotionsverfahren gab.

Ja

7. Ich bestätige, dass ich die Promotionsordnung der Medizinischen Fakultät der Technischen Universität Dresden anerkenne.

8. Ich habe die Zitierrichtlinien für Dissertationen an der Medizinischen Fakultät der Technischen Universität Dresden zur Kenntnis genommen und befolgt.

Ort, Datum

Unterschrift des Doktoranden

Dresden University of Technology **Annex 2**
Faculty of Medicine Carl Gustav Carus
Doctorate Regulations of 24th July 2011

I herewith confirm that the following currently applicable legal requirements have been observed in connection with my thesis

□ Favourable opinion of the Ethics Commission in case of clinical studies, epidemiological studies with personal references or contexts covered by the law on medical devices.

Case ref. no of the responsible Ethics Commission: NA

□ Observance of the stipulations of animal welfare legislation

Case ref. no. of the approving authority for the project/participation:

Landesdirektion Sachsen Ethics Committees Germany (AZ.: 24D-9168, 11-1/2013-14, TV38/2015, T12/2016 and T13/2016, TVV50/2017, TVV45/2018, TVV33-2019).

□ Observance of the stipulations of genetic engineering legislation

Project number: Az.: 54-881 1 .7 1 1210

□ Observance of the data privacy rules of the Faculty of Medicine and University Clinic Carl Gustav Carus.

Place, date

Signature of the candidate

Technische Universität Dresden **Anlage 2**
Medizinische Fakultät Carl Gustav Carus
Promotionsordnung vom 24. Juli 2011
Erklärungen zur Eröffnung des Promotionsverfahrens

Hiermit bestätige ich die Einhaltung der folgenden aktuellen gesetzlichen Vorgaben im Rahmen meiner Dissertation

□ das zustimmende Votum der Ethikkommission bei Klinischen Studien, epidemiologischen Untersuchungen mit Personenbezug oder Sachverhalten, die das Medizinproduktegesetz betreffen
Aktenzeichen der zuständigen Ethikkommission: NA

□ die Einhaltung der Bestimmungen des Tierschutzgesetzes
Aktenzeichen der Genehmigungsbehörde zum Vorhaben/zur Mitwirkung:

Landesdirektion Sachsen Ethics Committees Germany (AZ.: 24D-9168, 11-1/2013-14, TV38/2015, T12/2016 and T13/2016, TVV50/2017, TVV45/2018, TVV33-2019).

□ die Einhaltung des Gentechnikgesetzes
Projektnummer: Az.: 54-881 1 .7 1 1210

□ die Einhaltung von Datenschutzbestimmungen der Medizinischen Fakultät und des Universitätsklinikums Carl Gustav Carus.

Ort, Datum

Unterschrift des Doktoranden

9. Acknowledgments

There are not enough words to express my gratitude for all your teachings and help during all this period. Professor Nikolay Ninov, I will always bring all your teachings to the next projects and research. I assure you that I will always keep improving.

During all this travel, you always gave me the guidance to keep moving in the right direction. There we go, we managed to explore a bit some of the β-cell biology *in vivo*. Cheer to my TAC members and guides: Dr. Monika Ehrhart-Bornstein, Ph.D. Suzanne Eaton, Ph.D. Stefan R. Bornstein, Dr. Anthony Gavalas, Prof. Stephan Speier. And special thanks to Prof. Guy Rutter, Dr. Victoria Salem and Dr. Maximina Yun. I will keep on discovering more things and thanks for all your teachings.

Thank you Mom, Dad, Elena, Nayeli, Victoria, Sofia and Alberto. You are my Suns, the bright sun that always keeps me warm. Especially you Mom and Dad, you two are one of the few teachers about life I have had. And no matter the distance or the time, we will always be together.

Also, when we talk is like time have not passed at all. Thank you Pricilla Cuellar Medina, Juan Rafael Tontle Pena and Manuel Hernández, I managed somehow to make the dream I was always talking about to come true.

At the age of 17, I promised to study my doctorate in diabetes... What a “bad” decision. A long road that took me more than 15 years of pursuit. I ended up leaving my family to make my Bachelor and Masters at the UNAM in Cuernavaca. Thanks to that, I met all my old friends from Genómicas, I will always love you guys. Zarco, Stephanie, Silvia, Akram, Robert, Daniel, Soto, Willy, Rocio and Sol, We will always Rock! Thank you Dr. Sergio Encarnación, Dr. Alberto Checa, Dr. Andrés Andrade, Dra. Abigail Trejo, Magdalena Hernández, Sandra Contreras and Gabriel Martínez Batallar. The proteomics rocks!

Acknowledgements

Thank you Dr. Federico Sánchez Rodríguez and Dra. Yvonne Rosenstein, you inspired me to eat the world and assure the next step!

We managed to enter the program, and one by one we are finishing the PhD. Cheers to you guys: Heba Nabil, Juan Manuel Iglesias Artola, Soña Michlikova, Julien Delpier, Lenka Belicova. Riccardo Maraspini and Fabian Bergemann, we are almost finish!

Afterwards I started my first PhD at the other side of the Ocean, in Dresden Germany. However it was not in diabetes… I was supposed to study the progenitors of the adrenal gland because obviously life is not that easy. After 10 year of constant struggle, when I was at the moment to start my doctorate in diabetes, I was rejected to do so, because I lacked experience in confocal microscopy... If it weren't for all the people who helped me and supported me on all the struggles, I would not be here at the end of this dream and the beginning of a new stage. Thank you Dra. Guadalupe Sosa, you were part of my strength to keep me trying all over again against all odds.

Thank you Dr. Monika Ehrhart-Bornstein, Dra. Maria F. Rubin de Celis, Dra. Charlotte Steenblock, Dr. Christian G. Ziegler, Uta Lehnert and Linda Friedrich. You gave me the first chance to come to Dresden, and we explored a bit of the adrenal gland biology!

Special thanks to the DIBGS-BB PhD office, Arantxa Sanchéz and Marleen Frankee you keep us safe from paper work. During the rocky training in the DIGS-BB PhD program, I learned from Kei, how to do single-cell laser ablations in alive Zebrafish. Cheers to Mansi, Kei and Stephano, thanks to your teachings I somehow convinced Prof. Nikolay to give a chance to make my PhD on his lab. Later, Evelyn Abraham and Anja Machate were also very kind and help me to improve the laser ablation and to get some special transgenic lines. Thanks a lot for your extra help!

Second chances hardly exist in life. So if it were to happen to you, you better grab it, seize the opportunity, no matter what. There was no way I would let this second chance to be missed. Then, after asking Prof. Nikolay how the β-cells would respond after the ablation of some of them, I was at the beginning of this long-sought dream. I directly learned cloning and live imaging from Prof. Nikolay, and up to today we have created more than 20 transgenic lines and we have developed the techniques for high-speed and high-resolution live imaging, and probably we are the first ones in the whole world to control with light the β-cells in an alive organism. Of course, we are still going for more!

Acknowledgements

As they say by teaching you will learn, and by learning you will teach. Hopefully I taught you guys something while I was learning from you my beloved master´s students: Rajanya Ghosh, Hannah Hiepe, Anabel Villanueva, Ahsan Javed and Daniel Silva Apango, keep learning, keep growing, develop your mission and hope to see your results soon.

None of you were only labmates, for me, you were my teachers and friends, Sarah Birke, Dr. Sharan Janjua, Dr. Sumeet Pal Singh, Dr. Judith Konatz, Silvia Palme, Dr. Ezz Aldid Ahmed Alfar, Özge Kayisoglu, Theresa Hartmann, Nadeem Akhbar, Alicja Korpowska, Margrit Kamel, Halyna Karpusha, Alisa Hnatiuk, Prateek Chawla, Emirhan Tasöz, Rebecca Soliwoda and Ilka Drange. We were somehow united by the desired of knowing more, to experiment, to learn and discover. So, thank you all, for all this wonderful time and let´s stay hungry, self-motivated and never stop. Remember, there is no tomorrow, there is only today!

During this dream, I also experience the joy of working together, the so-called collaboration. Meeting you and working together was something incredible, my biggest respect for such professional people, you remind me, that even when I think I am working too much, there are people doing twice as much as me. Verena Kapert, Anastasia Tsakmaki, Keiichi Katsumoto, Dra. Vicky Salem, Dra. Sara Sofia Deville and Dr. Nico Scherf. Now, finally I understood what team work is. The task might look unsurmountable, but together we can!

As I mention, I did not have "*experience*" in microscopy, how can you have experience if you don't get the chance to try? Thank you Silke Tulok and Anja Nobst. You two were the first people who let me play with confocal microscopes. I still remember joking about a touch-pad for a microscope when I had only use manual epifluorescent microscope with manual camera and a memory of 512MB... Then, I "discovered" the Spinning disk, Confocal, Light-Sheet, SPIM, Epiflourescent, Apotmes and many more. We did 1500μm^3 in cleared adrenal glands in the Light-Sheet with David Accardi, together with Maria and Verena. What an achievement! Thanks a lot guys, you were very supportive in letting me try and we succeeded!

Soon after, the biggest challenge was here: Calcium imaging *in vivo*. No more fixed easy samples, we needed to go faster, with lower laser, with higher resolution… in other words, we needed to reach the limits of microscopy *in vivo*. And here you guys where the difference. Thanks to the CMCB - Light Microscopy Facility. Thanks to Dr. Hella Hartmann, Dr. Ruth Hans, Ellen Geibel, Dr. Britta Schroth-Diez, Dr. Markus Burkhardt and Dr. Ali Gheisari, you saved me so many times. I loved when we presented on the Tim2020, it is engrained in my mind, as the Zeiss representative was saying: I would never dare to give a workshop like this, where too many things can go wrong. Immediately I answered: at the contrary, too many

things can go right… you know why? Because you were always there, and you would solve any possible limitation. There is no roof, is only in our minds. Now, we are as fast as the β-cells and we even managed to do *in vivo* optogenetics, controlling single-cells within the living zebrafish larvae. Thank you all, and keep being Faster-Bigger-Better!

All this work is impossible without the support of the magnificent facilities of the CMCB. The Fish facility always made an amazing work for growing fish and keeping them in excellent conditions. Thanks for all your help Marika Fischer, Jitka Michling, Daniela Mögel, Rosi Winze, Katja Bernhardt and Dr. Judith Konatz. Without all of you, no zebrafish project could have been done.

Also, thanks to the Flow Cytometry Facility, especially to Anne Gompf. And also to the sequencing facility, especially to Andreas Dahl and Alexopoulou Dimitra. Cheers, we all together, explored how the transcriptomic profile of the β-cells is affected by inflammation!

Along the way of the doctorate studies in Germany I met with incredible people, in the MTZ I met you guys: Eduardo Rojo, Philip Muennighoff, Ricardo Lira, Santiago Cañon, Isha Swagata, Verena Kappert and Anica Kurzbach. Then in the CRTD I manage to make more friends: Lisa Nauman, Mehmet Ilyas, Probesh Bhattarai, Violeta Mashkaryan, Jochen Krattenmachen, Herr Teije, David Arturo. And of course from all the other non-academic places: Chris Koschenz, Aparna, Yanca, Iva Velinova, Katrin Walzac, Mali, Mattias, Mrinaly, Nokul, Luisa Grube, David Ortegón, Susann Riedel, Simona Bobnar, Giovanni De Ghantuz, Helena, Janine, Enrique Calvera, Andrés, Ana Barrios, Fabian, Christian Javier Castaño, Militza Caballero Pino, Flor Venini, Manuel Vázquez Requena, Uli Ulrik, Stephan Hawer, Nefer, Anika Nguyen, José, Tanja, Camila Avella, Mo Huiyu and Armand Muñoz. Hopefully the new friendship we have just made can grow stronger in the following years. We have had countless adventures and still all those to come!

Finally, you will always be one of my Suns, Silvia (Chocolatito) Catalina Cometta Conde. Thanks for the beautiful memories, they will always bring me happiness.

And remember, do not ever accept a first no… Find the way around, since life is only testing how strong your resolution is. Thank you all, and see you in the next adventure!

Kind regards,
Luis D.